Chapter 3: Observations: Ocean

Coordinating Lead Authors: Monika Rhein (Germany), Stephen R. Rintoul (Australia)

Lead Authors: Shigeru Aoki (Japan), Edmo Campos (Brazil), Don Chambers (USA), Richard Feely (USA), Sergey Gulev (Russia), Gregory C. Johnson (USA), Simon Josey (UK), Andrey Kostianoy (Russia), Cecilie Mauritzen (Norway), Dean Roemmich (USA), Lynne Talley (USA), Fan Wang (China)

Contributing Authors: Michio Aoyama, Molly Baringer, Nick Bates, Timothy Boyer, Robert Byrne, Stuart Cunningham, Thierry Delcroix, John Dore, Paul Durack, Rana Fine, Melchor González-Dávila, Nicolas Gruber, Mark Hemer, David Hydes, Stanley Jacobs, Torsten Kanzow, David Karl, Alexander Kazmin, Samar Khatiwala, Joan Kleypas, Kitack Lee, Calvin Mordy, Jon Olafsson, James Orr, Alejandro Orsi, Igor Polyakov, Sarah G. Purkey, Bo Qiu, Gilles Reverdin, Anastasia Romanou, Raymond Schmitt, Koji Shimada, Lothar Stramma, Toshio Suga, Taro Takahashi, Toste Tanhua, Hans von Storch, Xialoan Wang, Rik Wanninkhof, Susan Wijffels, Philip Woodworth, Igor Yashayaev, Lisan Yu

Review Editors: Howard Freeland (Canada), Yukihiro Nojiri (Japan), Ilana Wainer (Brazil)

Date of Draft: 16 December 2011

Notes: TSU Compiled Version

Table of Contents

Executive Summary

It is virtually certain that the upper ocean has warmed since 1970, when observations covering most of the global ocean become available. This result is consistently supported by three independent methods of observation including (i) the subsurface measurements of temperature described here, (ii) sea surface temperature data from satellites (Chapter 2) and in situ measurements from surface drifters and ships, and (iii) the record of sea level rise, which is known to include a substantial component due to thermal expansion (Section 3.7 and Chapter 13). Instrumental biases in historical upper ocean temperature measurements have been identified and largely removed, reducing a spurious decadal variation in upper ocean heat content present in analyses included in AR4. Largest warming is found near the sea surface (>0.1°C per decade in the upper 75 m), decreasing to about 0.017°C per decade by 700 m. The surface intensification of the warming signal increases the thermal stratification of the upper ocean by about 4% (between 0 and 200 m depth) over the 43-year record. Sparse sampling in space and time makes assessment of deep ocean temperature and heat content variability less certain than that for the upper ocean. Any trend in global ocean temperatures between 2000 and 4000 m depth is indistinguishable from zero. It is likely that the densest water mass fed by sinking of cold water around Antarctica has warmed at least since 1990.

Ocean warming accounts for more than 90% of the increase in heat energy stored by the Earth system over the last 40 years. Estimates of the trend in upper ocean heat content between 1970 and 2009 range from 37 to 42 x 10^{21} J decade^{-1}. The high agreement between two estimates using different strategies to map temperature changes in data-poor regions increases confidence in the conclusion that upper ocean heat content has increased.

Robust changes in ocean salinity have been observed throughout much of the ocean, both at the sea surface and in the ocean interior. Over the last fifty years, the mean regional pattern of sea surface salinity has been enhanced: saline surface waters in the evaporation-dominated mid-latitudes have become more saline, while the relatively fresh surface waters in rainfall-dominated tropical and polar regions have become fresher. Similarly, the interbasin contrast between saline Atlantic and fresh Pacific surface waters has increased. These changes are consistent with an intensification of the water cycle as the lower atmosphere has warmed, reflecting the ability of warmer air to contain more moisture. Changes in salinity have been observed in the ocean interior as well. Both, the subduction of surface water mass anomalies and the movement of density surfaces have contributed to the salinity changes on observed depth levels. Changes in freshwater flux and the migration of surface density outcrops caused by surface warming (e.g., to regions of lower or higher surface salinity) have likely both contributed to the formation of salinity anomalies on density surfaces.

The observed increase in upper ocean heat content is equivalent to a mean net heat flux into the ocean of <0.5 W m^{-2}. This signal is too small to detect in surface flux datasets, whose uncertainty is more than an order of magnitude larger than this. It is also not yet possible to establish whether there is a significant trend in evaporation – precipitation (E-P) over the past 50 years from surface flux observations; analyses for the shorter period 1987-2006 show significant interannual variability but no evidence for a trend in global mean E-P. There is evidence for an increase in wind stress in the Southern Ocean in recent decades that is linked to changes in the Southern Annular Mode (SAM) of atmospheric variability. While observations remain limited, it is likely that significant wave height has increased over the North Pacific since 1900, the North Atlantic since 1950 and the Southern Ocean over the last two decades. Extreme wave heights have likely increased over the past 60 years, in keeping with increases in extreme winds.

Changes in the temperature and salinity of the upper ocean have resulted in changes in the properties of major water masses in each of the ocean basins. Overall, in many regions of the ocean, there has been a tendency towards an increase in the stratification of the upper ocean, and a decline in ventilation, consistent with the observed tendency for declining oxygen in much of the upper ocean. Many of the water mass changes are broadly consistent with those expected from a warming climate and an enhanced hydrological cycle. For example, the intermediate depth salinity minimum waters in both hemispheres (AAIW, NPIW) have warmed, freshened, and shifted to lighter densities over the last forty years. However, the presence of energetic interannual to multi-decadal variability driven by climate modes like the El Nino – Southern Oscillation (ENSO), the North Atlantic Oscillation (NAO) and the SAM makes it difficult to detect significant trends from the short and incomplete observational record.

Recent observations have strengthened evidence for variability in major ocean circulation systems on time scales from years to decades. Much of the variability observed in ocean currents can be linked to changes in wind forcing, including changes in winds associated with the modes of climate variability. Given the short duration of direct measurements of ocean circulation, it is not possible to distinguish multi-decadal trends from decadal variability.

Global mean sea level (GMSL) has been rising since 1900 at a rate of 1.7 ± 0.2 mm yr^{-1} (90% confidence). Changes over periods from ten to twenty years can be several times larger than this in some regions, driven by changes in large-scale winds and ocean circulation. There is growing evidence that the rate of GMSL rise since 1990 is higher than in any comparable period since 1950. Thermal contributions to sea level change can be estimated reliably since 1970 and show the upper 700 m has been contributing 0.6 ± 0.2 mm yr^{-1} of sea level change. Warming below 1000 m is likely contributing another 0.14 ± 0.08 mm yr^{-1} of sea level rise, at least since the early 1990s. The two major components of sea level change (upper ocean warming and ocean mass change) can now be measured, but reliable estimates are only available since 2005. These recent observations indicate that the sea level budget can close, so with continued measurements of sea level rise and its components, one should be able to better quantify and attribute sea level change in the future. A rise in mean sea level is largely responsible for an increase in extreme sea level events and stronger storm surges in coastal areas.

The biogeochemical state of the ocean has changed. Three different methods to estimate the inventory of anthropogenic carbon dioxide (C_{ant}) agree within the uncertainties of each approach (±26 PgC) and provide high confidence that the ocean inventory of C_{ant} has increased, from 114 ± 22 PgC in 1994 to 151 ± 26 PgC in 2010. The marginal seas contribute an additional 6% to the global inventory. In general, observations of C_{ant} inventory changes are in broad agreement with the expected change resulting from the increase in atmospheric CO_2 concentrations and change in atmospheric O_2/N_2 ratios.

The uptake of CO_2 by the ocean has resulted in a gradual acidification of seawater. Long time series from several ocean sites show declines in pH in the mixed layer between -0.0015 and -0.0024 yr^{-1}, consistent with results from repeat pH measurements on ship transects spanning much of the globe. It is virtually certain that the pH decline in the surface ocean is solely attributable to the uptake of anthropogenic CO_2. In the ocean interior, pH can also be modified by natural physical and biological processes over decadal time scales.

Taken together, the observations summarized in this chapter provide strong evidence that the physical and biogeochemical state of the oceans has changed during the past forty years. The consistency of the observed patterns of change with known physical and chemical processes in the ocean enhances the level of confidence associated with this conclusion.

3.1 Introduction

The oceans influence climate by storing and transporting vast quantities of heat, freshwater, and carbon. The ocean has a large thermal inertia, both because of the large heat capacity of sea water relative to air and because ocean circulation connects the surface and interior ocean. More than three quarters of the total exchange of water between the atmosphere and the earth's surface through evaporation and precipitation takes place over the oceans. The ocean contains 60 times more carbon than the atmosphere and is at present absorbing 25% of human emissions of carbon dioxide, acting to slow the rate of climate change. It further slows the rate of climate change by taking up large amounts of heat. The ocean is also capable of relatively rapid change, with the potential for climate feedbacks. The evolution of climate on time-scales from weeks to millennia is therefore closely linked to the ocean.

The large inertia of the oceans means that they naturally integrate over short-term variability and often provide a clearer signal of longer-term change than other components of the climate system. Observations of ocean change therefore provide a means to track the evolution of climate change. Such observations also provide a rigorous and relevant test for climate models.

Documenting and understanding change in the ocean remains a challenge because of the paucity of long-term measurements of the global ocean. Despite the limited records, AR4 reported trends in ocean heat content, sea level, regional patterns of salinity, and biogeochemical parameters. The historical data sets at the heart of these conclusions are now being extended with much more comprehensive global observations. The Argo array of profiling floats is now providing year-round measurements of temperature and salinity in the upper 2000 m for the first time. The satellite altimetry record is now approaching twenty years in length. Longer continuous time series of important components of the meridional overturning circulation are being collected. While these recent data sets do not solve the problem of a lack of historical data, by documenting the seasonal and interannual variability they help estimate longer-term trends and their uncertainties from the incomplete observational record. Significant progress has also been made in removing biases and errors in the historical measurements. The spatial and temporal coverage of biogeochemical measurements in the ocean has expanded. As a result of these advances, there is now stronger evidence for change in the ocean and our understanding of the causes of ocean change is improved.

This chapter summarizes the observational evidence of change in the ocean, with an emphasis on basin- and global-scale changes relevant to climate.

3.2 Changes in Ocean Temperature and Heat Content

3.2.1 Background: Instruments and Sampling

While temperature is the most often measured subsurface ocean parameter, these measurements were generally not designed to assess long-term changes. Historically, a variety of instruments have been used, with different accuracies, sampling depths, and precision. Both the mix of instruments and the overall sampling patterns have changed in time and space (Boyer et al., 2009), complicating efforts to determine and interpret long-term change. Since AR4 the significant impact of measurement biases in some of these instruments (the XBT and MBT) on estimates of ocean temperature changes and upper ocean heat content anomalies (hereafter UOHCA) has been recognized (Gouretski and Koltermann, 2007). Careful comparison of measurements from the less accurate instruments with those from the more accurate ones has allowed some of the biases to be identified and mitigated (Gouretski and Reseghetti, 2010; Ishii and Kimoto, 2009; Levitus et al., 2009; Wijffels et al., 2008). One major consequence of this bias mitigation has been the reduction of an artificial decadal variation in upper ocean heat storage that was apparent in the observational assessment for AR4, in notable contrast to climate model output.

Upper ocean temperatures (hence heat content anomalies) vary significantly over multiple time-scales ranging from seasonal (e.g., Roemmich and Gilson, 2009) to decadal (e.g., Carson and Harrison, 2010). Given the close relation between ocean warming and sea level rise, together with the evidence of decadal and longer time-scale variability in global sea level rise (see 3.7), upper ocean heat content likely also varies on these longer time-scales.

The large amplitude of variations on shorter time and spatial scales might make estimating globally averaged temperature changes difficult in light of sparse historical sampling patterns. However, at least an error analysis that subsamples the recently well-resolved satellite record of SSH (and exploits its relation to UOHCA) indicates that the historical data set begins to be reasonably well suited for this purpose starting around 1967 (Lyman and Johnson, 2008). Error estimates in another UOHCA study (Domingues et al., 2008), with uncertainties that shrink as sampling improves around 1970, support this conclusion, so this assessment focuses on changes since 1970.

3.2.2 Upper Ocean Temperature

Recent estimates of upper ocean temperature change (Gouretski and Reseghetti, 2010; Ishii and Kimoto, 2009; Levitus et al., 2009; Lyman et al., 2010) differ from one another in their corrections for measurement biases noted above, but also in their treatment of unsampled regions. Those based on optimal interpolation (e.g., Ishii and Kimoto, 2009; Levitus et al., 2009) assume no temperature anomaly in unsampled regions, while other studies (Lyman and Johnson, 2008) assume that the averages of sampled regions are representative of the global mean in any given year, and others (e.g., Domingues et al., 2008) use ocean statistics (from satellite altimeter data) to extrapolate anomalies to sparsely sampled areas and estimate uncertainties. These differences in approach can lead to significant divergence in areal averages in sparsely sampled regions (e.g., the extra-tropical Southern Hemisphere prior to Argo). For well-sampled regions and times, the various analyses of temperature changes yield similar results.

Zonally averaged upper ocean temperature trends from 1970–2009 show warming at nearly all latitudes and depths (Figure 3.1a), with the exception of four small bands of cooling. Although the warming is more prominent in the northern hemisphere, the greater volume of the southern ocean increases the contribution of its warming to global heat content. A maximum in warming at 70–30°S is present but not as strong as in other analyses (Gille, 2008), likely because the data are relatively sparse in this location. Another maximum is present at 25–65°N. Both extend to 700 m (Levitus et al., 2009, Figure 3.1a). The warming is broadly consistent with poleward displacement of the mean temperature field. The warming observed in the upper Southern Ocean is thought to be at least partly owing to southward shifts of the Antarctic Circumpolar current that are in turn largely driven by southward migration and intensification of the westerly winds related to SAM (Böning et al., 2008; Gille, 2008; Sokolov and Rintoul, 2009). Other zonally-averaged temperature changes, for example cooling between 30°S and the equator (Figure 3.1a), are also consistent with poleward displacement of the mean field. That is, where the mean temperature field cools toward the pole, a poleward displacement would cause warming, and vice versa.

Globally averaged ocean temperature anomalies as a function of depth and time (Figure 3.1b) reveal warming at all depths in the upper 700 m over the relatively well-sampled 40-year time-period considered. Strongest warming is found closest to the sea surface, and the near-surface record is consistent with independently measured sea surface temperature (Chapter 2). The global average warming over this period exceeds 0.1°C per decade in the upper 75 m, decreasing to 0.017°C per decade by 700 m (Figure 3.1b).

The surface intensification of the warming signal means that the thermal stratification of the upper ocean has increased. A time-series of globally averaged temperature difference from 0 to 200 m (Figure 3.1c) shows thermal stratification has increased by about 4% over the 40-year record. An increase in thermal stratification is widespread in all the oceans, except the Southern Ocean south of about 40°S, based on the Levitus et al. (2009) temperature anomaly fields.

[INSERT FIGURE 3.1 HERE]

Figure 3.1: a) Zonally-averaged temperature trends (latitude versus depth, colors in °C per decade) for 1970–2009, with zonally averaged mean temperature over-plotted (black contours in °C). **b)** Globally-averaged temperature anomaly (time versus depth, colors in °C). **c)** Globally-averaged temperature difference between the ocean surface and 200-m depth (black: annual values, red: 5-year running mean). All plots are constructed from the optimal interpolation analysis of Levitus et al. (2009).

A potentially important impact of ocean warming is the effect on sea ice, floating glacial ice, and ice sheet dynamics (see Chapter 4). Warm ocean waters have been linked to increased melt of outlet glaciers in both Greenland (Holland et al., 2008; Straneo et al., 2010) and Antarctica (Jacobs et al., 2011; Rignot et al., 2008;

Shepherd et al., 2004; Wahlin et al., 2010). In the Arctic Ocean, subsurface pulses of relatively warm water of Atlantic origin can be traced around the Eurasian Basin from 2003–2005 (Dmitrenko et al., 2008), their warmth intensifying further through 2007 (Polyakov et al., 2010). This warming Atlantic Water has also shoaled, by 75–90 m, in the water column, and model results suggest that it might affect melting of sea ice (Polyakov et al., 2010). Arctic surface waters have warmed, likely from changes in albedo from 1993 to 2007 due to the sea ice melt, which may be driving further reductions in sea ice (Jackson et al., 2010).

3.2.3 Upper Ocean Heat Content

Global UOHCAs have been estimated from ocean temperature measurements starting in the 1950s (e.g., Domingues et al., 2008; Ishii and Kimoto, 2009; Levitus et al., 2009). Data used in AR4 included substantial XBT and MBT instrument biases that introduced a spurious warming in the 1970s and cooling in the early 1980s. More recent analyses based on corrected data show more monotonic, and larger increases in UOHCA since 1970 (Figure 3.2). Ocean state estimates that assimilated partially corrected data also showed this artificial decadal variability (Carton and Santorelli, 2008), while more recent estimates assimilating better corrected data sets result in reduced decadal variability (Giese et al., 2011). With increasing convergence on instrument bias correction since AR4, the next largest sources of error are the different assumptions regarding UOHCAs for sparsely sampled regions (Lyman et al., 2010). For the time period 1969 to 2003, linear trends of 24×10^{21} J decade^{-1} (Ishii and Kimoto, 2009), 32×10^{21} J decade^{-1} (Levitus et al., 2009), and 41×10^{21} J decade^{-1} (Domingues et al., 2008) were reported. For the time period 1970 to 2009, differences between two estimates using different methods of estimating temperature anomalies in sparsely sampled regions give an indication of the remaining instrument bias correction, data quality control, and mapping uncertainties (Figure 3.2). Although there are still apparent interannual variations about the upward trend of global UOHCA, different global estimates have variations at different times and for different periods, suggesting that sub-decadal variability in the time rate of change is still quite uncertain in the historical record.

Both of the estimates in Figure 3.2 show that upper ocean heat content has increased from 1970 to the present. Fitting linear trends to UOHCA estimates for the relatively well-sampled period from 1970–2009 yields a power of 117 (±96) TW (10^{12} W) for an analysis mapped with optimal interpolation (Levitus et al., 2009), and 133 (±21) TW for one mapped using spatial functions estimated from recent data (Domingues et al., 2008). Uncertainties are calculated as 95% confidence intervals for an ordinary least squares fit, taking into account the reduction in the degrees of freedom implied by the temporal correlation of the residuals. The rates of energy gain agree within their uncertainties, both are positive, and both are different from zero at 95% confidence.

[INSERT FIGURE 3.2 HERE]

Figure 3.2: Observation-based estimates of annual global mean ocean heat content anomaly in ZJ (10^{21} J) from 0–700 m from Levitus et al. (2009) (green line) and Domingues et al. (2008) (orange line) with one standard error uncertainty estimates (shading). The error estimates of Levitus et al. (2009) are simply the standard deviation of four seasonal estimates for each year, and do not reflect the full uncertainty, whereas the larger error estimates of Domingues et al. (2008) reflect data distributions and ocean statistics. The curves are plotted relative to their 1970 values.

3.2.4 Deep Ocean Temperature and Heat Content

As noted in AR4, warming over multi-decadal time-scales extends below 700 m (Levitus et al., 2005). Below 700 m the data coverage is too sparse to produce annual global heat content anomalies. Global sampling of the ocean below 2000 m is limited to a number of repeat oceanographic transects, many occupied only in the last few decades, and several time-series stations, some of which extend over decades. This sparse sampling in space and time makes assessment of global deep ocean heat content variability less certain than that for the upper ocean, especially at mid-depths, where vertical gradients are still sufficiently large for transient variations (ocean eddies, internal waves, and internal tides) to alias estimates made from sparse data sets. Nevertheless, there is sufficient information to conclude that the warming of the global ocean from circa 1992–2005 is probably not distinguishable from zero from about 2000–3000 m, but is greater than zero below that depth (Figure 3.3a).

[INSERT FIGURE 3.3 HERE]

Figure 3.3: a) Areal mean warming rates versus depth (thick lines) with 95% confidence limits (shading), both global (orange) and for the Southern Ocean south of the Sub-Antarctic Front SAF (purple). **b)** Mean warming rate below 4000 m (colorbar) estimated for deep ocean basins (thin black outlines) and centred on 1992–2005. Stippled basin warming rates are not significantly different from zero at 95% confidence. The mean warming rate for 1000–4000 m south of the SAF (purple line) is also given (purple number) with its 95% confidence interval. Data from Purkey and Johnson (2010).

In the Southern Ocean, much of the water column warmed between 1992 and 2005 (Purkey and Johnson, 2010). The warming is largest near the sea floor (i.e., below 4000 m), which is ventilated by sinking of Antarctic Bottom Water (AABW) around Antarctica (Orsi et al., 1999). The rate of warming is largest in basins that are effectively ventilated by AABW, and attenuates towards the north (Figure 3.3b). The warming of the global abyssal ocean below 4000 m depth and the Southern Ocean below 1000 m combined amount to a heating rate of 48 (±32) TW, centred on 1992–2005 (Purkey and Johnson, 2010). Their 95% uncertainty estimates may be too small, especially in the shallower portions of the ocean, since they assume the usually sparse sampling in each deep ocean basin analyzed is representative of the mean trend in that basin. Global scale abyssal warming on relatively short multi-decadal time-scales is possible because of teleconnections established by planetary waves originating within the Southern Ocean, reaching even such remote regions as the North Pacific (Masuda et al., 2010).

In the North Atlantic, strong decadal variability in NADW temperature and salinity, largely associated with the North Atlantic Oscillation (NAO) (e.g., Yashayaev, 2007), complicates efforts to determine long-term trends from the relatively short record. In addition, there is longer multi-decadal variability in the North Atlantic Ocean heat content (e.g., Polyakov et al., 2010).

3.2.5 Conclusion

It is virtually certain that the upper ocean has warmed since circa 1970, with the warming strongest near the sea surface. This result is supported by three independent and consistent methods of observation including (i) the subsurface measurements of temperature described here, (ii) sea surface temperature data (Section 2.2.2) from satellites and in situ measurements from surface drifters and ships, and (iii) the record of sea level rise, which is known to include a substantial component due to thermosteric expansion (Section 3.7 and Chapter 13). The greatest remaining uncertainty in the upper ocean temperature evolution is in the magnitude and pattern of warming at high southern latitudes. For the deep ocean, sparse sampling below 2000 m is the greatest obstacle. Strongest warming is found closest to the sea surface (>0.1°C per decade in the upper 75 m), decreasing to about 0.017°C per decade by 700 m. The surface intensification of the warming signal increases the thermal stratification of the upper ocean by about 4% (between 0 and 200 m depth) over the 43-year record. It is likely that global ocean warming reaches a minimum at mid-depth (roughly 2500 m) and increases below that. It is very likely that waters of Antarctic origin have warmed overall throughout the water column in the Southern Ocean at a rate of about 0.03°C per decade, and below 4000 m since circa 1990 at a global average rate of < 0.01°C per decade.

[START BOX 3.1 HERE]

Box 3.1: Change in Global Energy Inventory

Earth has been in radiative imbalance, with more energy entering than exiting the top of the atmosphere, for some decades (Murphy et al., 2009). Small amounts of this excess energy warm the atmosphere and continents, evaporate water, and melt ice, but the bulk of it warms the oceans (Box 3.1, Figure 1). The ocean dominates the change in energy because of its large mass and high heat capacity compared to the atmosphere. Also, as a fluid, the oceans can transfer heat rapidly by ocean currents and turbulence, in contrast to the continents and ice. In addition, the oceans also have a very low albedo and effectively absorb solar radiation.

[INSERT BOX 3.1, FIGURE 1 HERE]

Box 3.1, Figure 1: Plot of energy change inventory in ZJ (10^{21} J) within distinct components of Earth's climate system relative to and starting from 1970 unless otherwise indicated. The combined upper and deep ocean warming (dark purple) dominates; ice melt (light purple; for glaciers and ice caps, Greenland starting from 1992, Antarctica starting from 1992, and Arctic sea ice starting from 1979); continental warming (orange); and atmospheric warming (red; starting from 1979) make smaller contributions. The ocean uncertainty also dominates the total uncertainty (dotted lines about the sum of all four components).

The global atmospheric energy change inventory accounting for specific heating and water evaporation is estimated by combining satellite estimates from 80°S to 80°N of lower tropospheric (Mears and Wentz, 2009b) and lower stratospheric (Mears and Wentz, 2009a) temperature anomalies by the ratio of the portions of atmospheric mass they sample (0.88 and 0.12, respectively). These temperature anomalies are converted to energy changes using a total atmospheric mass of 5.14×10^{21} g, a mean total water vapor mass of 1.27×10^{19} g (Trenberth and Smith, 2005), a heat capacity of 1 J g^{-1} $°C^{-1}$, a latent heat of vaporization of 2,464 J g^{-1}, and a fractional increase of integrated water vapor content of 0.075 $°C^{-1}$ (Held and Soden, 2006). Smaller changes in potential and kinetic energy are neglected here. Standard deviations for each year of data are used for uncertainties, and the time-series starts in 1979.

A global average rate of continental warming and its uncertainty has been estimated from borehole temperature profiles from 1500–2000 at 50-yr intervals (Beltrami et al., 2002). The 1950–2000 estimate is extended into the first decade of the 21st century, although that extrapolation is almost certainly an underestimate of the energy absorbed as land surface temperatures for years since 2000 are some of the warmest on record (Section 2.2.1).

All annual ice melt rates (for glaciers and ice-caps, ice sheets, and sea ice from Chapter 4) are converted into energy change using a heat of fusion (334×10^3 J kg^{-1}) and density (920 kg m^{-3}) for freshwater ice. Warming of the ice from sub-freezing temperatures takes fractionally more energy, and the heat of fusion and density of ice may vary slightly among the different ice types, but these second order effects are neglected here.

For the oceans an estimate of global upper (0–700 m depth) ocean heat content change using ocean statistics to extrapolate to sparsely sampled regions and estimate uncertainties (Domingues et al., 2008) is used, starting in 1970 (see Section 3.2). For the deep ocean a uniform rate of energy gain 20 (±22) TW (10^{12} W) is used for 1970–1991 from a linear fit to annual values of the global mean ocean heat gain for 700–3000 m depth (Levitus et al., 2005). The uncertainty assumes the value for each year is independent. For the deep ocean from 1992–2009 the uniform rate of energy gain of 49 (±34) TW represents the sum of average deep (1000–2000 m) Southern Ocean and deeper global ocean (2000 m to the bottom) warming rates centred on 1992–2005 (Purkey and Johnson, 2010), extrapolated through 2009.

There is unequivocal evidence that Earth has gained substantial energy from 1970–2009 — an estimated first-difference change of 219 (±50) ZJ (10^{21} J), with a rate of 180 TW (10^{12} W) from a linear fit over that time period (Box 3.1, Figure 1). From 1993–2009 the estimated energy gain is 100 (±42) ZJ (10^{21} J) with a rate of 176 TW. Ocean warming dominates the total energy change inventory, accounting for an estimated 90–93% on average from 1970–2009. Melting ice (including Arctic sea ice, ice sheets, and glaciers) accounts for 4% of the total, and warming of the continents 3–4%. Warming of the atmosphere makes up the remaining 0–1%. The ocean component of the 1993–2009 rate of energy gain is 156 TW, equivalent to a global mean net air-sea heat flux of 0.43 W m^{-2}, and that for 1970–2009 is 165 TW, implying a mean net air-sea heat flux of 0.46 W m^{-2}.

[END BOX 3.1 HERE]

3.3 Changes in the Salinity and Freshwater Budget

3.3.1 Introduction

The ocean plays a pivotal role in the global water cycle: 86 % of the evaporation and 78 % of the precipitation occurs over the ocean (Schmitt, 2008). The salinity of the surface ocean largely reflects this exchange of freshwater, with high surface salinity generally found in regions where evaporation exceeds precipitation, and low salinity found in regions of excess precipitation. Ocean circulation also affects the regional distribution of surface salinity. The subduction of surface waters transfers the surface salinity signal into the ocean interior, so that subsurface salinity distributions are also linked to patterns of evaporation, precipitation, and continental run-off at the sea surface. At high latitudes, melting and freezing of ice (both sea ice and glacial ice) can also influence salinity.

The water cycle is expected to intensify in a warmer climate, because warm air can contain more moisture. The dominant effect is due to the Clausius – Clapeyron relation: water vapour pressure increases by about 7% per degree C (at the current global average temperature of about 14°C), with substantialy smaller increases in global precipitation per unit warming expected because of feedbacks and atmospheric dynamics (e.g., Held and Soden, 2006; Wentz et al., 2007) (Section 12.4.3). The water vapour content of the atmosphere has increased since the 1970s, at a rate consistent with the observed warming (Section 2.3). However, observations of precipitation and evaporation are sparse and uncertain, particularly over the ocean where most of the exchange of moisture occurs. The uncertainties in some of the individual terms are so large that it is not yet possible to detect robust trends in the water cycle from these observations (Section 3.4). Ocean salinity, on the other hand, naturally integrates the small difference between these two terms and has the potential to act as a rain gauge (Yu, 2011). Diagnosis and understanding of ocean salinity trends is also important because salinity changes affect circulation and stratification, and therefore the ocean's capacity to store heat and carbon as well as biological productivity.

In AR4, surface and subsurface salinity changes consistent with a warmer climate were highlighted, based on linear trends over 50 years in the historical global salinity data set (Boyer et al., 2005) as well as on more regional studies. Additional observations, improvements in the availability and quality of historical data, and new analysis approaches now allow a more complete assessment of changes in salinity.

3.3.2 Global to Basin-Scale Trends

The salinity of near-surface waters is changing on global and basin scales, with increase in the more evaporative regions and decrease in the precipitation-dominant regions in almost all ocean basins. All salinity values quoted in the chapter are expressed on the Practical Salinity Scale 1978 and are unit-less.

3.3.2.1 Sea Surface Salinity

Robust and consistent multi-decadal trends in sea surface salinity have been found in studies published since AR4 (Boyer et al., 2007; Durack and Wijffels, 2010; Hosoda et al., 2009; Roemmich and Gilson, 2009), confirming the trends reported in AR4 based mainly on Boyer et al. (2005). The spatial pattern of surface salinity change is similar to the distribution of surface salinity itself: salinity tends to increase in regions of high mean salinity, where evaporation exceeds precipitation, and tends to decrease in regions of low mean salinity, where precipitation dominates (Figure 3.4). For example, the surface salinity maxima formed in the evaporation-dominated subtropical gyres have increased in salinity. The surface salinity minima at subpolar latitudes and the intertropical convergence zones have freshened. Interbasin salinity differences are also enhanced: the relatively salty Atlantic has become more saline on average, while the relatively fresh Pacific has become fresher (Durack and Wijffels, 2010). The exception is the subpolar North Atlantic (Hosoda et al., 2009), which is dominated by decadal variability from atmospheric modes like the NAO. Fifty-year salinity trends are statistically significant at the 99% level over 43.8% of the global ocean surface (Durack and Wijffels, 2010).

[INSERT FIGURE 3.4 HERE]

Figure 3.4: a) The 1950–2000 climatological-mean surface salinity. Contours every 0.5 are plotted in black. **b)** The 50-year linear surface salinity trend [(50 year)$^{-1}$]. Contours every 0.2 are plotted in white. Regions where the resolved linear trend is not significant at the 99% confidence level are stippled in grey. Composite of Durack and Wijffels (2010) and Hosoda et al. (2009).

3.3.2.2 Upper Ocean Salinity

Changes in surface salinity are transferred into the ocean interior by subduction and flow along ventilation pathways. Consistent with observed changes in surface salinity, robust multi-decadal trends in subsurface salinity have been detected (Böning et al., 2008; Boyer et al., 2005; Durack and Wijffels, 2010; Helm et al., 2010; Wang et al., 2010). Global zonally-averaged 50-year salinity changes on pressure surfaces in the upper 2000 m show increases in salinity in the salinity maxima in the upper thermocline of the subtropical gyres, freshening of the low salinity intermediate waters sinking in the Southern Ocean (Subantarctic Mode Water abd Antarctic Intermediate Water) and North Pacific, (North Pacific Intermediate Water) (Durack and Wijffels, 2010; Helm et al., 2010), and freshening of the shallow freshwater pool near the equator (see Section 3.5).

Change in subsurface salinity at a given location and depth may reflect water-mass changes driven by changes in surface fluxes or the movement of water-masses (e.g., due to wind-driven changes in ocean circulation). Analysis of property changes in the ocean interior on surfaces of constant pressure and surfaces of constant density allows changes in water mass properties to be distinguished from vertical or lateral displacement of isopycnals (Bindoff and McDougall, 1994). Both processes are found to contribute to changes in subsurface salinity (Durack and Wijffels, 2010). Density layers that are ventilated in precipitation-dominated regions are observed to freshen, while those ventilated in evaporation-dominated regions have increased in salinity, consistent with an enhancement of the mean surface freshwater flux pattern (Helm et al., 2010). In addition, warming of the upper ocean has caused a generally poleward shift of isopycnals. The observed pattern of change in subsurface salinity is also consistent with subduction and ventilation along isopycnal outcrops migrating through the mean surface salinity field: salinity has increased on layers that have moved to regions of higher mean salinity, and decreased along layers that have moved into regions of lower mean salinity (Durack and Wijffels, 2010). A quantitative assessment of the relative contribution of changes in freshwater fluxes and migration of isopycnal outcrops to the observed change in salinity has not yet been made.

3.3.3 Regional Changes in Salinity

Regional changes in ocean salinity reinforce the conclusion that regions where precipitation dominates evaporation have generally become wetter, while regions of net evaporation have become drier. In the high-latitude regions, higher runoff, increased melting of ice, and changes in freshwater transport by ocean currents have likely also contributed to observed salinity changes (Bersch et al., 2007; Jacobs and Giulivi, 2010; Polyakov et al., 2008).

3.3.3.1 Pacific and Indian Oceans

In the tropical Pacific, surface salinity has declined in the precipitation-dominated western equatorial regions and in the South Pacific Convergence Zone by 0.1 to 0.3 in 50 years, while surface salinity has increased in the evaporation-dominated zones in the southeastern and north-central tropical Pacific (Cravatte et al., 2009). The fresh, low density waters in the warm pool of the western equatorial Pacific have expanded in area as the surface salinity front has migrated eastward by 1500–2500 km in 50 years (Cravatte et al., 2009; Delcroix et al., 2007). Similarly, in the Indian Ocean, the net precipitation regions in the Bay of Bengal and the warm pool contiguous with the tropical Pacific warm pool have been freshening, while the saline Arabian Sea and south Indian Ocean have been getting saltier (Durack and Wijffels, 2010).

In the North Pacific, the subtropical thermocline has freshened by 0.1 since the early 1990s, following surface freshening that began around 1984 (Ren and Riser, 2010); the freshening extends down through the intermediate water that is formed in the northwest Pacific (Nakano et al., 2007), continuing the freshening documented by Wong et al. (1999). Warming of the sutface water that subduct to supply the intermediate water is one reason for this signal, as the fresh water from the subpolar North Pacific now enters the subtropical thermocline at lower density.

3.3.3.2 North Atlantic

The net evaporative North Atlantic has become saltier as a whole over the past 50 years (Boyer et al., 2007; Durack and Wijffels, 2010). The maximum increase in the upper 700m of 0.006 per decade (between 1955 and 1959 and 2002 and 2006) occurred in the Gulf Stream region (Wang et al., 2010). During the same time period, the upper 700m of the subpolar North Atlantic freshened by up to 0.002 per decade (Wang et al., 2010), while an increase in surface salinity was found between the periods 1960–89 and 2003–07 (Hosoda et al., 2009). Decadal and multi-decadal variability in the subpolar gyre and Nordic Seas is vigorous and has been related to various climate modes such as the NAO, the Atlantic multidecadal oscillation (AMO), and even ENSO (Polyakov et al., 2005; Yashayaev and Loder, 2009), obscuring long-term trends. The 1970s–

1990s freshening of the northern North Atlantic and Nordic Seas (Curry and Mauritzen, 2005; Curry et al., 2003; Dickson et al., 2002) reversed to salinification (0–2000m depth) starting in the late 1990s (Boyer et al., 2007; Holliday et al., 2008), and the propagation of this signal could be followed along the eastern boundary from the Northeast Atlantic south of 60°N to Fram Strait at 89°N (Holliday et al., 2008). Advection has also played a role in moving higher salinity subtropical waters to the subpolar gyre (Bersch et al., 2007; Hatun et al., 2005; Lozier and Stewart, 2008). The variability of the cross equatorial transport contribution to this budget is highly uncertain. Reversals of surface salinity of similar amplitude and duration than in the last 50 years are apparent in the early 20th century (Reverdin, 2010; Reverdin et al., 2002).

3.3.3.3 Arctic Ocean

Freshwater in the form of sea ice in the Arctic has declined significantly in recent decades (Kwok et al., 2009), but lack of historical observations makes it difficult to assess long-term trends in ocean salinity for the Arctic as a whole (Rawlins et al., 2010). Over the 20th century (1920–2003) the central Arctic Ocean became increasingly salty in the upper 150m with a rate of freshwater loss of 239±270 km^3 per decade, while the Siberian Shelf became fresher (Polyakov et al., 2008). Both trends are modulated by strong multidecadal variability. For instance, the central Arctic Ocean freshened between the periods 1992–1999 and 2006–2008 (Rabe et al., 2011). Ice production and sustained draining of freshwater from the Arctic Ocean in response to winds are suggested as key contributors to the salinification of the upper Arctic Ocean over recent decades (Polyakov et al., 2008).

Over the Siberian shelf where river discharge has increased (Shiklomanov and Lammers, 2009), long-term (1920–2003) freshwater content trends show a general freshening tendency with a rate of 29±50 km^3 per decade (Polyakov et al., 2008). Upper ocean freshening has also been observed regionally in the southern Canada basin from 1950–1980s to 1990–2000s (Proshutinsky et al., 2009; Yamamoto-Kawai et al., 2009), while the salinity of the upper ocean has increased in the Eurasian basin (McPhee et al., 2009). The contrasting changes in different regions of the Arctic have been attributed to the effects of Ekman transport and sea ice formation and melt.

3.3.3.4 Southern Ocean

Widespread freshening (trend of -0.01 per decade, significant at 95% confidence) of the upper 1000 m of the Southern Ocean was inferred by taking differences between modern data (mostly Argo) and a long-term climatology along mean streamlines (Böning et al., 2008). Both a southward shift of the Antarctic Circumpolar Current and water-mass changes contribute to the observed trends (Meijers et al., 2011). Increased inflow of glacial meltwater linked to ocean warming is likely responsible (Jacobs et al., 2011; Rignot et al., 2008; Shepherd et al., 2004) for the freshening between 1958 and 2008 (Jacobs and Giulivi, 2010) of High Salinity Shelf Water (one of the components of AABW) in the Ross Sea. AABW freshening is discussed in Section 3.5.4.

3.3.4 Evidence for Change of the Global Water Cycle from Salinity

The large scale spatial pattern of the changes in salinity observed at the sea surface is consistent with the hypothesis that the water cycle is intensifying as the planet warms. The striking similarity between the salinity trends and both the mean salinity pattern and the distribution of evaporation – precipitation (Figure 3.4) suggests the global hydrological cycle has been enhanced, as anticipated from thermodynamics and projected by climate models. Surface salinity differences between the Atlantic and Pacific has increased by about 2% per decade over the last 50 years (Durack and Wijffels, 2010). A similar conclusion was reached in AR4 (Bindoff et al., 2007). The more recent studies, based on expanded data sets and new analyses approaches, have substantially increased the level of confidence in the inferred change in the global water cycle (e.g., Durack and Wijffels, 2010; Helm et al., 2010; Hosoda et al., 2009; Roemmich and Gilson, 2009; Stott et al., 2008), (Figure 3.5).

[INSERT FIGURE 3.5 HERE]

Figure 3.5: Zonally integrated freshwater content changes (km^3 per degree of latitude) for the latter half of the 20th century in the upper 500 m over the one-degree zonal belt of the World Ocean (upper panel), and Atlantic, Pacific, and Indian Oceans (lower panel). The time period is from the late 1950s to 2000s (Boyer et al., 2005; solid lines) and 1950–

2000 (Durack and Wijffels, 2010; broken lines). Calculations are done according to the method of Boyer et al. (2007). Error estimates are 90% confidence intervals.

3.3.5 Conclusion

Robust changes in ocean salinity have been observed throughout much of the ocean, both at the sea surface and in the ocean interior. Over the last fifty years, the mean regional pattern of sea surface salinity has been enhanced: saline surface waters in the evaporation-dominated mid-latitudes have become more saline, while the relatively fresh surface waters in rainfall-dominated tropical and polar regions have become fresher. Similarly, the interbasin contrast between saline Atlantic and fresh Pacific surface waters has increased. These changes are consistent with an intensification of the water cycle as the lower atmosphere has warmed, reflecting the expected and observed increased water vapour content of the warmer air (Section 2.3).

Changes in salinity have been observed in the ocean interior as well. Both, the subduction of surface water mass anomalies and the movement of density surfaces have contributed to the salinity changes on observed depth levels. Changes in freshwater flux and the migration of surface density outcrops caused by surface warming (e.g., to regions of lower or higher surface salinity) have likely both contributed to the formation of salinity anomalies on density surfaces.

3.4 Changes in Ocean Surface Fluxes

3.4.1 Introduction

Exchanges of heat, water and momentum (wind stress) at the sea surface are important factors for driving the ocean circulation. Changes in air-sea fluxes may result from variations in the driving surface meteorological state variables (air temperature and humidity, wind speed, cloud cover, precipitation, SST) and can impact both water-mass formation rates and ocean circulation. Air-sea fluxes also influence temperature and humidity in the atmosphere and, therefore, the hydrological cycle and atmospheric circulation. Any anthropogenic climate change signal in surface fluxes is expected to be small compared to their natural variability and associated uncertainties. AR4 concluded that, at the global scale, the accuracy of the observations is insufficient to permit a direct assessment of anthropogenic changes in surface fluxes. As described below, while substantial progress has been made since AR4, that conclusion still holds for this assessment.

The net air-sea heat flux is the sum of two turbulent (latent and sensible) and two radiative (shortwave and longwave) components; we adopt a sign convention in which ocean heat gain from the atmosphere is positive. The latent and sensible heat fluxes are computed from the state variables using bulk parameterizations; they primarily depend on the products of wind speed and the vertical near-sea-surface gradients of humidity and temperature respectively. The air-sea freshwater flux is the difference of precipitation (P) and evaporation (E). It is linked to heat flux through the relationship between evaporation and latent heat flux. Thus, when considering potential trends in the global hydrological cycle, consistency between observed heat budget and evaporation changes is required in areas where evaporation is the dominant term in hydrological cycle changes. Ocean surface shortwave and longwave radiative fluxes can be inferred from satellite measurements using radiative transfer models, or computed using empirical formulae, involving astronomical parameters, atmospheric humidity, cloud cover and SST. The wind stress is given by the product of the wind speed squared and the drag coefficient. For detailed discussion of all terms see for example Gulev et al. (2010) and Josey (2011).

3.4.2 Air-Sea Heat Flux

3.4.2.1 Turbulent Heat Fluxes and Evaporation

Latent and sensible heat fluxes show strong regional variations (with annual mean heat loss ranging from close to zero to near -250 W m^{-2}) and have pronounced seasonal cycles. Estimates of these terms have many potential sources of error (e.g., sampling issues, instrument biases, uncertainty in the flux computation algorithms) which are difficult to quantify and strongly spatially variable (Gulev et al., 2007). The overall uncertainty of each term is likely in the range 10–20 % for the annual mean global value. In the case of the larger latent heat flux term, this corresponds to an uncertainty of up to 20 W m^{-2} (note the sensible heat flux is an order of magnitude smaller than the latent in the global annual mean). Spurious temporal trends may also arise, in particular as a result of variations in instrument type. In comparison, changes in global mean values of individual heat flux components expected as a result of anthropogenic climate change are at the level of < 2 W m^{-2} over the past 50 years (Pierce et al., 2006).

Many new turbulent heat flux datasets have become available since AR4 including products based on atmospheric reanalyses, satellite and in situ observations, and hybrid datasets that combine information from these three different sources (Gulev et al., 2010). It is not possible to identify a single best product as each has its own strengths and weaknesses; several are highlighted here, for a full discussion see the review of Gulev et al. (2010). The Hamburg Ocean Atmosphere Parameters and Fluxes from Satellite Data product (Andersson et al., 2011) provides turbulent heat flux (and precipitation) fields developed from observations at microwave and infrared wavelengths. However, in common with other satellite based datasets, it only spans a relatively recent period (in this case 1987–2005) and is thus of limited utility for identifying changes in these fields. A significant advance in flux dataset development methodology is the Objectively Analysed Air-Sea heat flux (OAFlux) product that covers 1958–2010 and for the first time synthesizes state variables (sea surface temperature, air temperature and humidity, wind speed) from reanalyses and, where available, from satellite observations, prior to flux calculation (Yu and Weller, 2007). By combining these data sources, OAFlux avoids the severe spatial sampling problems that limit the usefulness of datasets based on ship observations and offers significant potential for studies of temporal variability. However, the balance of data sources used for OAFlux changed significantly in the mid-1980s, with the advent of satellite data, and the consequences of this change need to be assessed. In an alternative approach, Large and Yeager (2009) modified the NCEP/NCAR reanalysis state variables prior to flux calculation using various adjustment techniques, to produce the Coordinated Ocean Research Experiments (CORE) turbulent fluxes for 1948–2006. When combined with satellite based radiative flux estimates, CORE provides a globally balanced net heat flux field for forcing ocean models. However, the adjustments employed were based on satellite and in situ based observations spanning only limited periods (e.g., 1999–2004 for the wind speed adjustment) and the CORE product contains several fields that are climatological means prior to 1984. Thus it is not clear to what extent CORE can be reliably used for studies of interdecadal variability.

Analysis of OAFlux suggests that global mean evaporation exhibits variability at interdecadal timescales (Li et al., 2011; Yu, 2007, and Figure 3.6 left panel) although the impact of varying data sources on this variability has not yet been investigated. Time series of global mean latent and sensible heat flux determined from OAFlux are shown in Figure 3.6 centre and right hand panels. The latent heat flux variations closely follow those in evaporation (with allowance for the sign definition which results in negative values of latent heat flux corresponding to positive values of evaporation) but do not scale exactly as there is an additional minor dependence on sea surface temperature through the latent heat of evaporation. The overall time series from 1958–2010 provides no evidence for a trend in global mean evaporation.

[INSERT FIGURE 3.6 HERE]

Figure 3.6: Time series of globally averaged annual mean ocean evaporation (E), latent and sensible heat flux from 1958 to 2010 determined from OAFlux (shaded bands show uncertainty estimates; updated from Yu (2007)).

3.4.2.2 Surface Fluxes of Shortwave and Longwave Radiation

The shortwave flux component has strong regional variations with annual mean values up to about 250 W m^{-2} in the Tropics and a pronounced seasonal cycle. The longwave flux is less variable with annual mean losses typically in the range -30 to -70 Wm^{-2} depending on location. Estimates of these terms are available from in situ climatologies (that employ empirical formulae requiring ship observer estimates of cloud cover), from atmospheric reanalyses, and, since the 1980s, from satellite observations. As is the case for turbulent fluxes, these sources have many potential sources of error (e.g., uncertainty in the empirical formulae, sampling issues, representation of cloud in the reanalyses, and changing satellite sensors) which are difficult to quantify and strongly spatially dependent. The overall uncertainty of each term is again likely in the range of 10-20 % for the annual mean at a given location (Gulev et al., 2010). High accuracy in-situ radiometer measurements are available at many sites over land since the 1960s, allowing analysis of decadal variations in the surface shortwave flux (Wild, 2009; Chapter 2). However, this is not the case over the oceans, where there are very few in-situ measurements. Instead it is necessary to rely on satellite observations, which are less accurate (compared to in-situ determination of radiative fluxes), restrict the period that can be considered to the mid-1980s onwards, but do provide homogeneous sampling.

Estimates based on data over both ocean and land show increases of the globally averaged solar radiation (global brightening) by about 3 W m^{-2} per decade from 1991–1999 (Romanou et al., 2006; Wild et al., 2005) and have been attributed predominantly to aerosol optical depth decreases and cloud changes (Cermak et al., 2010; Mishchenko and Geogdzhayev, 2007). The brief interlude of global brightening in the 1990s has been preceded and followed by periods of decreasing surface insolation (global dimming) by about 2.5 W m^{-2} per decade for 1983–1991 and 5 W m^{-2} per decade for 1999–2004; over the full period 1983–2004 there is no significant trend (Hinkelman et al., 2009). Patterns of regional variability may differ significantly from the global signal (Hinkelman et al., 2009). Analysis of ISCCP-FD radiative fluxes for the period 1984–2000 by Romanou et al. (2007) shows a small increase of 1 W m^{-2} per decade in the surface shortwave radiation averaged over the global oceans with larger regional positive trends in the Pacific and North Atlantic tropics and negative trends in the mid-latitudinal North Pacific, Southern Atlantic and southern half of the Indian Ocean. Ship-based and reanalysis estimates of radiative flux variability over the oceans prior to the advent of satellite observations in the 1980s are unlikely to be accurate enough to detect global trends of <5 W m^{-2} per decade primarily due to space-time inhomogeneity of sampling in ship-based estimates and uncertainty in the radiative schemes employed in reanalyses.

3.4.2.3 Net Heat Flux and Ocean Heat Storage Constraints

The most reliable source of information for changes in the global mean net heat flux comes from the constraints provided by analyses of changes in ocean heat storage. The estimate of increase in global ocean heat content for 1970–2009 quantified in Box 3.1 corresponds to an increase in mean net heat flux from the atmosphere to the ocean of 0.46 W m^{-2}. This flux is small, and extremely challenging to detect from observations given the strength of signals associated with natural variability, the uncertainties in the flux estimates, and the lack of satellite measurements prior to the 1980s. Closure of the global mean net heat flux budget to within 20 W m^{-2} has still not been reliably achieved (e.g., Trenberth et al., 2009). Since AR4, some studies have shown consistency in regional net heat flux variability at sub-basin scale since the 1980s; notably in the Tropical Indian Ocean (Yu et al., 2007) and North Pacific (Kawai et al., 2008). However, detection of a change in surface fluxes responsible for the long-term ocean warming remains beyond the ability of currently available observational surface flux datasets.

3.4.3 Ocean Surface Precipitation and Freshwater Flux

Precipitation observations are available from remote sensing since 1979 and have been used by Smith et al. (2009) to reconstruct precipitation for the period 1900–2008 over 75° S – 75 ° N by means of a Canonical Correlation Analysis (CCA) with SST and SLP (Figure 3.7). The CCA makes use of correlation fields between precipitation and SST / SLP that are determined using remote sensing data from the Global Precipitation Climatology Project (GPCP) for 1979–2003. The reconstruction shows both centennial and decadal variability in ocean precipitation. The trend from 1900 to 2008 is 0.006 mm day^{-1} per decade, corresponding to an increase of nearly 2 mm per month over the 108-yr period. The trend for the more recent period 1950–2008 is 0.012 mm day^{-1} per decade which is nearly twice that for the whole period. For the period of overlap from 1979, the Smith et al. (2009) reconstruction time series is consistent (as is to be expected) with the corresponding time series determined directly from the GPCP data (Figure 3.7). Analysis of the GPCP data alone has revealed a slightly increasing global mean precipitation of 0.015 mm day^{-1} per decade from 1979 to 2005 with a stronger increase over the tropical ocean of 0.06 mm day^{-1} per decade (Gu et al., 2007).

Trenberth et al. (2011) assess the hydrological cycles in eight current atmospheric reanalyses and their time variability. For the recent period 1989 onwards, they find little consistency of the changes in ocean precipitation in the MERRA and ERA-Interim reanalyses with the GPCP dataset.

[INSERT FIGURE 3.7 HERE]

Figure 3.7: Long-term reconstruction of ocean precipitation (annual values – thin black line, low-pass filtered data – bold grey line) over 75°S – 75°N by Smith et al. (2009) as well as GPCP-derived ocean precipitation over the same

latitudinal range (annual values – thin blue line, low-pass filtered data – cyan bold line). Precipitation anomalies were taken relative to the 1979–2007 period.

By combining data from OAFLUX for E and GPCP for P, Schanze et al. (2010) examine variations in the global mean ocean net surface freshwater flux (E-P) for 1987 to 2006. There is significant interannual variability within this period but no evidence for a trend in global mean E-P. Schanze et al. (2010) find that use of satellite data prior to 1987 is limited by discontinuities in the record attributable to variations in data type and such variations also affect atmospheric reanalysis fields. Thus, it is not yet possible to establish whether there is a significant trend in E-P over the past 50 years.

3.4.4 Wind Stress

Wind stress fields are available from reanalyses, satellite-based datasets, and in situ observations. Yang et al. (2007) found a positive trend of Southern Ocean surface zonal wind stress from 1980 to 2000 using the ECMWF Re-analysis (ERA40) averaged over 45–60°S, satellite (SSM/I) winds and island station data. The trend has a strong seasonal dependence with largest values of about 0.02 N m^{-2} per decade in January at 55–60°S. They argue that the strengthening is closely linked with changes in the Southern Annular Mode (SAM). Xue et al. (2010) analysed wind stress for a range of ocean regions in several reanalyses as part of an evaluation of variability in the recent NCEP-CFSR reanalysis. They considered a somewhat broader Southern Ocean region (45–70°S) and longer period (1979–2009), and found significant wind stress trends in the NCEP-1 and NCEP-2 reanalyses but not NCEP-CFSR (Figure 3.8). For 2003 onwards, all three reanalyses (NCEP-1, NCEP-2 and NCEP-CFSR) covering this period considered by Xue et al. (2010) show zonal wind stress increasing over the Southern Ocean.

[INSERT FIGURE 3.8 HERE]
Figure 3.8: Time series of 1-year running mean of zonal mean wind stress over the Southern Ocean (45–70°S) for NCEP-CFSR (red), NCEP R1 (cyan, labelled NCEP-1), NCEP/NCAR R2 (dark blue line, labelled NCEP-DOE) and ERA-40 (green line). Units are N m^{-2} (Xue et al., 2010).

Atmospheric reanalyses have also been used to link wind stress changes to atmospheric teleconnection patterns. In particular, changes in wind stress curl over the North Atlantic from 1950 to early 2000s from NCEP-1 and ERA-40 have leading modes that are highly correlated with the NAO and East Atlantic circulation patterns; each of these patterns demonstrates a positive trend over the period from the early 1960s to the late 1990s (Sugimoto and Hanawa, 2010).

In the period prior to the NCEP-1 and ERA-40 reanalyses, attempts have been made to reconstruct the wind stress field in the Tropics by making use of the relationship between wind stress and SST/SLP in combination with historic datasets of these fields. Using this approach, Deng and Tang (2009) reconstructed time series of the wind stress over the Equatorial Pacific for 1875–1947 and found significant interannual and multidecadal variability over this period.

3.4.5 Changes in Surface Waves

Surface wind waves are generated by direct wind forcing and are partitioned into two components, namely wind sea (wind-forced waves propagating slower than surface wind) and swell (resulting from the wind sea development and propagating typically faster than surface wind). Significant wave height (SWH) represents the measure of the wind wave field consisting of wind sea and swell and is frequently attributed to the highest one-third of wave heights. Local wind changes influence wind sea properties, while changes in remote storms affect swell. Wind sea integrates characteristics of atmospheric dynamics over different scales and could serve as an indicator of climate variability and change. Variability patterns of wind sea and surface wind may not necessarily be consistent since wind sea integrates wind properties over a larger domain. Global and regional time series of wind sea characteristics are available from buoy data, Voluntary Observing Ship (VOS) reports, satellite measurements, and model wave hindcasts. No source is superior, as all have their strengths and weaknesses.

AR4 reported statistically significant positive SWH trends during 1900–2002 in the North Pacific (up to 8 cm per decade) and stronger trends (up to 14 cm per decade) from 1950 to 2002 for most of the mid-latitudinal North Atlantic and North Pacific, with insignificant trends, or small negative trends, in most other regions (Trenberth et al., 2007). Since AR4, further studies have provided confirmation of previously reported trends with more detailed quantification and regionalization.

At the centennial scale, hindcasts based on 20C Reanalyses (Wang et al., 2009) for 1871–2008 confirm an increase in SWH over the subtropical and mid-latitude Pacific, but indicate no significant trends in the mid-latitude North Atlantic. Starting from the 1950s, however, both observational data and forced model experiments are in agreement (Figure 3.9), indicating trends in SWH varying from 8 cm per decade to 20 cm per decade in winter months in the North Atlantic with smaller magnitudes in the North Pacific (Gulev and Grigorieva, 2006; Sterl and Caires, 2005; Wang and Swail, 2006; Wang et al., 2009). An ERA-40-WAM model hindcast covering 1958–2002 (Semedo et al., 2011) also shows an upward trend in both wind sea and swell heights in the North Atlantic and the North Pacific with the changes in SWH (1.18% per decade in the North East Pacific and nearly 1% per decade in the North East Atlantic) mainly related to the increase in swell heights. There is also evidence of increasing peak wave period during 1953–2009 in the Northeast Atlantic of up to 0.1 s per decade (Dodet et al., 2010), confirmed by the hindcast of Wang et al. (2009) for the same period. Trends in extreme waves have been reported in numerous locations since the late 1970s, including the North American Atlantic coast (Komar and Allan, 2008), the North American Pacific coast (Menendez et al., 2008), the western tropical Pacific (Sasaki et al., 2005) and south of Tasmania (Hemer, 2010).

[INSERT FIGURE 3.9 HERE]

Figure 3.9: [PLACEHOLDER FOR SECOND ORDER DRAFT: Global map of trends in SWH. Figure will be available for SOD.]

Analysis of reliable long-term trends in SWH in the Southern Hemisphere remains a challenge due to limited in-situ data and temporal in-homogeneity in the data used for reanalysis products. Studies comparing altimeter-derived SWH with data from buoys and output from models indicate that while there are some areas with statistically significant increases in waves, they occur in a narrower area than the models predict, or with smaller trends (Hemer, 2010; Hemer et al., 2010). Positive trends in the data occur mainly south of 45°S (Hemer et al., 2010). In the South Atlantic Ocean, in the area of the South American shelf between 30°S and 40°S, Dragani et al. (2010) reported a 7% increase in SWH during the 1990s and early 2000s, confirmed by TOPEX altimetry, in-situ data and a SWH hindcast model forced by NCEP winds.

Young et al. (2011) compiled global maps of trends for 1985–2008 in mean surface wind speed and mean SWH using measurements from up to 7 altimeter missions. For the mean SWH they report weak statistically significant positive linear trends of up to 0.25–0.5% per year in the Southern Ocean and negative trends in the Central North Pacific and many regions of the Northern Hemisphere oceans. The Northern Hemisphere mean SWH trends are of opposite sign, and thus inconsistent, with those in wind speed — the latter being primarily positive. Nevertheless, for the higher percentiles of SWH (90^{th} and, especially, 99^{th}), strong positive trends up to more than 1% per year were identified in the Southern Ocean, North Atlantic, and North Pacific, and these trends are consistent with the tendencies in extreme wind speeds. Young et al. (2011) note that because of the relatively short length of the dataset it is not possible to determine whether their results reflect long-term trends in SWH and wind speed, or are part of a multidecadal oscillation.

In conclusion, it is likely that SWH has been increasing over much of the North Pacific since 1900, and in the North Atlantic from the 1950s. In the Southern Ocean, south of 45°S, this tendency holds over the last two decades. It is also likely that extreme wave heights have been growing over the last 60 years.

3.4.6 Conclusions

The global mean net heat flux signal expected from observed ocean heat content changes is extremely small (<0.5 W m^{-2}) and beyond the detection ability of currently available observational surface flux datasets. It is not yet possible to establish whether there is a significant trend in E-P over the past 50 years from surface observations; an analysis for the shorter period 1987–2006 shows significant interannual variability but no evidence for a trend in global mean E-P. There is increasing evidence for a strengthening of the wind stress field in the Southern Ocean in recent decades that is linked to changes in the Southern Annular Mode (SAM) of atmospheric variability. Information on Significant Wave Height (SWH) trends is severely limited by available data but SWH has likely increased over the North Pacific since 1900, the North Atlantic since 1950 and the Southern Ocean over the last two decades, the trends are consistent with the tendencies in extreme wind speeds.

3.5 Changes in Water-Mass Properties and Ventilation

3.5.1 Introduction

To a large degree, water-mass properties are set at the sea surface through interaction between the ocean and the overlying atmosphere (and ice, in polar regions). The water characteristics resulting from these interactions (e.g., temperature, salinity, dissolved gas concentrations, and dissolved nutrients concentrations) are transferred into the ocean interior in a process known as subduction or ventilation, and slowly modified by mixing and for some substances biogeochemical cycling as the water masses are advected by the large-scale flow. The formation and subduction of water masses largely determine the ocean's capacity to store heat, freshwater, carbon, oxygen, and other properties relevant to climate. Water masses therefore provide a useful perspective on ocean change. In this section, evidence for changes in the major water masses of the world ocean is summarized.

The changes evident in zonally averaged temperature, salinity, and density (Figure 3.10) reflect changes in water-mass properties and ventilation as well as changes in circulation that result in vertical or horizontal migration of density layers. The tendency for warming of the upper ocean and a decrease (increase) of salinity in higher (lower) latitudes discussed in Section 3.2 and 3.3 are clearly evident in the zonally-averaged fields. The density of the surface layers has generally declined, increasing the upper ocean stratification. Stronger stratification inhibits ventilation, consistent with the observed tendency for declining oxygen in much of the upper ocean (discussed in Section 3.8).

3.5.2 North Atlantic

The North Atlantic is strongly influenced by atmospheric modes of variability (NAO). In the Northeast Atlantic, a high NAO index leads to colder, fresher, and denser Subpolar Mode Water (SPMW) than during periods of low NAO (Johnson and Gruber, 2007). These changes are consistent also in the Subarctic Intermediate water and the Mediterranean Outflow Water, both ventilated elsewhere, implying that NAO-related circulation changes (northwestward contraction of the subpolar gyre) seems the most likely cause of these variations (Johnson and Gruber, 2007), and not changes in local buoyancy fluxes (Johnson and Gruber, 2007; Sarafanov et al., 2008).

The North Atlantic Deep Water (NADW) has several components, the shallowest being Labrador Sea Water (LSW). LSW exhibits strong decadal variability in temperature and salinity. Since the mid-1990s, LSW warmed and got saltier (Yashayaev and Loder, 2009). Parallel to that, ventilation weakened and the density of LSW decreased (Kieke et al., 2006). Since 1997, only lighter modes ($27.68 < \sigma_\Theta < 27.74$ kg m^{-3} vs. $27.74 < \sigma_\Theta < 27.80$ kg m^{-3}) have been ventilated [(!!! INVALID CITATION !!!)], while for the time period 1970–1997, the formation of denser LSW (σ_Θ =27.74-27.80 kg/m^3) was more dominant (LeBel et al., 2008). The LSW formation rate decreased from 7.7 Sv (10^6 m^3 s^{-1}) in 1997–1999 to roughly 0.5 Sv in 2003–2005 (Rhein et al., 2011), mostly due to changes in the local buoyancy fluxes (Yashayaev and Loder, 2009), related to the NAO. The reduced ventilation also affected the anthropogenic carbon inventory of the subpolar North Atlantic, the inventory increase was much smaller than expected (Steinfeldt et al., 2009).

The dense part of the NADW consists of water overflowing the sills between Greenland and Scotland. The salinity of the Faroe Bank overflow, especially in its warmer reaches, increased substantially since 1995, implying a density increase on the order of 0.01 kg/m^{-3} (Hansen and Osterhus, 2007). The other main overflow, through Denmark Strait, shows large interannual variability in temperature and salinity for the last 10 years, but no trend. The freshening trend observed since the mid-1960s in both overflows and highlighted in AR4 has stopped in the mid-1990s (Dickson et al., 2008).

3.5.3 North Pacific

In the North Pacific a freshening is found in the subtropical main thermocline, starting in the early 1990s (Ren and Riser, 2010). The spatial pattern and long-term evolution of the freshening could be an indication of an intensifying hydrological cycle, but other processes like the poleward migration of the winter outcrop position into areas with higher precipitation are also likely (Ren and Riser, 2010).

Oxygen data spanning time scales of 50 years to a decade show decreasing concentrations in the subpolar North Pacific. Oxygen concentrations in the eastern and western subarctic gyre decrease at a rate of 7 µmol kg^{-1} per decade superimposed on a bidecadal oscillation (Aleutian Low and 18.6-year nodal tide). Oxygen decreased from the mid-1980s to late 1990s throughout the upper subarctic waters, extending to the subtropical gyre in the eastern Pacific (Mecking et al., 2006; Mecking et al., 2008; Whitney et al., 2007). The decline was largest near the base of the mode water. Changing CFC ages of the water masses, and modeling studies indicate that reduced ventilation and subduction (Deutsch et al., 2006; Mecking et al., 2006; Mecking et al., 2008) related to increased stratification as well as freshening, warming and shoaling of the mixed layer (Whitney et al., 2007) are responsible for the oxygen decline rather than changes in oxygen utilization.

North Pacific Intermediate Water (NPIW) has steadily warmed, by roughly 0.5°C from 1955 to 2004 in the northwestern North Pacific, accompanied by significant oxygen reduction (Nakanowatari et al., 2007), and has also freshened since 1960 (Kouketsu et al., 2009). The trends are strongest in the formation area of NPIW. There are some indications, although inconclusive, that increased air temperature during the cold season and a decrease in sea-ice extent is linked to the property changes of NPIW (Nakanowatari et al., 2007). In contrast, decadal variability of the ventilation of the North Pacific Subtropical Mode Water (STMW) is mainly influenced by circulation variability and not so much by air-sea flux changes (Qiu and Chen, 2006).

3.5.4 Southern Hemisphere Subtropical Gyres

Comparison of changes in CFC concentrations between WOCE data from the decade of the 1990s and CLIVAR data of the 2000s show a distinct asymmetric behaviour between the southern and northern hemispheres. There are larger increases of CFC concentrations with time in the Southern Hemisphere, as the subtropical gyres there reach deeper and the Subantarctic Mode Water (SAMW) and Antarctic Intermediate Water (AAIW) formation rates are higher compared with those of their Northern counterparts (e.g., Fine et al., 2001). The characteristic of larger CFC concentration increases in Southern Hemisphere subtropical gyres is consonant with the oxygen distributions. These CFC and oxygen increases on intermediate surfaces are consistent with a decadal intensification of wind stress curl associated with an increase in the SAM, which affects all three connected Southern Hemisphere subtropical gyres (e.g., Ridgway and Dunn, 2007; Roemmich et al., 2007; Speich et al., 2007). Thus, when looking at the limited time period over the decade between WOCE and CLIVAR a larger increase in Southern Hemisphere ventilation than the Northern on lower thermocline and intermediate-level isopycnals is consistent with SAM variability.

3.5.5 Southern Ocean

Since the 1970s, the salinity minimum of the AAIW shoaled (30–50 dbar $decade^{-1}$), warmed (0.05°–0.15°C $decade^{-1}$) and became less dense (up to 0.03 kg m^{-3} $decade^{-1}$). The trends are strongest near the formation regions in the southeast Pacific and Atlantic (Schmidtko and Johnson, 2011). Similar trends were observed at the mid-latitude of the Indian Ocean, where salinity of the SAMW and AAIW decreased since the 1960s, and the pycnostad core of the SAMW and the salinity minimum of AAIW shifted to lighter densities. The trend is more prominent in the eastern region near the source than in the west (Kobayashi et al., 2011). The freshening along isopycnals in the Southern Ocean including the AAIW had been interpreted as being caused by an intensification of the hydrological cycle (Helm et al., 2010), but other mechanisms could also be invoked. For instance, in the South Atlantic, the AAIW changes in salinity are linked with changes in the Agulhas leakage related to atmospheric variability (SAM) rather than intensification of the hydrological cycle (McCarthy et al., 2011). The freshening of the AAIW in the Drake Passage observed since 1970 was linked to freshening of Winter Water (WW) involved in AAIW formation (Garabato et al., 2009). WW freshening was caused by increased precipitation and a retreat of the winter sea ice edge west of the Antarctic Peninsula, presumably forced by an interdecadal trend in the SAM and regional positive feedbacks in the air–sea ice coupled climate system. Poleward migration of isopycnal outcrops with surface warming is also likely to contribute to the observed salinity changes (Durack and Wijffels, 2010).

The AABW has warmed and freshened in recent decades, most noticeably near its source regions (Aoki et al., 2005; Johnson et al., 2008b; Kouketsu et al., 2011; Purkey and Johnson, 2010; Rintoul, 2007), but with warming detectable into the North Pacific and even the North Atlantic oceans. In the Indian Ocean, AABW in the Australian-Antarctic Basin and the Princess Elizabeth Trough has warmed and freshened between the 1990s and the 2000s (Johnson et al., 2008a; Rintoul, 2007). In the Pacific sector, closest to Antarctica, there are indications of abyssal freshening, consistent with long-term freshening in some of the Antarctic source regions for these waters (Jacobs, 2004; Jacobs and Giulivi, 2010). Warming of the abyssal waters derived from Antarctica has been observed throughout the Pacific, all the way to the Aleutian Islands (Fukasawa et al., 2004; Johnson et al., 2007; Kawano et al., 2006). In the Atlantic, repeat hydrography show that abyssal waters have warmed considerably over the last few decades in all the deep western basins of the South Atlantic (Johnson and Doney, 2006) and in the western basins of the North Atlantic as well (Johnson et al., 2008b). More frequent bottom temperature data in a few deep passages such as the Vema Channel (Zenk and Morozov, 2007) and the equatorial Atlantic (Andrié et al., 2003) also show monotonic warming since around 1990.

[INSERT FIGURE 3.10 HERE]

Figure 3.10: [PLACEHOLDER FOR SECOND ORDER DRAFT] Upper 2000 m zonal average distribution of changes in salinity (row 1), neutral density (row 2), and potential temperature (row 3), for the Atlantic (column 1), Pacific (column 2) and Indian (column 3) oceans over the past 50 years (1950–2000). Mean density is overlaid in black (contour interval 1.0 kg m^{-3} – thick contours, and 26.5 to 27.75 in increments of 0.25 kg m^{-3} – thin contours), and density changes are contoured in white (contour interval 0.1 kg m^{-3} from -0.3 to +0.3 kg m^{-3}). Data from Durack and Wijffels (2010). Main intermediate water masses are indicated in row 1.

3.5.6 Conclusions

Changes in the temperature and salinity of the upper ocean have resulted in changes in the properties of major water masses in each of the ocean basins. Overall, there has been a tendency towards an increase in stratification of the upper ocean, and a decline in ventilation, in many regions of the ocean. Many of the changes are broadly consistent with those expected from a warming climate and an enhanced hydrological cycle. For example, the intermediate depth salinity minimum waters in both hemispheres. However, the presence of strong interannual variability driven by atmospheric modes of variability like the NAO and SAM together with the absence of long-term, continuous, measurements means that it is often not possible to isolate significant trends from interannual to multi-decadal variability.

3.6 Evidence for Change in Ocean Circulation

3.6.1 Observing Ocean Circulation Variability

The present-day ocean observing system includes global observations of velocity made at the sea surface by the Global Drifter Program (Dohan et al., 2010), and at 1000-m depth by the Argo Program (Freeland et al., 2010). In addition, Argo observes the geostrophic shear between 2000 m and the sea surface. These two recently implemented observing systems, if sustained, will continue to document the large-spatial scale, long-timescale variability of circulation in the upper ocean.

Historical measurements of ocean circulation are much sparser, so estimates of decadal and longer changes in circulation are very limited. Since 1992, high-precision satellite altimetry has measured the time variations in sea surface height (SSH), whose horizontal gradients are proportional to the surface geostrophic velocity. In addition, mostly during 1991–1997, single global top-to-bottom hydrographic survey was carried out by the World Ocean Circulation Experiment (WOCE), measuring geostrophic shear as well as mid-depth velocity. A subset of WOCE and pre-WOCE transects is being repeated at 5–10 year intervals (Hood et al., 2010).

Foci of ocean circulation studies in relation to climate include variability in the wind-driven gyres (Section 3.6.2) and changes in the meridional overturning circulations (MOCs, Section 3.6.3 and 3.6.4) influenced by buoyancy loss and water-mass formation. The MOCs are responsible for much of the ocean's capacity to carry excess heat from the tropics to middle latitudes, and also are important in the ocean's sequestration of carbon. The connections between ocean basins (Section 3.6.5) have also been subject to study because of the significance of inter-basin exchanges in wind-driven and thermohaline variability, and also because these can be logistically advantageous regions for measurement ("chokepoints"). In the following, the best-studied and most significant aspects of circulation variability and change are assessed including wind-driven circulation in the Pacific, the Atlantic and Antarctic MOCs, and selected interbasin exchanges.

An assessment is now possible of the recent mean and the changes in global geostrophic circulation over the previous decade (Figure 3.11, and discussion in Section 3.6.2). In general, changes in the slope of SSH across ocean basins indicate changes in the major gyres and the interior component of MOCs (western boundary-current components may also be important but are not resolved in these observations). Changes occurring in high gradient regions such as the Antarctic Circumpolar Current (ACC) indicate shifts in the location of those currents.

[INSERT FIGURE 3.11 HERE]

Figure 3.11: The mean SSH (cm, black contours) for the Argo era is the sum of the geostrophic pressure field at 1000 m based on Argo trajectory data (Katsumata and Yoshinari, 2010) plus the relative pressure field (0/1000 dbar steric height) based on Argo profile data from Roemmich and Gilson (2009). The SSH trend (cm decade^{-1}, color shading) for the period 1993–2009 is based on the AVISO altimetry "reference" product (Ducet et al., 2000). Spatial gradients in the SSH trend are proportional to changes in surface geostrophic velocity.

3.6.2 Wind-Driven Circulation Variability in the Pacific Ocean

The upper Pacific Ocean is less influenced than the Atlantic by the deep MOC (the North Pacific has no deep water formation), and variability in the horizontal gyre circulations of the Pacific is mostly wind-driven. Consistent changes in circulation throughout the Pacific in the past two decades are seen with good agreement among satellite ocean data, in-situ ocean measurements, and wind stress forcing.

The subarctic gyre in the North Pacific poleward of about 40°N consists of the Alaska Gyre to the east and the Western Subarctic Gyre (WSG) to the west. Over the past two decades, the cyclonic Alaska Gyre has strengthened while shrinking in size. The shrinking is due to strengthening and northward expansion of the North Pacific Current (NPC, the high gradient region centred about 40°N in Figure 3.11) and has been described using the satellite altimeter, XBT/hydrography, and, more recently, Argo profiling float data (Cummins and Freeland, 2007; Douglass et al., 2006). A similar trend is detected in the WSG, with the northern WSG in the Bering Sea strengthened while the southern WSG south of the Aleutian Islands has weakened. These decadal changes are attributable to strengthening and northward expansion of the Pacific High and Aleutian Low atmospheric pressure systems over the subarctic North Pacific Ocean (Carton et al., 2005).

Accompanying the NPC's northward expansion, the subtropical gyre in the North Pacific also expanded along its southern boundary over the past two decades. The North Equatorial Current (NEC) shifted southward along the 137°E meridian (Qiu and Chen, 2011, also note the SSH increase east of the Philippines in Figure 3.10 indicating the southward shift). The NEC's bifurcation latitude along the Philippine coast migrated southward from a mean latitude of 13°N in the early 1990s to 11°N in the late 2000s (Qiu and Chen, 2010). These changes are due to a strengthening of the Walker circulation generating a positive wind stress curl anomaly (Mitas and Clement, 2005; Tanaka et al., 2004). This regional wind stress curl anomaly is also responsible for the enhanced regional sea level rise, >10 mm yr^{-1}, in the western tropical North Pacific Ocean (Timmermann et al., 2010, Figure 3.10). The 20-year timescale expansion of the North Pacific subtropical gyre has high confidence due to the good agreement seen in satellite altimetry, subsurface ocean data, and wind stress changes.

Variability in the mid-latitude South Pacific over the past two decades is characterized by a broad increase in SSH in the 35°S–50°S band and a lesser increase or decrease south of 50°S along the path of the ACC (Figure 3.11). These dipolar SSH fluctuations are induced by the intensification in the Southern Hemisphere westerlies, generating positive and negative wind stress curl anomalies north and south of 50°S. In response, the southern limb of the South Pacific subtropical gyre has intensified in the past two decades (Cai, 2006; Qiu and Chen, 2006; Roemmich et al., 2007) along with a southward expansion of the East Australian Current (EAC) into the Tasman Sea (Hill et al., 2008; Ridgway, 2007). The intensification in the South Pacific gyre extends to a greater depth than that in the North Pacific gyre (Roemmich and Gilson, 2009). As in the north, the 20-year changes in the South Pacific are seen with high confidence as they occur consistently in multiple lines of medium and high quality data.

The strengthening of southern hemisphere westerlies is a multi-decadal signal (as seen in decreasing trends in high southern latitude sea level pressure, see Box 2.2, Figure 1), and the multi-decadal warming in the Southern Ocean (e.g., Figure 3.1) is consistent with a poleward displacement of the ACC (Gille, 2008) and the southern limb of the subtropical gyres. The warming and corresponding sea level rise signals are not confined to the South Pacific, but are seen globally in zonal mean fields (e.g., at 40°S in Figure 3.11). Alory et al. (2007) describe the broad warming consistent with a southward shift of the ACC in the South Indian Ocean. In the Atlantic, a southward trend in the location of the Brazil-Malvinas confluence (at around 39°S) is described from surface drifters and altimetry by Lumpkin and Garzoli (2011), and in the location of the Brazil Current separation point from sea surface temperature and altimetry by Goni et al. (2011).

3.6.3 The Atlantic Meridional Overturning Circulation (AMOC)

[INSERT FIGURE 3.12 HERE]

Figure 3.12: The AMOC is a time-varying streamfunction in the vertical-meridional plane that can be calculated from the zonal integral of the meridional velocity in an east–west section across an ocean basin The AMOC is primarily a two-layer system, with an upper limb moving northward between the surface and approximately 1200 m depth and a mass-balancing lower limb return flow between approximately 1200 m and 5000 m. Transports are given in units of Sverdrups (Sv; where 1 Sv = 10^6 m^3 s^{-1}). 1. RAPID/MOCHA array at 26.5°N (red): The array monitors the top-to-bottom Atlantic wide circulation, ensuring a closed mass balance across the section, and hence a direct measure of the upper and lower limbs of the AMOC. 2. 41°N (black): An index of maximum AMOC strength from Argo float measurements in the upper 2000 m only, combined with satellite altimeter data. The lower limb is not measured. 3. MOVE at 16°N (blue): Transport of North Atlantic Deep Water in the lower limb of the AMOC between 1100m and 4800m depth between the Caribbean and the mid-Atlantic Ridge. This transport is thought to be representative of maximum MOC variability based on model validation experiments. The temporal resolution of the three timeseries is ten days for 16°N and 26°N and one month for 41°N. In this figure the data have been three month low-pass filtered and the means and standard deviations are of the low-pass timeseries.

Observations of the AMOC are directed toward detecting possible long-term changes in its amplitude, its northward energy transport, and in the ocean's capacity to absorb excess heat and greenhouse gases, as well as characterizing short-term variability and its relationship to changes in forcing. The overturning circulation is a global-scale phenomenon, with a bottom limb of Antarctic Bottom Water spreading northward below the AMOC. Variability of this bottom limb is discussed in Section 3.6.4.

Presently, changes in the AMOC are being estimated on the basis of direct observations of the full MOC at 26.5°N by the RAPID/MOCHA array (Cunningham et al., 2007; Johns et al., 2011; Kanzow et al., 2007) or of observations that target one component of the AMOC (e.g., a specific current or ocean layer, e.g., Kanzow et al., 2008; Meinen et al., 2010; Toole et al., 2011; Willis, 2010). Other estimates of the temporal evolution of the AMOC are indirect, from measurements of forcing fields such as air-sea fluxes (e.g., Grist et al., 2009; Josey et al., 2009; Marsh, 2000; Speer, 1997), or from properties that may be related to AMOC changes, such as abyssal temperature or salinity (e.g., Johnson et al., 2008b), changes in water-mass formation rates (e.g., Kieke et al., 2007; Myers and Donnelly, 2008), or coastal sea level (Bingham and Hughes, 2009).

Longer, continuous time series of components of the AMOC have been obtained using moored instrumentation, e.g., inflow into the Arctic through Fram Strait (since 1997, Schauer and Beszczynska-Möller, 2009), dense inflows across sills between Greenland and Scotland (since 1999 and 1995 respectively, Olsen et al., 2008), and North Atlantic Deep Water carried southward within the Deep Western Boundary Current - at 53°N (since 1997, Fischer et al., 2010), at 39°N (Line W, since 2004, Toole et al., 2011), and at 16°N since 2000 (Kanzow et al., 2009). The overturning circulation is a global-scale phenomenon, but few time series exist in the other ocean basins.

The only array to continually observe the full AMOC is located at 26.5°N, the RAPID/MOCHA array (Cunningham et al., 2010). Since 2004, both the vertical structure and the strength of the AMOC (Cunningham et al., 2007; Kanzow et al., 2007; Kanzow et al., 2010) and the meridional heat flux associated with it (Johns et al., 2011) have been monitored continuously (Figure 3.12). These data show a mean AMOC magnitude (±annual mean error) of 18 ± 1.3 Sv between April 2004 and April 2009, with 10-day values ranging from 3–32 Sv, the difference of the annual mean from year to year was as high as 5 Sv. There is a large seasonal cycle with amplitude 6.7 ± 1.2 Sv. The mean meridional heat transport at this latitude is

1.33 ± 0.12 PW (Johns et al., 2011), of which 90% is carried by the AMOC. At periods greater than 180 days the variance of the upper-mid ocean transport dominates AMOC variance. From 2004 to 2009 the standard deviation of annual mean transports is 0.9 Sv. During this period there are no trends.

To estimate AMOC strength and variability at 41°N, Willis (2010) combines velocities from Argo drift trajectories, Argo temperature and salinity profiles and satellite altimeter data (Figure 3.12). Here the AMOC magnitude is 15.5 Sv ± 2.2 from 2002–2009 (Figure 3.12). This study suggests an increase in the AMOC strength of about 2.4 Sv from 1993–2010, though of uncertain confidence because it is based on SSH alone in the pre-Argo interval of 1993–2001.

At 16°N, geostrophic array-based observations of the southward transport of North Atlantic Deep Water (NADW) in the depth range 1100 to 4700 m have been made continuously since 2000 (Kanzow et al., 2008). These measurements of the southward flow of NADW in the western basin may be representative of overall AMOC transport and variability. They suggest that the southward transport of NADW has been declining between 2000 and 2009 by roughly 3 Sv (Figure 3.12). However, given the large intraseasonal to interannual variability the possible decline is not significant at 95% confidence (Send et al., 2011).

The measured or inferred AMOC estimates at 16°N, 26.5°N, and 41°N have time series of length nine, eight, and seven years respectively (Figure 3.12). All show a substantial variability of ~3-5 Sv for three month low-pass time series, with a peak-to-peak interannual variability of 5 Sv. The shortness of these time series, and the relatively large interannual variability emerging in them suggests that trend estimates be treated cautiously. At 16°N and 41°N no trends are seen at 95% confidence interval. This result also holds at 26.5°N for the period 2004–2009.

Indirect estimates of the annual average AMOC strength and variability can be made (Grist et al., 2009; Josey et al., 2009) from diapycnal transports driven by air-sea fluxes (NCEP-NCAR reanalysis fields from 1960 to 2007) or by inverse techniques (Lumpkin and Speer, 2007). Decadal fluctuations of up to 2 Sv are seen, but no trend. The decadal variability is generally in phase from 30-80°N, except in the 1990s when anomalies north and south of 60°N are out of phase. Consistent with Grist et al. (2009), the sea level index of the strength of the AMOC, based on several coherent western boundary tide gauge records between 39°N and 43°N at the American coast (Bingham and Hughes, 2009) shows no long-term trend from 1960 to 2007. Similarly, none of the direct, continuous transport estimates of single components of the AMOC such as the Florida Current (going back to 1982; Meinen et al., 2010); the overflows entering the Atlantic across Greenland-Scotland Ridge (going back to 1995; Olsen et al., 2008) or the DWBC at the exit of the Labrador Sea (going back to 1997; Fischer et al., 2010) exhibit long-term trends at 95% significance.

Measurements of the AMOC and of circulation elements contributing to it, at various latitudes and covering different time periods, agree that the range of inter-annual variability is 5 Sv (Figure 3.12). These estimates do not have trends, in either the subtropical or the subpolar gyre. The observational record of AMOC variability, however, is short, and taken together there is no evidence for or against a meridionally coherent change in the transport of the AMOC.

3.6.4 The Antarctic Meridional Overturning Circulation

Below the AMOC, Antarctic Bottom Water sinks around Antarctica and spreads northward ventilating the bottom-most portions of much of the ocean (Orsi et al., 1999). Observed widespread warming of Antarctic Bottom Water in recent decades (Section 3.5.4) implies a concomitant reduction in its northward spread. Reductions of 1-4 Sv in northward transports of AABW across 24°N have been estimated by geostrophic calculations using repeat oceanographic section data between 1981 and 2004 in the North Atlantic Ocean (Johnson et al., 2008b) and between 1985 and 2005 in the North Pacific (Kouketsu et al., 2009). A global full-depth ocean data assimilation study also shows a reduction of northward AABW flow across 35°S of ~2 Sv in the South Pacific starting around 1985 and ~1 Sv in the western South Atlantic starting around 1975 (Kouketsu et al., 2011). These reductions are supported by estimates of trends in basin-wide inventories of AABW, with an even stronger global contraction rate of 8.3 (±2.6) Sv (in the southernmost basins around Antarctica) for AABW with $\theta < 0°C$ between the 1980s and 2000s (Purkey and Johnson, 2011). The analyses are all based on a relatively sparse global network of oceanographic sections that have been revisited at roughly decadal intervals since the 1980s or 1990s, making assessment of time-scales or variability prior to the 1980s difficult.

3.6.5 Water Exchange Between Ocean Basins

3.6.5.1 The Indonesian Throughflow (ITF)

The transport of water from the Pacific to the Indian Ocean via the Indonesian archipelago is the only low-latitude exchange between oceans, and is significant because it is a fluctuating sink/source for very warm tropical water in the two oceans. ITF transport has been estimated from hydrographic and XBT transects between Australia and Indonesia and from moorings in the principal Indonesian passages. The most comprehensive observations were obtained in 2004–2006 in three main passages by the INSTANT mooring array (Sprintall et al., 2009), and show a transport of 15.0 (±4) Sv. On a longer timescale, Wainwright et al. (2008) analyzed data along the IX1 Australia-Indonesia XBT transect and found a change in the slope of the thermocline for data before and after 1976, indicating a decrease in geostrophic transport by 23%, consistent with a weakening of the trade winds (e.g., Vecchi et al., 2006). Other transport estimates based on the IX1 transect show correlation with ENSO variability (Potemra and Schneider, 2007) and no significant trend for the period since 1984 having continuous sampling along IX1 (Sprintall et al., 2002). Overall, there is not sufficient evidence to conclude with high confidence that a trend in ITF transport has been seen.

3.6.5.2 The Antarctic Circumpolar Current (ACC)

Westerly winds in the Southern Ocean have increased since the 1970’s, associated with a positive trend in the Southern Annular Mode (Marshall, 2003). Coarse resolution climate models (e.g., Fyfe and Saenko, 2006) suggest the ACC transport should increase with increasing wind stress. While a few observational studies have found evidence for correlation between SAM and ACC transport on subseasonal to interannual scales (e.g., Hughes et al., 2003; Meredith et al., 2004), there is no observational evidence of an increase in ACC transport associated with the multi-decadal trend in wind forcing over the Southern Ocean. Repeat hydrographic sections in Drake Passage (e.g., Cunningham et al., 2003; Gladyshev et al., 2008; Koshlyakov et al., 2007; Koshlyakov et al., 2011), south of Africa (Swart et al., 2008) and south of Australia (Rintoul et al., 2002) reveal moderate variability but no evidence of trends in these short and discontinuous records. A comparison of recent Argo data and a long-term climatology showed that the slope of density surfaces (hence baroclinic transport) associated with the ACC had not changed in recent decades (Böning et al., 2008). Models that resolve eddies also suggest the ACC transport is relatively insensitive to trends in wind forcing, consistent with the ACC being in an “eddy-saturated” state where increases in wind forcing are largely compensated by changes in the eddy field (Hallberg and Gnanadesikan, 2006; Spence et al., 2010). While there is no evidence for multi-decadal changes in transport of the ACC, observations of changes in temperature, salinity and sea surface height indicate the current system has shifted polewards along with a poleward shift in the westerly winds in recent decades (Böning et al., 2008; Gille, 2008; Sokolov and Rintoul, 2009).

3.6.5.3 North Atlantic / Nordic Seas Exchange

There is inconclusive evidence of changes during the past two decades in the flow across the Greenland-Scotland Ridge, which connects the North Atlantic with the Norwegian and Greenland Seas. Hakkinen and Rhines (2009), analyzing surface drifter tracks in the North Atlantic, found a greater tendency after 2000 for drifters in the North Atlantic Current to continue northward across 50°N rather than recirculate toward the southeast. However, a recent surface drifter study in the Nordic Seas (Andersson et al., 2011) finds no change in the surface currents between the two time periods. Moreover, direct measurements since 1994 of the warmest northward flow across the Faroe Shetland Channel (>8°C; roughly 4 Sv), show no trend in the transport (Mauritzen et al., 2011).

The two primary pathways for the deep southward overflows across the Greenland-Scotland Ridge are the Denmark Strait and Faroe Bank Channel. Moored measurements of the Denmark Strait overflow demonstrate significant interannual transport variations (Macrander et al., 2005), but the time-series is not long enough to detect a multi-decadal trend. Similarly, a ten-year time-series of moored measurements in the Faroe Bank channel (Olsen et al., 2008) does not show a trend in transport.

3.6.6 Conclusion

In summary, recent observations have strengthened evidence for variability in major ocean circulation systems on time scales from years to decades. Much of the variability observed in ocean currents can be linked to changes in wind forcing, including changes in winds associated with the modes of climate variability. Given the short duration of direct measurements of ocean circulation, it is not possible to distinguish multi-decadal trends from decadal variability.

3.7 Sea Level Change, Including Extremes

3.7.1 Observations of Long-Term Trends and Patterns in Sea Level

Direct observations of sea level change have been made regularly at a number of tide gauge sites since the late 1800s, and a much smaller number of records extend back to the 18th century. Satellite radar altimeters have nearly global coverage, but have reported measurements only over the last two decades. Although the two approaches differ in the measurements technique, the spatial and temporal sampling, the length of the record, and the reference frames used, numerous studies have compared the two and verified that they agree at the level of 0.5 mm yr^{-1} or better over periods of a decade and longer (Beckley et al., 2010; Merrifield et al., 2009; Nerem et al., 2010).

Tide gauges with long records show increasing sea level since 1900 (Figure 3.13), and numerous studies have averaged sea level change from available observations to examine global mean sea level (GMSL) (e.g., Douglas, 2001). However, comparing tide gauges in different regions (Figure 3.13) demonstrates that sea level change can vary significantly from one area to another on periods from a decade to several decades. Changes over 10–20 years can be several times larger than the long-term trend, and can often be of different sign even when the tide gauges border the same ocean (e.g., New York and Newlyn in Figure 3.13). Much of these decadal fluctuations have been linked to either redistribution of heat and salt related to changing large-scale ocean circulation (Section 3.6) or changes nearer the coast driven by in the alongshore wind variations (Sturges and Douglas, 2011). While GMSL is a convenient metric for understanding sea level change, regional sea level change can be significantly larger or smaller than the change in GMSL on periods of several decades.

[INSERT FIGURE 3.13 HERE]
Figure 3.13: 3-year running mean sea level from long tide gauge records from the Permanent Service for Mean Sea Level (PSMSL), corrected for Glacial Isostatic Adjustment (GIA) (Peltier, 2004), after Woodworth et al. (2009).

Tide gauge records need to be corrected for vertical land motion (VLM) before they can be interpreted in terms of changes in the volume of the ocean. Older studies only accounted for glacial isostatic adjustment (GIA) of the solid earth (Peltier, 2001). However, in many areas with tectonic activity or ground-water mining, GIA is not the largest source of vertical land motion and using only a GIA model may potentially bias the true rate. Some authors choose gauges that have no evidence of tectonic activity or subsidence in order to reduce this potential bias (e.g., Holgate, 2007). More recently, efforts to place global positioning system (GPS) receivers at tide gauge sites have allowed a better quantification of the uncertainty of not correcting for the full VLM when computing GMSL. While rates of GMSL rise computed with and without VLM from GPS do differ, the results are well within their uncertainties (± 0.5 mm yr^{-1}, 90% confidence) (Merrifield et al., 2009; Woeppelmann et al., 2009), which gives increased confidence that the 20th Century GMSL rates based on tide gauge data are not biased high due to unmodeled vertical land motion at the gauges. A GIA correction must also be applied to convert sea level measured by satellite altimetry to water volume change (Peltier, 2001), correcting for the change in location of the ocean bottom relative to the reference frame of the satellite.

Multiple methods have been used to compute GMSL from tide gauges. These range from using the average rates from very long, nearly continuous records (Douglas, 2001; Holgate, 2007), to using shorter records and filters to separate nonlinear trends from decadal-scale quasi-periodic variability (Jevrejeva et al., 2006; Jevrejeva et al., 2008), to computing regional sea level for specific basins then averaging based on the ocean area covered (Jevrejeva et al., 2006; Jevrejeva et al., 2008; Merrifield et al., 2009), to projecting tide gauge records onto empirical orthogonal functions (EOFs) computed from modern altimetry (Church et al., 2004) or EOFs from ocean models (Llovel et al., 2009). The time-series from different approaches generally agree within two standard deviations (~90% confidence) at most time scales (Figure 3.14a). The rate from 1901 to 2010 using the Church and White (2011) analysis is 1.6 ± 0.2 mm yr^{-1} (90% confidence). Other published estimates for similar time intervals agree with this estimate within the uncertainty.

[INSERT FIGURE 3.14 HERE]

Figure 3.14: Global mean sea level from the different measuring systems as they have evolved in time. **a)** Yearly average GMSL reconstructed from tide gauges (1900–2010) by two different approaches (Church and White, 2011; Jevrejeva et al., 2008), **b)** total GMSL (1970–2010) from tide gauges along with the thermosteric component (3-year running mean) estimated from in situ temperature profiles (updated from Domingues et al., 2008), **c)** total GMSL (1993–2010) from tide gauges, along with measurement from altimetry (Nerem et al., 2010) smoothed with a 1-year running mean, and thermosteric component, **d)** the total sea level (nonseasonal) from altimetry and computed from the mass component (GRACE) and steric component (Argo) from 2005–2010 (Leuliette and Willis, 2011). All uncertainty bars are one standard error as reported by the authors. The thermosteric component is just a portion of total sea level, and is not expected to agree individually with total sea level. The time-series are plotted relative to 5-year mean values that start at **a)** 1900, **b)** 1970, **c)** 1993, and **d)** 2005.

There is a statistically significant increase in GMSL rate as one starts the calculation from later times (Table 3.1). The most recent period, which corresponds to the 17-year long record of continuous satellite altimeter missions, has a rate of 3.3 ± 0.2 mm yr^{-1} (90% confidence) (Beckley et al., 2010; Leuliette and Scharroo, 2010; Nerem et al., 2010, Figure 3.12). Tide gauge measurements give a statistically consistent result over the same period (Merrifield et al., 2009), so there is high confidence that this change in observed rate of sea level rise is real and not an artefact of the different sampling or instruments.

Regional rates of sea level change are often higher or lower than the global mean on interdecadal periods (Figure 3.13). It is difficult to map these patterns from tide gauge data directly, except on the very broadest scales. Global maps can be reconstructed using EOFs (e.g., Church et al., 2004; Llovel et al., 2009), but the patterns are still highly uncertain, as the method relies on assuming that the EOFs since 1993 represent patterns in previous decades. However, regional rates are known globally to high precision using satellite altimetry since 1993, and results have shown a persistent pattern of change, with rates in the Warm Pool of the western Pacific up to 3 times larger than GMSL, while rates over much of the Eastern Pacific from 1993 to 2010 are near zero or negative (Beckley et al., 2010).

It is still uncertain how long such large-scale patterns of regional sea level change can last, but based on the tide-gauge records (Figure 3.12; Merrifield et al., 2009; Sturges and Douglas, 2011), large departures from the GMSL rate can persist regionally for several decades. There is growing evidence that sea level trends in different ocean basins have become more consistent over the last 20 years than in previous decades (Jevrejeva et al., 2006; Merrifield et al., 2009). In previous decades sea level change over the Southern Ocean (where they can be observed) were out of phase with the tropics and Northern Hemisphere, but after 1990, sea level rise in the Southern Ocean has been largely in phase with the rest of the world's oceans (Merrifield et al., 2009).

3.7.2 Observations of Decadal Variations and Accelerations in GMSL

Individual tide gauge record (Figures 3.13) show that large regional decadal variations exist, with deviations that are an order of magnitude larger than the global average and are often uncorrelated from one region to the other, except at the very longest periods. Whether such large decadal fluctuations also exist in GMSL is still not entirely clear. From the altimetry record, we know that significant interannual (less than 5-year) variations exist in GMSL, mainly due to ENSO (Nerem et al., 2010; Nerem et al., 1999). Many studies have attempted to quantify decadal (longer than 10-year) fluctuations in GMSL by examining trends over running 10-year or longer intervals in the GMSL time-series reconstructed from tide gauge data. While all have found significant decadal variations in GMSL (Church and White, 2006; Holgate, 2007), with rates of sea level rise in the 1930s and 1940s being higher than the present rates, the calculations from different authors disagree at more than ± 2 mm yr^{-1} before 1950, suggesting the uncertainty is still high before this period. Only for trends longer than 15 years and using data after 1950 is uncertainty (90% confidence) lower than ± 0.5 mm yr^{-1} (Church and White, 2011; Merrifield et al., 2009). While there is growing evidence that the higher trend in GMSL since 1990 is at the upper end of observed trends over the last 50 years (Church and

White, 2011; Merrifield et al., 2009), the uncertainty caused by sparse observations with large, uncorrelated decadal variations makes it impossible to determine conclusively whether similar large trends in GMSL occurred in the period between 1700 and 1950.

In light of the large decadal variability in regional sea level and still uncertain decadal variations in GMSL, it is difficult to quantify accelerations in GMSL. Estimates have been made of an acceleration term by fitting a quadratic to data at individual tide gauges (Houston and Dean, 2011; Woodworth et al., 2011; Woodworth et al., 2009) as well as to reconstructed time-series of GMSL (Church and White, 2006; Church and White, 2011; Jevrejeva et al., 2008). Church and White (2006) find that the estimated acceleration term from 1880 to 2009 is 0.009 ± 0.003 mm yr^{-2} (1 standard deviation), which is consistent with other estimates of GMSL (Jevrejeva et al., 2008), as well as from individual long tide gauges (Woodworth et al., 2011; Woodworth et al., 2009). Houston and Dean (2011) found only insignificant acceleration terms in tide gauge data along the North American coastline and some evidence of a negative acceleration; however, only a small number of tide gauges in their study extended before 1930. This result is consistent with the study of Woodworth et al. (2009) who found that the "acceleration" is better approximated by changes in the linear trend at discrete intervals, especially an increase around 1920–1930. Because of this behaviour of observed sea level, an estimated quadratic ("acceleration") term will only be significantly positive if data before 1920 are used (Rahmstorf and Vermeer, 2011), while the term will be smaller and more uncertain if only data after 1920 are used. Thus, while there is evidence of an increase in the rate of GMSL rise around 1920–1930, it is still unclear that the change is a continuous acceleration.

3.7.3 Measurements of Components of Sea Level Change

Sea level will rise as the ocean warms or water is added to it by changes in the global water cycle, run-off, or melt of ice sheets and glaciers. Tide gauges and satellite altimetry measure the combined effect of these two components. Although variations in the density related to upper-ocean salinity changes will cause regional changes in sea level, when globally averaged the effect on sea level rise is about an order of magnitude smaller than the thermal effects (Antonov et al., 2002). Most of the thermal contribution to sea level rise comes from the upper ocean (Section 3.1). Thermosteric sea level change is typically computed at annual or longer resolution from in situ temperature measurements, mainly in the upper 700 m of the ocean (Section 3.1). After correcting for the biases in older XBT data (Section 3.2), the rate of thermosteric sea level rise in the upper 700 m is 50% higher than estimates used for AR4 (Domingues et al., 2008; Wijffels et al., 2008). The warming of the upper ocean from 1970 to 2009 (Section 3.2) caused an estimated mean thermosteric rate of rise of 0.6 ± 0.2 mm yr^{-1} (90% confidence; Table 3.1, Figure 3.14b). Although still a short record, more numerous, better distributed, and higher quality CTD measurements from the Argo program are now being used to estimate the steric component above 1000 m (Cazenave et al., 2009; Leuliette and Miller, 2009; Llovel et al., 2011; Willis et al., 2008). These data are best suited for global analyses after 2005 (Leuliette and Willis, 2011). Published trends have been computed over periods from as short as 3 years and as long as 5 years, and values computed for periods after 2004 range from 0.3 to 0.8 mm yr^{-1}, with the most recent estimate from 2005 to 2010 falling in the middle (Leuliette and Willis, 2011; Table 3.1). Trends from 2005 to 2010 are still highly uncertain due to the short time-span, but are consistent with the longer-term estimates from XBTs. However, because less temporal averaging is necessary with Argo data, one can begin to measure steric changes on monthly time-scales (Figure 3.14d).

Observations of the contribution of deep-ocean warming to sea level rise are still highly uncertain due to limited historical data, especially in the Southern Ocean, and are generally computed over longer time scales and only to 3000 m depth (Levitus et al., 2005). However, using available repeat hydrographic sections occupied between 1980 and 2010, Purkey and Johnson (2010) and Kouketsu et al. (2011) have found a significant contribution from the deep ocean, with a significant fraction coming from the warming of the waters between 1000 and 4000 m within and south of the Sub-Antarctic Front (Figure 3.3a). The estimated total contribution of warming below 2000 m (below 1000 m in the Southern Ocean) to global mean sea level rise between circa 1992 and 2005 is 0.15 ± 0.10 mm yr^{-1} (95% confidence).

The mass component of mean sea level rise has only recently been measured by using satellite observations of time-variable gravity at monthly time-scales (Chambers et al., 2004). The published rates since 2003 range from 1 to 2 mm yr^{-1} (Cazenave et al., 2009; Leuliette and Miller, 2009; Leuliette and Willis, 2011; Willis et al., 2008; Willis et al., 2010), with the most recent estimate being 1.1 ± 0.6 mm yr^{-1} (90%

confidence level) from 2005 to 2010 (Leuliette and Willis, 2011; Table 3.1). This uncertainty includes that of the GIA correction required for satellite gravity measurements (Chambers et al., 2010). It will take a time-series much longer than a decade to average out significant transient interannual fluctuations in the ocean mass related to variations in the Earth's water cycle (Leuliette and Willis, 2011; Willis et al., 2008) and so determine the long-term rate of ocean mass increase with high confidence. Several studies have compared the sum of observed thermosteric and mass components with the total sea level data in order to quantify how well the sea level budget closes (Cazenave et al., 2009; Leuliette and Willis, 2011; Willis et al., 2008). Early attempts at closure suffered from problems due to biases in the altimetry (Nerem et al., 2010) and thermosteric data (Willis et al., 2010), sampling issues with the thermosteric data (Leuliette and Miller, 2009), and the GIA correction used (Chambers et al., 2010). After each of these issues has been addressed, the sea level budget closes within the uncertainty over a common time period (Leuliette and Willis, 2011; Figure 3.14d; Table 3.1), which gives increased confidence that the current ocean observing system is capable of resolving the long-term rate of sea level rise and its components, assuming continued measurements.

3.7.4 Extreme Sea Level and Storm Surges

As mean sea level rises, the frequency of events exceeding a certain threshold will increase. Since storm surge and extreme sea level events are often perceived as a regional problem, global analyses of the changes in storm surge are limited, and most reports are based on analysis of regional data (see Lowe et al., 2010 for a review). Methods used to derive changes in storm surges and extreme sea level rely either on the analysis of local tide gauge data, or on multi-decadal hindcasts of a dynamical model (WASA-Group, 1998). Most analyses have focused on specific regions and most do indicate extremes have been increasing, using various statistical measures (e.g., Church et al., 2006; D'Onofrio et al., 2008; Haigh et al., 2010; Letetrel et al., 2010; Marcos et al., 2009; Tsimplis and Shaw, 2010; Vilibic and Sepic, 2010). A global analysis of tide gauge records has been performed for data from the 1970s onwards when the 'global' data set has been reasonably copious Woodworth (Menendez and Woodworth, 2010; Woodworth and Blackman, 2004).

A primary focus of these studies is whether there is evidence for extremes having changed at different rates to MSL in recent years. Extreme sea levels have increased at most locations around the world, largely as a result of the change in MSL (Menendez and Woodworth, 2010). A related question concerns whether extreme levels have become more frequent at most locations since the 1970s. Again, while frequencies have increased, much of this is a result of the MSL change (Menendez and Woodworth, 2010) and climate signals like ENSO and NAO (e.g., Abeysirigunawardena and Walker, 2008; Haigh et al., 2010).

3.7.5 Conclusions

Globally averaged, sea level has been rising since 1900 at a rate of 1.7 ± 0.2 mm yr^{-1} (90% confidence). In some regions, changes over periods from ten to twenty years can be several times larger than this, driven by decadal changes in the large-scale winds and ocean circulation. There is growing evidence that the rate of GMSL rise since 1990 is the highest it has been over a comparable period since 1950. Thermal contributions to sea level change can only be estimated reliably since 1970 and show the upper 700 m was been contributing 0.6 ± 0.2 mm yr^{-1} of sea level change. Warming below 1000 m is likely contributing another 0.14 ± 0.08 mm yr^{-1} of sea level rise, at least since the early 1990s. Although we can now measure the two major components of sea level change (upper ocean warming and ocean mass change), reliable estimates are only available since 2005. These recent observations indicate that the sea level budget can close, so with continued measurements of sea level rise and its components, one should be able to better quantify and attribute sea level change in the future. Finally, there is increasing evidence for increasing extreme sea level and stronger storm surges in coastal areas, attributed mainly to rising mean sea level.

Table 3.1: Estimated trends in GMSL and components over different periods from representative time-series. Trends and uncertainty have been estimated from a time-series provided by the authors using ordinary least squares with the uncertainty representing the 90% confidence interval. The model fit for yearly averaged time-series was a bias + trend; the model fit for monthly and 10-day averaged data was a bias + trend + seasonal sinusoids.

Quantity	Period	Trend (mm yr-1)	Source	Resolution

GMSL	1901–2010	1.6 ± 0.2	Tide Gauge Reconstruction (Church and White, 2011)	Yearly
	1901–1990	1.5 ± 0.2	Tide Gauge Reconstruction (Church and White, 2011)	Yearly
	1971–2010	2.0 ± 0.3	Tide Gauge Reconstruction (Church and White, 2011)	Yearly
	1993–2010	2.8 ± 0.5	Tide Gauge Reconstruction (Church and White, 2011)	Yearly
	1993–2010	3.3 ± 0.2a	Altimetry (Nerem et al., 2010)	10-day
	2005–2010	2.1 ± 0.4a	Altimetry (Nerem et al., 2010)	10-day
Thermosteric Component (upper 700 m only)	1971–2010	0.6 ± 0.2	XBT Reconstruction (updated from Domingues et al., 2008)	3-year running means
	1993–2010	0.7 ± 0.3	XBT Reconstruction (updated from Domingues et al., 2008)	3-year running means
	2005–2010	0.5 ± 0.5	Argo (Leuliette and Willis, 2011)	Monthly
Thermosteric Component (below 2000 m)	1992–2005	0.15 ± 0.10b	Deep hydrographic sections (Purkey and Johnson, 2010)	Trend only
Ocean Mass Component	2005–2010	1.1 ± 0.5c	GRACE (Leuliette and Willis, 2011)	Monthly
Thermosteric + Mass	2005–2010	1.6 ± 0.5 c	GRACE + Argo (Leuliette and Willis, 2011)	Monthly

[a]Does not include potential systematic error due to drift of altimeter, estimated to be ± 0.4 mm yr-1 (Beckley et al., 2010; Nerem et al., 2010), which would increase uncertainty to ± 0.4 mm yr-1 from 1993-2010 using the root-sum-square (RSS) of the two uncertainty values.
bTrend value taken from Purkey and Johnson (2010), Table 1. Uncertainty represents the 95% confidence interval.
c Does not include potential systematic error due to GIA correction, estimated to be ± 0.3 mm yr-1 (Chambers et al., 2010), which would increase uncertainty to ± 0.6 mm yr-1 using the RSS of the two uncertainty values.

3.8 Ocean Biogeochemical Changes, Including Anthropogenic Ocean Acidification

3.8.1 Ocean Carbon

The reservoir of inorganic carbon in the ocean is roughly 60 times that of the atmosphere. Thus, even small changes in the ocean reservoir may have a significant impact on the atmospheric concentration of CO_2. The fraction of dissolved inorganic carbon (DIC) in the ocean due to increased atmospheric CO_2 concentrations (i.e., the anthropogenic CO_2, C_{ant}) cannot be measured directly but various techniques exist to infer C_{ant} from observations of interior ocean properties. Currently, approximately 25% of the CO_2 released to the atmosphere by burning of fossil fuels and land-use change enters the ocean across the air-sea interface. The global ocean inventory of C_{ant} (excluding marginal seas) in 2010 is estimated via a Green function approach to be 151 ± 26 PgC (Khatiwala et al., 2009). The corresponding uptake rate was 2.5 ± 0.6 PgC yr^{-1}, consistent with the 2.2 ± 0.6 Pg C yr^{-1} value estimated on the basis of atmospheric O_2/N_2 measurements from 1993 to 2003 (Manning and Keeling, 2006) and 2.0 ± 1.0 Pg C yr^{-1} from surface water CO_2 partial pressure (pCO_2) measurements normalized to the year 2000 (Takahashi et al., 2009). Some model outputs indicate that the sum of both the uptake of anthropogenic CO_2 emissions plus the natural carbon uptake by the oceans has increased (Le Quere et al., 2009), while others were interpreted differently with no clear trend in the rate of uptake (Gloor et al., 2010; Sarmiento et al., 2010). At the regional scale, significant spatial and temporal variations in uptake due to changes in wind, temperature, evaporation/precipitation, ocean circulation, and biological production have been observed, which are often related to climate modes such as the ENSO and NAO (Bates, 2007; Feely et al., 2006).

3.8.1.1 Long-Term Trends and Variability in the Ocean Uptake of Carbon from Observations

The air-sea flux of CO_2 is computed from the observed CO_2 partial pressure difference across the air-water interface (ΔpCO_2), the solubility of CO_2 in seawater, and the gas transfer velocity (Wanninkhof et al., 2009). Significant uncertainties exist in global and regional fluxes due to the limited geographic and temporal coverage of the ΔpCO_2 measurement as well as uncertainties in wind forcing and transfer velocity parameterizations. The air-sea flux is frequently related to climate modes such as ENSO. For example, in the Eastern and Central Equatorial Pacific increases in ΔpCO_2 between El Niño and La Niña can reach over 100 µatm (Feely et al., 2006). However, fluxes are often impacted by shorter-term forcing variability. Therefore, most regional estimates of decadal trends in fluxes are uncertain (± 50%), and no robust global trends in CO_2 fluxes based on this approach alone have been obtained. Some quantitative information on regional trends of surface ocean pCO_2 and uptake are available for selected locations.

Globally, the ΔpCO_2 remains unchanged, i.e., on average, surface ocean waters have kept pace with the atmospheric CO_2 increase although ΔpCO_2 varies geographically. While these local variations have little effect on the atmospheric CO_2 growth rate in the short term, they provide important information on changes in the functioning of the ocean and possible longer-term climate feedbacks. Regional changes in CO_2 effluxes in response to El Niño and La Niña have been observed in the Pacific, along with an appreciable overall increase in efflux in the Equatorial Pacific since 1998–2000 due a change in circulation associated with the Pacific Decadal Oscillation (PDO) and increasing winds (Feely et al., 2006). The North Atlantic has seen a dramatic decrease in CO_2 uptake of 0.24 Pg C yr^{-1} over the decade from 1994 to 2003 (Schuster and Watson, 2007) with a partial recovery since then (Watson et al., 2009). No clear correlation with the predominant climate index in the North Atlantic, the NAO, has been found, although Bates (2007) suggests that several indices contribute to the flux anomalies, often with appreciable lags. The Southern Ocean has seen decreased uptake in response to SAM related increases in wind that in turn have increased surface divergence, upwelling and outgassing of natural CO_2 (Metzl, 2009).

3.8.1.2 Variations in CO_2 Inventories with Time over the Past Four Decades

Three independent data-based estimates for the global ocean inventory of C_{ant} for the reference year 1994 are now available: (1) 106 ± 17 PgC based on the ΔC^* method (Sabine et al., 2004); (2) 107 ± 14 PgC based on the transit time distribution (TTD) method (Waugh et al., 2006); and (3) 114 ± 22 PgC using a Green function approach (Khatiwala et al., 2009). All three approaches assume steady state ocean circulation and use tracer information, which tends to underestimate natural variability and changes in ocean biogeochemistry. The first two methods additionally assume constant air-sea disequilibrium of CO_2 over the industrial period while the third approach relaxes this assumption, resulting in a time-evolving reconstruction of C_{ant} in the ocean over the industrial period. Even though these estimates agree within their uncertainty, there are significant differences in the distribution of C_{ant}, particularly at high latitudes. An update of the third approach for 2010 yields a global inventory of 151 ± 26 PgC (Figure 3.15).

[INSERT FIGURE 3.15 HERE]

Figure 3.15: Compilation of the 2010 column inventories (mol m^{-2}) of anthropogenic CO_2: the global Ocean excluding the marginal seas (updated from Khatiwala et al., 2009) 151 ± 26 PgC; Arctic Ocean (Tanhua et al., 2009) 2.6 – 3.4 PgC; the Nordic Seas (Olsen et al., 2010) 1.0 – 1.5 PgC; the Mediterranean Sea (Schneider et al., 2010) 1.5 – 2.4 PgC; the East Sea (Sea of Japan) (Park et al., 2006) 0.40 ± 0.06 Pg C.

Perturbations in oceanic DIC concentrations due to anthropogenically forced changes in large-scale circulation, ventilation, or biological activity are not considered in these estimates, although errors introduced due to neglecting these changes are likely much smaller than the inherent uncertainty of the methods. The change in DIC or C_{ant} concentration between two time periods, i.e., the storage rate, is less dependent on such assumptions. Regional observations of the storage rate are in broad agreement with the expected storage rate of C_{ant} resulting from the increase in atmospheric CO_2 concentrations, but with significant spatial and temporal variations (Figure 3.16); i.e., the North Atlantic is an area with high variability in circulation and deep water formation, influencing the C_{ant} inventory and its changes. As a result of the decline in the Labrador Sea Water (LSW) formation rates since 1997 (Rhein et al., 2011), the C_{ant} increase between 1997 and 2003 was smaller in the subpolar North Atlantic than expected from the atmospheric increase, in contrast to the subtropical and equatorial Atlantic (Steinfeldt et al., 2009). Perez et al. (2010a) also noticed the dependence of the C_{ant} storage rate in the North Atlantic on the NAO, with high C_{ant} storage rate during phases of high NAO (i.e., high LSW formation rates) and low storage during phases of low NAO (low formation). Wanninkhof et al. (2010) confirmed the lower inventory increase in the North Atlantic compared to the South Atlantic.

[INSERT FIGURE 3.16 HERE]

Figure 3.16: Top: maps of storage rate distribution of anthropogenic carbon (mol m^{-2} y^{-1}) for the three ocean basins (Atlantic, Pacific, and Indian Ocean) averaged over 1980–2005 estimated by the Green function approach (Khatiwala et al., 2009). Bottom: Corresponding storage rates as observed from repeat hydrography cruises. Measurements for the northern hemisphere are drawn as solid lines, the tropics as dash-dotted lines, and dashed lines for the southern hemisphere; the color schemes refer to different studies. Estimates of uncertainties are shown as vertical bars with matching colors on the right hand side of the panels. The solid black line represents the basin average storage rate using the same Green function approach (Khatiwala et al., 2009). Data sources as indicated in the legend are: 1) (Wanninkhof et al., 2010), 2) (Murata et al., 2008), 3) (Friis et al., 2005), 4) (Tanhua et al., 2007), 5) (Olsen et al., 2006), 6) (Perez et al., 2008), 7) (Murata et al., 2007), 8) (Murata et al., 2009), 9) (Sabine et al., 2008), 10) (Peng et al., 2003), 11) (Wakita et al., 2010), 12) (Matear and McNeil, 2003), 13) (Peng et al., 1998), and 14) (Murata et al., 2010).

3.8.2 Anthropogenic Ocean Acidification

The uptake of carbon dioxide by the ocean changes the chemical balance of seawater through the thermodynamic equilibrium of CO_2 with seawater. Dissolved CO_2 forms a weak acid and, as CO_2 in seawater increases, the pH and carbonate ion concentration $[CO_3^{2-}]$ of seawater decrease. The mean pH of surface waters ranges between 7.8 and 8.4 in the open ocean, so the ocean remains mildly basic (pH>7) at present (Orr et al., 2005). Ocean uptake of CO_2 results in gradual acidification of seawater; this process is termed ocean acidification (Caldeira and Wickett, 2003). A decrease in ocean pH of 0.1 corresponds to a 26% increase in the concentration of H^+ in seawater. The consequences of changes in pH, carbonate ion, and saturation states for $CaCO_3$ minerals on marine organisms and ecosystems remain poorly understood.

Direct observations of oceanic dissolved inorganic carbon (DIC = CO_2 + carbonate + bicarbonate) and computed partial pressure of CO_2 (pCO_2) reflect changes in both the natural carbon cycle and the uptake of anthropogenic CO_2 from the atmosphere. Ocean time series stations in the North Atlantic and North Pacific record decreasing pH (Figure 3.17) with rates ranging between -0.0015 and -0.0024 per year (Bates, 2007; Dore et al., 2009; Gonzalez-Davila et al., 2010; Olafsson et al., 2009; Santana-Casiano et al., 2007). The greatest change occurs in the western subtropical North Atlantic and in the Iceland Sea during winter. Directly measured pH differences in the surface mixed layer along repeat transects in the central North Pacific Ocean where pH measurements between Hawaii and Alaska showed a -0.0017 yr^{-1} decline in pH between 1991 and 2006, which is in agreement with observations at the time series sites (Figure 3.16, Table 3.1, Byrne et al., 2010). This rate of pH change was also consistent with the repeat transects of CO_2 and pH measurements in the western Pacific (winter: -0.0018 ± 0.0002 yr^{-1}; summer: -0.0013 ± 0.0005 yr^{-1}) (Midorikawa et al., 2010).

[INSERT FIGURE 3.17 HERE]

Figure 3.17: Long-term trends of surface seawater pCO_2 (top), pH (middle), and carbonate ion (bottom) concentration at three subtropical ocean time series in the North Atlantic and North Pacific Oceans, including: **a)** Bermuda Atlantic Time-series Study (BATS, 31°40′N, 64°10′W; **green**) and Hydrostation S (32°10′, 64°30′W) from 1983 to present (published and updated from Bates, 2007); **b)** Hawaii Ocean Time-series (HOT) at Station ALOHA (A Long-term Oligotrophic Habitat Assessment; 22°45′N, 158°00′W; **orange**) from 1988 to present (published and updated from Dore et al., 2009), and; **c)** European Station for Time-series in the Ocean (ESTOC, 29°10′N, 15°30′W; **blue**) from 1994 to present (published and updated from Gonzalez-Davila et al., 2010). Atmospheric pCO_2 (**black**) from Hawaii is shown in the top panel. Lines show linear fits to the data, whereas Table 3.2 give results for harmonic fits to the data (updated from Orr, 2011).

Seawater chemistry changes at the ocean time series sites and in the North Pacific Ocean result from uptake of anthropogenic CO_2 (Doney et al., 2009), but also include other changes imparted by local physical and biological variability. As an example, while pH changes in the mixed layer of the North Pacific Ocean can be explained solely in terms of equilibration with atmospheric CO_2, declines in pH between 800 m and the mixed layer between 1991 and 2006 were attributed in approximately equal measure to anthropogenic and natural variations (Byrne et al., 2010). Figure 3.18 (Byrne et al., 2010) shows pH changes between the surface and 1000 m that were attributed solely to the effects of anthropogenic CO_2. The summary observations given in Table 3.1, which include both anthropogenic and natural variations, show that seawater pH and $[CO_3^{2-}]$ have decreased by 0.03–0.04 and ~8–10 µmoles kg^{-1}, respectively, over the last 20 years (Table 3.2: 1988–2009 trends). Over longer time periods, anthropogenic changes in ocean chemistry are likely to become increasingly prominent relative to changes imparted by physical and biological variability. An anthropogenically induced decrease in surface water pH of 0.08 from 1765 to 1994 for the global ocean was calculated from the estimated uptake of atmospheric CO_2 (Sabine et al., 2004), with the largest reduction (-0.10) in the northern North Atlantic and the smallest reduction (-0.05) in the subtropical South Pacific. These results are consistent with the generally lower buffer capacities of the high latitude oceans compared to lower latitudes (Egleston et al., 2010).

[START BOX 3.2 HERE]

Box 3.2: Ocean Acidification

What is ocean acidification? Ocean acidification refers to a reduction in pH of the ocean over an extended period, typically decades or longer, caused primarily by the uptake of carbon dioxide from the atmosphere. Ocean acidification can also be caused by other chemical additions or subtractions from the oceans that are natural (e.g., increased volcanic activity, methane hydrate releases, long-term changes in net respiration) or human-induced (e.g., release of nitrogen and sulfur compounds into the atmosphere). Anthropogenic ocean acidification refers to the component of pH reduction that is caused by human activity.

Since the beginning of the industrial era, the release of carbon dioxide (CO_2) from our collective industrial and agricultural activities has resulted in atmospheric CO_2 concentrations that have increased from approximately 280 ppm to about 392 ppm. The atmospheric concentration of CO_2 is now higher than experienced on Earth for at least the last 800,000 years and is expected to continue to rise (Luthi et al., 2008). The oceans have absorbed approximately 150 billion tons of carbon from the atmosphere over the last two and a half centuries (Le Quere et al., 2009). This natural process of absorption has benefited humankind by significantly reducing the greenhouse gas levels in the atmosphere and minimizing some of the impacts of global warming. However, the ocean's uptake of carbon dioxide is having a significant impact on the chemistry of seawater. The average pH of ocean surface waters has already fallen by about 0.1 units, from about 8.2 to 8.1, since the beginning of the industrial revolution (Feely et al., 2009; Orr et al., 2005; Figure 1). Estimates of future atmospheric and oceanic carbon dioxide concentrations indicate that, by the end of this century, the average surface ocean pH could be lower than it has been for more than 20 million years (Caldeira and Wickett, 2003).

The major controls on seawater pH are atmospheric CO_2 exchange, the production and remineralization of dissolved and particulate organic matter in the water column, and the formation and dissolution of calcium carbonate minerals. Oxidation of organic matter lowers dissolved oxygen concentrations, adds CO_2 to solution, reduces carbonate ion, and lowers the pH of seawater in subsurface waters (Byrne et al., 2010). As a result of these processes, minimum pH values in the oceanic water column are generally found near the depths of the oxygen minimum layer. When CO_2 reacts with seawater it forms carbonic acid which is highly reactive and reduces the concentration of carbonate ion, critical to shell formation for marine animals such as corals, plankton, and shellfish. This process could affect some of the most fundamental biological and chemical processes of the sea in coming decades (Doney et al., 2009; Fabry et al., 2008).

Anthropogenic ocean acidification may produce far-reaching consequences of the buildup of human-induced carbon dioxide in the atmosphere. Results from laboratory, field, and modeling studies, as well as evidence from the geological record, clearly indicate that marine ecosystems are highly susceptible to the increases in oceanic CO_2 and the corresponding decreases in pH and carbonate ion (Doney et al., 2009; Fabry et al., 2008). While some species, such as seagrasses, appear to benefit from ocean acidification, many calcifying species such as clams, oysters, and corals will be increasingly affected by a decreased capability to produce their shells or skeletons (Hendriks et al., 2010; Kroeker et al., 2010). Other species of fish and shellfish will also be negatively impacted in their physiological responses due to a decrease in pH levels. Ocean acidification is an emerging scientific issue and much research is needed before all of the ecosystems responses are well understood. However, to the limit that the scientific community understands this issue right now, the potential for environmental, economic, and societal risks is high (Cooley et al., 2009)

[INSERT BOX 3.2, FIGURE 1 HERE]

Box 3.2, Figure 1: National Center for Atmospheric Research Community Climate System Model 3.1 (CCSM3)-modeled decadal mean pH at the sea surface centered around the years 1875 (top) and 1995 (middle). Global Ocean Data Analysis Project (GLODAP)-based pH at the sea surface, nominally for 1995 (bottom). Deep coral reefs are indicated with darker gray dots; shallow-water coral reefs are indicated with lighter gray dots. White areas indicate regions with no data (after Feely et al., 2009).

[INSERT BOX 3.2, FIGURE 2 HERE]

Box 3.2, Figure 2: Distribution of: **a)** pH and **b)** CO_3^{2-} ion concentration in the Pacific, Atlantic, and Indian oceans. The data are from the World Ocean Circulation Experiment/Joint Global Ocean Flux Study/Ocean Atmosphere Carbon Exchange Study global CO_2 survey (Sabine, 2005). The lines show the mean pH (solid line to panel), aragonite (solid line bottom panel), and calcite (dashed line bottom panel) saturation CO_3^{2-} concentration for each of these basins (modified from Feely et al., 2009).

[END BOX 3.2 HERE]

[INSERT FIGURE 3.18 HERE]

Figure 3.18: ΔpH_{ant}: pH change attributed to the uptake of anthropogenic carbon between 1991 and 2006, at about 150°W, Pacific Ocean (from Byrne et al., 2010).

Table 3.2: Published and updated long-term trends of atmospheric (pCO_2^{atm}) and seawater carbonate chemistry (i.e., surface-water pCO_2, pH, $[CO_3^{2-}]$, and aragonite saturation state Ω_a) at four ocean time series in the North Atlantic and North Pacific oceans: (1) Bermuda Atlantic Time-series Study (BATS, 31°40′N, 64°10′W) and Hydrostation S (32°10′, 64°30′W) from 1983 to present (Bates, 2007); (2) Hawaii Ocean Time-series (HOT) at Station ALOHA (A Long-term Oligotrophic Habitat Assessment; 22°45′N, 158°00′W) from 1988 to present (Dore et al., 2009); (3) European Station for Time-series in the Ocean (ESTOC, 29°10′N, 15°30′W) from 1994 to present (Gonzalez-Davila et al., 2010); and (4) Iceland Sea (IS, 68.0°N, 12.67°W) from 1985 to 2006 (Olafsson et al., 2009). Trends at the first three time series site are from observations that have been seasonally detrended. Also reported are the wintertime trends in the Iceland Sea as well as the pH difference trend for the North Pacific Ocean between transects in 1991 and 2006 (Byrne et al., 2010) and repeat sections in the western North Pacific between 1983 and 2008 (Midorikawa et al., 2010).

Site	Period	pCO_2^{atm} (μatm yr^{-1})	pCO_2^{sea} (μatm yr^{-1})	pH^* (yr^{-1})	$[CO_3^{2-}]$ (μmol kg^{-1} yr^{-1})	Ω_a (yr^{-1})
a. published trends						
BATS	1983–2005[a]	1.78 ± 0.02	1.67 ± 0.28	-0.0017 ± 0.0003	-0.47 ± 0.09	-0.007 ± 0.002
	1983–2005[b]	1.80 ± 0.02	1.80 ± 0.13	-0.0017 ± 0.0001	-0.52 ± 0.02	-0.006 ± 0.001
ALOHA	1988–2007[c]	1.68 ± 0.03	1.88 ± 0.16	-0.0019 ± 0.0002	-	-0.0076 ± 0.0015
	1998–2007[d]	-	-	-0.0014 ± 0.0002	-	-
ESTOC	1995–2004[e]	-	1.55 ± 0.43	-0.0017 ± 0.0004	-	-
	1995–2004[f]	1.6 ± 0.7	1.55	-0.0015 ± 0.0007	-0.90 ± 0.08	-0.0140 ± 0.0018
IS	1985–2006[g]	1.69 ± 0.04	2.15 ± 0.16	-0.0024 ± 0.0002	-	-0.0072 ± 0.0007[g]
N.Pacific	1991–2006[h]	-	-	-0.0017	-	-
N.Pacific	1983–2008[i]	Summer 1.54 ± 0.08 Winter 1.65 ± 0.05	Summer 1.37 ± 0.33 Winter 1.58 ± 0.12	Summer -0.0013 ± 0.0005 Winter -0.0018 ± 0.0002		
Coast of western N.Pacific	1994-2008[k]	1.99 ± 0.02	1.54 ± 0.33	0.0020 ± 0.0007		-0.012 ± 0.005

b.updated trends[j,l]						
BATS	1983–2009	1.66 ± 0.01	1.92 ± 0.08	-0.0019 ± 0.0001	-0.59 ± 0.04	-0.0091 ± 0.0006
	1985–2009	1.67 ± 0.01	2.02 ± 0.08	-0.0020 ± 0.0001	-0.68 ± 0.04	-0.0105 ± 0.0006
	1988–2009	1.73 ± 0.01	2.22 ± 0.11	-0.0022 ± 0.0001	-0.87 ± 0.05	-0.0135 ± 0.0008
	1995–2009	1.90 ± 0.01	2.16 ± 0.18	-0.0021 ± 0.0002	-0.80 ± 0.08	-0.0125 ± 0.0013
ALOHA	1988–2009	1.73 ± 0.01	1.82 ± 0.07	-0.0018 ± 0.0001	-0.52 ± 0.04	-0.0083 ± 0.0007
	1995–2009	1.92 ± 0.01	1.58 ± 0.13	-0.0015 ± 0.0001	-0.40 ± 0.07	-0.0061 ± 0.0028
ESTOC	1995–2009	1.88 ± 0.02	1.83 ± 0.15	-0.0017 ± 0.0001	-0.72 ± 0.05	-0.0123 ± 0.0015
IS	1985–2009[l]	1.75 ± 0.01	2.07 ± 0.15	-0.0024 ± 0.0002	-0.47 ± 0.04	-0.0071 ± 0.0006
	1988–2009[l]	1.70 ± 0.01	1.96 ± 0.22	-0.0023 ± 0.0003	-0.48 ± 0.05	-0.0073 ± 0.0008
	1995–2009[l]	1.90 ± 0.01	2.01 ± 0.37	-0.0022 ± 0.0004	-0.40 ± 0.08	-0.0062 ± 0.0012

[*]pH on the total scale
[a]Bates (2007, Table 1) - simple linear fit
[a]Bates (2007, Table 2) - seasonally detrended (including linear term for time)
[c]Dore et al. (2009) - linear fit with calculated pH and pCO2 from measured DIC and TA(full time series); corresponding Ω_a from Feely et al. (2009)
[d]Dore et al. (2009) - linear fit with measured pH (partial time series)
[e]Santana-Casiano et al. (2007) - seasonal detrending (including linear terms for time and temperature)
[f]González-Dávila et al. (2010) - seasonal detrending (including linear terms for time, temperature, and mixed-layer depth)
[g]Olafsson et al. (2009) - multivariable linear regression (linear terms for time and temperature) for winter data only
[h]Byrne et al. (2010) - meridional section originally occupied in 1991 and repeated in 2006
[i]Midorikawa et al. (2010) - winter and summer observations along 137°E
[j]Trends are for linear time term in seasonal detrending with harmonic periods of 12, 6, and 4 months. Harmonic analysis made after interpolating data to regular monthly grids (except for IS, which was sampled much less frequently):
1983–2009 = Sep 1983 to Dec 2009 (BATS/Hydrostation S sampling period),
1985–2009 = Feb 1985 to Dec 2009 (IS sampling period),
1988–2009 = Nov 1988 to Dec 2009 (ALOHA/HOT sampling period), and
1995–2009 = Sep 1995 to Dec 2009 (ESTOC sampling period).
[k]Ishii et al (2011) - seasonally detrended time-series observations in the coast of western N. Pacific
[l]Atmospheric pCO_2 trends computed from same harmonic analysis (12-, 6-, and 4-month periods) on the GLOBALVIEW-CO2 (2010) data product for the marine boundary layer referenced to the latitude of the nearest atmospheric measurement station (BME for Bermuda, MLO for ALOHA, IZO for ESTOC, and ICE for Iceland)
[l]Winter ocean data, collected during dark period (between 19 January and 7 March), as per Olafsson et al. (2009) to reduce scatter from large interannual variations in intense short-term bloom events, undersampled in time, fit linearly (y=at+bT+c)

3.8.3 Oxygen

The assessment of long-term changes in dissolved oxygen is limited by data quality issues, and the general sparseness of marine observations. Nevertheless, thanks to the early introduction of standardized methods and the relatively wide interest in the distribution of oxygen, the historical record of marine oxygen observations is richer than that of nearly all other biogeochemical parameters. To date, the most thorough assessment of global-scale oxygen changes in open ocean environments reveals overall a decreasing trend in the last 20–50 years, i.e., a large-scale deoxygenation of the ocean's thermocline at a rate of about 3–5 µmol kg^{-1} $decade^{-1}$, but with strong regional differences (Keeling et al., 2010).

The long-term deoxygenation of the open ocean thermocline is consistent with the expectation that warmer waters can hold less oxygen (solubility effect), and that warming-induced stratification leads to a decrease in the resupply of oxygen into the thermocline from near surface waters (stratification effect). Models suggest a heat uptake to oxygen loss ratio of about 6 to 7 nmol O_2 per joule of warming, which is about twice the value expected from the reduction of the oxygen solubility alone, meaning that increased stratification is of about equal importance as the solubility effect. Detailed analysis of time series records from a few selected spots with sufficient data coverage in the tropical ocean reveals negative trends for the last 50 years in all ocean basins (Stramma et al., 2008), resulting in a substantial expansion of the oxygen minimum zones there. A more spatially expansive analysis conducted by comparing data between 1960 and 1974 with those from 1990 to 2008 supports the spot analysis in that it identified oxygen decreases in most tropical regions with an average rate of 2–3 μmol kg^{-1} $decade^{-1}$ (Stramma et al., 2010). Also, many observations from the high latitudes tend to suggest decreasing oxygen levels (Keeling et al., 2010). Observations from one of the longest time series sites in the subpolar North Pacific (Station Papa, 50°N, 145°W) reveal a persistent declining trend in the thermocline for the last 50 years (Whitney et al., 2007), although this trend is superimposed on oscillations on timescales of a few years to two decades. Several tropical open ocean regions in the Atlantic, Indian and Pacific have also experienced a decrease in dissolved oxygen in the thermocline (Stramma et al., 2010; Figure 3.19).

[INSERT FIGURE 3.19 HERE]

Figure 3.19: Dissolved oxygen (DO) distributions (in μmol kg^{-1}) between 40°S and 40°N for: **a)** the climatological mean (World Ocean Database 2005) at 200 dbar, as well as changes between 1960 and 1974 and 1990 and 2008 of **b)** dissoved oxygen (ΔDO) at 200 dbar, **c)** apparent oxygen utilization at 200 dbar relative to oxgen saturation at the surface, and **d)** ΔDO vertically-averaged over 200–700 dbar. In **b)-d)** increases are red and decreases blue, and areas with differences below the 95% confidence interval are shaded by black horizontal lines (after Stramma et al., 2010).

Coastal regions have also experienced long-term oxygen changes. Bograd et al. (2008) reported a substantial reduction of the thermocline oxygen content in the southern part of the California Current from 1984 until 2002, resulting in a shoaling of the hypoxic boundary (60 μmol kg^{-1}). Off the Oregon coast, previously unreported hypoxic conditions have been observed on the inner shelf since 2000, with hypoxia being especially severe in 2006 (Chan et al., 2008). These changes along the west coast of North America appear to have been largely caused by the open ocean oxygen decrease and local processes associated with decreased vertical oxygen transport following near-surface warming and increased stratification. Gilbert et al. (2010) found evidence for greater oxygen decline rates in the coastal ocean than in the open ocean.

In nearshore areas, the analysis of oxygen changes has largely been driven by the observation of a strong increase in the number of hypoxic zones since the 1960s (Diaz and Rosenberg, 2008). The formation of hypoxic zones has been exacerbated by the increase of primary production and consequent worldwide coastal eutrophication fueled by riverine runoff of fertilizers and the burning of fossil fuels.

3.8.4 Regional and Long-Term Trends in Nutrient Distributions in the Oceans

Human impacts and shifting physical processes are altering the supply of nutrients to the oceans, thereby exerting a control on the magnitude and variability of the ocean's biological carbon pump. The large-scale warming of the surface oceans increase stratification (Section 3.2), thereby decreasing ventilation (Section 3.5) and the upward vertical flux of nutrients and, in low latitudes, reducing primary production. Satellite observations of chlorophyll found that oligotrophic gyres in four of the world’s major oceans expanded at average rates of 0.8% to 4.3% yr^{-1} from 1998 to 2006. consistent with reduced nutrient availability. In the ocean’s thermocline, given the current rate of deoxygenation and Redfield stoichiometry, nitrate and phosphate are expected to increase at rates of ~0.3–0.6 and ~0.02–0.04 μmol kg^{-1} $decade^{-1}$, respectively. This hypothesis was used to partially explain trends of increasing nutrient concentrations in upwelled water (Pérez et al., 2010b), and has been found in modeling studies (Rykaczewski and Dunne, 2010). Superimposed on the long-term trends are large interannual and multi-decadal fluctuations in nutrients. Modeling and observational studies demonstrate that these fluctuations are coupled with eddy pumping, and variability of mode water and the NAO in the Atlantic Ocean (Cianca et al., 2007; Pérez et al., 2010a); climate modes of variability in the Pacific Ocean (Di Lorenzo et al., 2009; Wong et al., 2007); and variability of subtropical gyre circulation in the Indian Ocean (Álvarez et al., 2011). As a likely consequence, recent changes in global net primary production have been dominated by natural, multi-year oscillations (e.g., ENSO) and clearly show the close coupling between ocean ecology and climate (Behrenfeld et al., 2006; Chavez et al., 2011).

3.8.5 Summary

The global ocean inventory of anthropogenic carbon in 2010 is estimated to be 151 ± 26 PgC, with a corresponding annual global uptake rate of 2.5 ± 0.6 PgC yr^{-1}. Ocean uptake of CO_2 results in gradual acidification of seawater and decreasing pH (i.e., anthropogenic ocean acidification) in surface waters with rates ranging between -0.0015 and -0.0024 per year. The long-term deoxygenation of the open ocean thermocline is consistent with the expectation that warmer waters can hold less oxygen, and that warming-induced stratification leads to a decrease in the resupply of oxygen into the thermocline from near surface waters. Models suggest a heat uptake to oxygen loss ratio of about 6 to 7 nmol O_2 per joule of warming, which is about twice the value expected from the reduction of the oxygen solubility alone, meaning that increased stratification is of about equal importance as the solubility effect. These results are consistent with the increasing supply of nitrate and phosphate in the thermocline.

3.9 Synthesis

Substantial progress has been made since AR4 in documenting and understanding change in the ocean. The major findings of this chapter are largely consistent with those in AR4, but in many cases statements can now be made with a greater degree of confidence. The level of confidence has increased because more data are available, biases in historical data have been identified and reduced, and new analytical approaches have been applied.

Significant changes have been observed in a number of ocean properties of relevance to climate (Figure 3.20). It is virtually certain that global mean sea level and the ocean inventory of anthropogenic carbon dioxide have increased since at least 1950, and that ocean heat content has increased since 1970 (when sufficient observations became available to make global estimates). It is likely that sea surface salinity has increased in regions where the salinity exceeds the global mean surface salinity and decreased in regions where salinity is less than the global mean value. The amplification of the contrast between regions of high and low sea surface salinity is consistent with expectations of an intensification of the global water cycle in a warming climate.

[INSERT FIGURE 3.20 HERE]

Figure 3.20: Time series of changes in large-scale ocean climate properties. Global ocean inventory of anthropogenic carbon dioxide is updated from Khatiwala et al. (2009). Global upper ocean heat content anomaly is updated from Domingues et al. (2008). Global mean sea level (GMSL) is from Church and White (2011). “High salinity” refers to the salinity averaged over regions where the sea surface salinity is greater than the global mean sea surface salinity from the World Ocean Database (2009) and "Low Salinity" to an average over regions with values below the global mean. Time series amplitudes are normalized by the differences between the last and first years of the records for easier comparison of trends in different properties.

Trends have been detected in a number of subsurface water properties, with varying levels of confidence (Figure 3.21). There is compelling and robust evidence that most of the ocean above 1000 m has warmed over at least the last forty years, with the strongest warming observed near the sea surface. There is high confidence in the rate and pattern of sea level rise since 1993 (top panel, Figure 3.20) based on near-global coverage of satellite altimetry and the agreement with independent measurements from tide gauges and estimates of thermal expansion. While salinity observations are less abundant than temperature observations, the high agreement between different analyses provides medium confidence that subsurface salinity has changed, with water masses formed and subducted in the precipitation-dominated mid- to high-latitudes becoming fresher, while water masses formed in the evaporation-dominated subtropics becoming saltier. Anthropogenic carbon dioxide is accumulating in surface waters and being carried into the interior, primarily by water masses formed in the North Atlantic and Southern Oceans. The accumulation of anthropogenic CO_2 is virtually certain to have caused the observed decline of pH and $CO_3^{=}$ in surface waters. As a result of changes in the temperature and salinity of surface waters, the density of the surface ocean has decreased, strengthening the stratification in the upper ocean. Observations of a decline in oxygen in thermocline waters in much of the global ocean are consistent with a reduction in ventilation caused by the increase in stratification, although the more limited oxygen data set means we have lower confidence in oxygen changes than for temperature and salinity. It is likely that the tropical oxygen minimum zones have expanded in recent decades.

[INSERT FIGURE 3.21 HERE]

Figure 3.21: Summary of observed changes in zonal averages of global ocean properties. Temperature trends (°C decade^{-1}) are indicated in color (red = warming, blue = cooling); salinity trends are indicated by contour lines (dashed = fresher; solid = saltier) for the upper 2000 m of the water column (50-year trends from data set of Durack and Wijffels (2010); trends significant at >90% confidence are shown). Arrows indicate primary ventilation pathways. The top panel shows the zonal mean trend in sea level from 1993-2007 from satellite altimetry (Merrifield et al., 2009). Changes in other physical and chemical properties are summarised to the right of the figure, for each depth range (broken axes symbols delimit changes in vertical scale). Increases are shown in red, followed by a plus sign; decreases are shown in blue, followed by a minus sign; the number of + and – signs indicates the level of confidence associated with the

observation of change (+++ = high confidence; ++ = medium confidence; + = low confidence). T = temperature, S = salinity, Strat = stratification, C_{ANT} = anthropogenic carbon, $CO_3^{=}$ = carbonate ion, NA = North Atlantic, SO = Southern Ocean, AABW = Antarctic Bottom Water. $S > \overline{S}$ refers to the salinity averaged over regions where the sea surface salinity is greater than the global mean sea surface salinity; $S < \overline{S}$ refers to the average over regions with values below the global mean.

The largest changes in the ocean inventory of heat, freshwater, anthropogenic carbon dioxide and other properties are observed along known ventilation pathways, where surface waters are transferred to the ocean interior, or in regions where changes in ocean circulation (e.g., contraction or expansion of gyres, or a southward shift of the Antarctic Circumpolar Current) result in large anomalies. The fact that the changes observed in a number of independent variables are consistent with each other and with well-understood dynamics of ocean circulation enhances confidence in the conclusion that the ocean state has changed.

For other properties of the ocean, the short and incomplete observational record is not sufficient to detect trends. For example, there is no observational evidence for or against a change in the strength of the AMOC, based on the short records presently available. However, recent observations have strengthened evidence for variability in major ocean circulation systems and water mass properties on time scales from years to decades. Much of the variability observed in ocean currents and in water masses can be linked to changes in surface forcing, including wind changes associated with the major modes of climate variability such as the NAO, SAM, ENSO, and the PDO.

Taken together, the observations summarised here give very high confidence that the physical and biogeochemical state of the oceans has changed. The spatial patterns of change are consistent with changes in the surface ocean (warming, changes in salinity and an increase in C_{ant}) and the subsequent propagation of anomalies into the ocean interior along ventilation pathways.

While improvements in the quality and quantity of ocean observations strengthen and extend conclusions reached in AR4, substantial uncertainties remain. In many cases, the observational record is still too short or incomplete to detect trends in the presence of energetic variability on time-scales of years to decades. Recent improvements in the ocean observing system, most notably the Argo profiling float array, mean that temperature and salinity are now being sampled routinely in most of the ocean above 2000 m depth for the first time. However, sparse sampling of the deep ocean and of many biogeochemical variables continues to limit our ability to detect and understand changes in the global ocean. Sustained global-scale observations will increase confidence in the assessment of ocean change, improve the ability to detect and attribute climate change, and provide guidance for improvement of climate models.

[START FAQ 3.1 HERE]

FAQ 3.1: Is the Ocean Warming?

Yes, the ocean is warming, although neither everywhere and nor constantly. The signature of warming emerges most clearly when considering long times (a decade or more) for averages over the whole globe.

Over time scales longer than a decade the average temperature of the upper ocean has increased at least since 1970, when data coverage began to be adequate for estimating global averages. Observations also suggest that the deepest and coldest waters of the world ocean have in general been warming since around 1990. Ocean temperature in a given location, on the other hand, can vary largely with the march of the seasons and can also fluctuate substantially from year-to-year or even decade-to-decade owing to variability in the heat exchange between ocean and atmosphere as well as variations in ocean currents.

Archived historical ocean temperature measurements extend back for centuries, but not until around 1970 are the measurements in any given year sufficient in number and sufficiently global in their spatial distribution to estimate global upper ocean temperature with high confidence. In fact, before the Argo program first achieved global coverage in 2004, the global average upper ocean temperature anomaly for any given year is sensitive to the methodology used to estimate it. In spite of the large uncertainty for most yearly means, the increase of the global mean over decadal time scales since 1970 is a robust result.

Temperature anomalies enter the subsurface ocean by multiple paths (FAQ3.1, Figure 1). In addition to mixing from above, colder waters from high latitude regions can sink down from the surface and slide equatorward under warmer waters from more tropical regions. As these sinking waters become warmer, they increase temperatures in the deep ocean much more quickly than would downward mixing of surface heating alone. There are a few locations — in the northern North Atlantic Ocean and the Southern Ocean around Antarctica — where ocean water is cooled enough so that it sinks to great depths, even to the ocean bottom. It spreads out from these locations to fill much of the rest of the deep ocean. The temperature of these deep waters varies from decade to decade in the North Atlantic, sometimes warming, sometimes cooling, depending on the prevailing winter atmospheric patterns there. Around Antarctica, the bottom waters appear to have been warming relatively fast since at least 1990, perhaps owing to the strengthening and poleward shift of the westerly winds around the Southern Ocean over the last several decades.

[INSERT FAQ 3.1, FIGURE 1 HERE]

FAQ 3.1, Figure 1: Ocean variability pathways. The ocean is stratified, with the coldest water in the deep ocean (lower panels, use upper right panel for orientation). Antarctic Bottom Water (dark blue) sinks around Antarctica and spreading northward along the ocean floor into the central Pacific (left, red arrow fading to white indicating warming with time) and western Atlantic (right, red arrow fading to white indicating warming with time) oceans, as well as the Indian Ocean (not shown). North Atlantic Deep Water, slightly warmer and lighter (lighter blue) sinks in the northern North Atlantic Ocean (right, red and blue arrow indicating decadal warming and cooling) and spreads south above the Antarctic Bottom Water and then around Antarctica and into the Pacific and Indian Oceans. Similarly, in the upper ocean (upper left panel, only Southern Hemisphere shown, but Northern Hemisphere similar) Intermediate Waters, still warmer (cyan) sink in subpolar regions (red arrows indicating warming with time) and slip equatorward under Subtropical Waters, yet warmer (green), which in turn sink (red arrows indicating warming with time) slip equatorward under tropical waters, the warmest and lightest (orange) in all three oceans. Excess heat or cold entering at the ocean surface (top squiggly red arrows) also mixes slowly downward (interior squiggly red arrows).

Estimates of change in global average ocean temperature have improved since AR4, largely through reductions in systematic measurement errors. Careful comparison of less accurate measurements with sparser but more accurate ones at nearby locations and times has made the historical record more consistent and removed spurious variability. With the biases ameliorated, it is seen that the global average ocean temperature has increased much more steadily from year to year than what was reported in AR4. However, the global average warming rate may not be uniform in time: There are years when it appears faster than average, and years where it seems to slow to almost nothing.

From the ocean surface to about 60-m depth, the global average ocean warming trend has been around 0.1°C per decade for the period 1970–2009. The global average upper ocean warming trend generally gets smaller from the surface to mid-depth, reducing to about 0.04°C per decade by 200 m and under 0.02°C per decade by 500 m. While the deep warming rates can also be small (for instance about 0.03°C per decade since the 1990s in the deep and bottom waters around Antarctica, and smaller in many other locations), they occur over a large volume, so the deep ocean warming contributes a notable fraction to the total increase in ocean heat content. To put the ocean's overall role in climate into context, it has absorbed between 91–94% of the total heat gain by the combined air, sea, land, and cryosphere between 1970 and 2009. In other words, as the Earth is absorbing more heat than it is emitting back into space, nearly all of the excess heat is entering the oceans and being stored there.

The ocean's large mass and high heat capacity (their product is over 1000 times the atmosphere's) mean that it can store huge amounts of energy. This fact, coupled with its long time-scales for exchange of water from the surface to its depths, means that the ocean has significant thermal inertia. It takes decades for near-surface ocean temperatures to adjust in response to climate forcing such as changes in greenhouse gas concentrations. It will take centuries to millennia for deep ocean temperatures to warm in response to changes occurring today. Thus, even if greenhouse gas concentrations could be held constant at their present levels into the future, Earth's surface would continue to warm for decades. Furthermore, sea level would continue to rise for centuries to millennia as the deep oceans continued to warm and expand (even absent the contributions of melting land ice).

[END FAQ 3.1 HERE]

[START FAQ 3.2 HERE]

FAQ 3.2: How Does Anthropogenic Ocean Acidification Relate to Climate Change?

Both climate change and anthropogenic ocean acidification are caused by increasing carbon dioxide concentrations in the atmosphere. Rising levels of CO_2, along with other greenhouse gases, indirectly alter the climate system by trapping heat that perturbs the Earth's radiation budget. Anthropogenic ocean acidification is a direct consequence of rising CO_2 concentrations as seawater absorbs CO_2 from the atmosphere.

Anthropogenic ocean acidification refers to an increase in the ocean's hydrogen ion concentration (in other words, a lowering of pH or increase in acidity) caused by human activities, including the uptake of atmospheric carbon dioxide (CO_2) derived from the burning of fossil fuels, land-use changes, and cement production. Implicit with the pH change are the associated changes in the concentrations of the dissolved carbon species ($CO_{2(aq)}$, H_2CO_3, HCO_3^-, CO_3^{2-}). Results from laboratory, field, and modeling studies, as well as evidence from the geological record, clearly indicate that marine ecosystems are highly susceptible to the increases in oceanic CO_2 and the corresponding decreases in pH (Doney et al., 2009). Ocean acidification describes the direction of pH change rather than the end point; that is, ocean pH is decreasing but is not expected to become acidic (pH<7).

[INSERT FAQ 3.2, FIGURE 1 HERE]

FAQ 3.2, Figure 1: Time series of atmospheric pCO_2 at the atmospheric Mauna Loa Observatory (top), surface ocean pCO_2 (middle), and surface ocean pH (bottom) on the island of Hawaii and Station ALOHA in the subtropical North Pacific north of Hawaii, 1988–2008 (after Doney et al., 2009; data from Dore et al., 2009).

Climate change and anthropogenic ocean acidification do not act independently, as both processes affect the exchange of CO_2 between the atmosphere and ocean. The CO_2 that is taken up by the ocean does not contribute to greenhouse warming. Ocean warming, however, reduces the solubility of carbon dioxide in seawater; and thus reduces the amount of CO_2 the oceans can absorb from the atmosphere. For example, under doubled preindustrial CO_2 concentrations and a 2°C temperature increase, seawater absorbs about 10% less CO_2 than it would with no temperature increase (compare columns 4 and 6 of Table 1), but the decrease in pH (i.e., the increase in hydrogen ion concentration) remains almost unchanged. Thus, a warmer ocean has less capacity to remove carbon dioxide from the atmosphere, but still experiences ocean acidification.

FAQ 3.2, Table 1: Oceanic pH and carbon system parameter changes for a CO_2 doubling from the preindustrial atmosphere without and with a 2°C warming.

Parameter	preindustrial (280 ppmv) 20°C	2x preindustrial (560 ppmv) 20°C	*(% change relative to preindustrial)*	2x preindustrial (560 ppmv) 22°C	*(% change relative to preindustrial)*
pH	8.1714	7.9202	-	7.9207	-
H^+ (µmol kg)	$6.739e^{-9}$	$1.202e^{-8}$	*(78.4)*	$1.200e^{-8}$	*(78.1)*
$CO_2(aq)$ (µmol kg)	9.10	18.10	*(98.9)*	17.2	*(89.0)*
HCO_3^- (µmol kg)	1723.4	1932.8	*(12.15)*	1910.4	*(10.9)*
CO_3^{2-} (µmol kg)	228.3	143.6	*(-37.1)*	152.9	*(-33.0)*
DIC (µmol kg)	1960.8	2094.5	*(6.82)*	2080.5	*(6.10)*

[END FAQ 3.2 HERE]

[START FAQ 3.3 HERE]

FAQ 3.3: Is There Evidence for Changes in the Earth's Water Cycle?

The Earth's water cycle involves evaporation and precipitation of moisture at the Earth's surface. Changes in the water vapour content of the atmosphere and in the salinity distribution in the ocean provide strong evidence that the water cycle is already responding to a warming climate.

The water cycle is expected to intensify in a warmer climate, because warmer air can be moister: the atmosphere can have about 7% more water vapour for each degree C of warming (see FAQ 12.2). Observations of the atmosphere since the 1970s do indeed show increases in surface and lower atmosphere water vapour at a rate consistent with the observed warming (Section 2.3).

Increases in precipitation, evaporation, and extreme hydrological events are projected to result from a warmer atmosphere, although not necessarily at the same rate as water vapour content (Section 12.4.3). Observing such changes directly and globally is difficult. Most of the exchange of freshwater between the atmosphere and the surface takes place over the 70% of the Earth's surface that is covered by ocean. Long-term measurements of precipitation are only available over land areas, and long-term measurements of evaporation are not available (Section 2.3). Land-based precipitation observations show increases in some regions and decreases in others, making it difficult to construct a globally integrated picture. From land-based observations it is likely that there have more extreme precipitation events, and more flooding associated with earlier snow melt at high latitudes, but there is strong regionality in the trends; land-based observations are not sufficient to provide evidence of changes in drought extremes (Section 2.7).

Ocean salinity, on the other hand, naturally integrates the net freshwater flux resulting from the difference between precipitation and evaporation and can therefore act as a sensitive and effective rain gauge. (Ocean salinity can also be affected by run-off of water from the continents and by the melting and freezing of sea ice or floating glacial ice. Freshwater added by melting of ice in glaciers and ice sheets on land will change global-averaged salinity, but changes to date are more than an order of magnitude smaller than can be detected from in ocean observations.)

The distribution of salinity at the ocean surface largely mirrors the distribution of evaporation – precipitation. High salinity is observed in the subtropics, where evaporation exceeds precipitation, and low salinity is observed at high latitudes and in the tropics, where there is more rainfall than evaporation. The Atlantic, the saltiest ocean basin, loses more freshwater through evaporation than it gains from precipitation, while the reverse is true for the Pacific. Transport of moisture as water vapour in the atmosphere connects the regions of net freshwater gain or loss by the ocean.

Changes observed in ocean salinity and atmospheric water vapour in the last 50 years provide strong evidence that the global water cycle is increasing in intensity as the Earth warms, as anticipated from the fact that warmer air can contain more moisture. Changes in surface salinity have reinforced the mean salinity pattern: the evaporation-dominated subtropical regions have become saltier, while the precipitation-dominated subpolar and tropical regions have become fresher. The observed changes in surface salinity are statistically significant at the 99% level of confidence over more than 40% of the surface of the global ocean (Durack and Wijffels, 2010).

[END FAQ 3.3 HERE]

References

Abeysirigunawardena, D. S., and I. J. Walker, 2008: Sea Level Responses to Climatic Variability and Change in Northern British Columbia. *Atmosphere-Ocean*, **46,** 277-296.

Alory, G., S. Wijffels, and G. Meyers, 2007: Observed temperature trends in the Indian Ocean over 1960-1999 and associated mechanisms. *Geophysical Research Letters*, **34**.

Álvarez, M., T. Tanhua, H. Brix, C. Lo Monaco, N. Metzl, E. L. McDonagh, and H. L. Bryden, 2011: Decadal biogeochemical changes in the subtropical Indian Ocean associated with Subantarctic Mode Water. *Journal of Geophysical Research-Oceans*, **116**.

Andersson, A., C. Klepp, K. Fennig, S. Bakan, H. Grassl, and J. Schulz, 2011: Evaluation of HOAPS-3 Ocean Surface Freshwater Flux Components. *Journal of Applied Meteorology and Climatology*, **50,** 379-398.

Andrié, C., Y. Gouriou, B. Bourlès, J. F. Ternon, E. S. Braga, P. Morin, and C. Oudot, 2003: Variability of AABW properties in the equatorial channel at 35°W. *Geophys. Res. Lett.*, **30,** 8007.

Antonov, J. I., S. Levitus, and T. P. Boyer, 2002: Steric sea level variations during 1957-1994: Importance of salinity. *Journal of Geophysical Research-Oceans*, **107**.

Aoki, S., S. R. Rintoul, S. Ushio, S. Watanabe, and N. L. Bindoff, 2005: Freshening of the Adelie Land Bottom Water near 140 degrees E. *Geophysical Research Letters*, **32**.

Bates, N. R., 2007: Interannual variability of the oceanic CO2 sink in the subtropical gyre of the North Atlantic Ocean over the last 2 decades. *Journal of Geophysical Research-Oceans*, **112,** -.

Beckley, B. D., et al., 2010: Assessment of the Jason-2 Extension to the TOPEX/Poseidon, Jason-1 Sea-Surface Height Time Series for Global Mean Sea Level Monitoring. *Marine Geodesy*, **33,** 447-471.

Behrenfeld, M. J., et al., 2006: Climate-driven trends in contemporary ocean productivity. *Nature*, **444,** 752-755.

Beltrami, H., J. E. Smerdon, H. N. Pollack, and S. P. Huang, 2002: Continental heat gain in the global climate system. *Geophysical Research Letters*, **29,** 3.

Bersch, M., I. Yashayaev, and K. P. Koltermann, 2007: Recent changes of the thermohaline circulation in the subpolar North Atlantic. *Ocean Dynamics*, **57,** 223-235.

Bindoff, N. L., and T. J. McDougall, 1994: DIAGNOSING CLIMATE-CHANGE AND OCEAN VENTILATION USING HYDROGRAPHIC DATA. *Journal of Physical Oceanography*, **24,** 1137-1152.

Bindoff, N. L., et al., 2007: Observations: Oceanic Climate Change and Sea Level. *Climate Change 2007: The Physical Science Basis. Contribution of Working Group I to the Fourth Assessment Report of the Intergovernmental Panel on Climate Change*, S. Solomon, et al., Eds., Cambridge University Press.

Bingham, R. J., and C. W. Hughes, 2009: Signature of the Atlantic meridional overturning circulation in sea level along the east coast of North America. *Geophysical Research Letters*, **36**.

Bograd, S. J., C. G. Castro, E. Di Lorenzo, D. M. Palacios, H. Bailey, W. Gilly, and F. P. Chavez, 2008: Oxygen declines and the shoaling of the hypoxic boundary in the California Current. *Geophysical Research Letters*, **35**.

Böning, C. W., A. Dispert, M. Visbeck, S. R. Rintoul, and F. U. Schwarzkopf, 2008: The response of the Antarctic Circumpolar Current to recent climate change. *Nature Geoscience*, **1,** 864-869.

Boyer, T., S. Levitus, J. Antonov, R. Locarnini, A. Mishonov, H. Garcia, and S. A. Josey, 2007: Changes in freshwater content in the North Atlantic Ocean 1955-2006. *Geophysical Research Letters*, **34**.

Boyer, T. P., S. Levitus, J. I. Antonov, R. A. Locarnini, and H. E. Garcia, 2005: Linear trends in salinity for the World Ocean, 1955-1998. *Geophysical Research Letters*, **32**.

Boyer, T. P., et al., 2009: World Ocean Database 2009, 216 pp.

Byrne, R. H., S. Mecking, R. A. Feely, and X. W. Liu, 2010: Direct observations of basin-wide acidification of the North Pacific Ocean. *Geophysical Research Letters*, **37**.

Cai, W., 2006: Antarctic ozone depletion causes an intensification of the Southern Ocean super-gyre circulation. *Geophysical Research Letters*, **33**.

Caldeira, K., and M. E. Wickett, 2003: Anthropogenic carbon and ocean pH. *Nature*, **425,** 365-365.

Carson, M., and D. E. Harrison, 2010: Regional Interdecadal Variability in Bias-Corrected Ocean Temperature Data. *Journal of Climate*, **23,** 2847-2855.

Carton, J. A., and A. Santorelli, 2008: Global Decadal Upper-Ocean Heat Content as Viewed in Nine Analyses. *Journal of Climate*, **21,** 6015-6035.

Carton, J. A., B. S. Giese, and S. A. Grodsky, 2005: Sea level rise and the warming of the oceans in the Simple Ocean Data Assimilation (SODA) ocean reanalysis. *Journal of Geophysical Research-Oceans*, **110**.

Cazenave, A., et al., 2009: Sea level budget over 2003–2008: A re-evaluation from GRACE space gravimetry, satellite altimetry and Argo. *Marine Geodesy*, **65,** 447 - 471.

Cermak, J., M. Wild, R. Knutti, M. I. Mishchenko, and A. K. Heidinger, 2010: Consistency of global satellite-derived aerosol and cloud data sets with recent brightening observations. *Geophysical Research Letters*, **37**.

Chambers, D. P., J. Wahr, and R. S. Nerem, 2004: Preliminary observations of global ocean mass variations with GRACE. *Geophysical Research Letters*, **31**.

Chambers, D. P., J. Wahr, M. E. Tamisiea, and R. S. Nerem, 2010: Ocean mass from GRACE and glacial isostatic adjustment. *Journal of Geophysical Research-Solid Earth*, **115**.

Chan, F., J. A. Barth, J. Lubchenco, A. Kirincich, H. Weeks, W. T. Peterson, and B. A. Menge, 2008: Emergence of anoxia in the California current large marine ecosystem. *Science*, **319,** 920-920.

Chavez, F. P., M. Messié, and J. T. Pennington, 2011: Marine primary production in relation to climate variability and change. *Annual Review of Marine Science*, **3,** 227-260.
Church, J. A., and N. J. White, 2006: A 20th century acceleration in global sea-level rise. *Geophysical Research Letters*, **33**.
Church, J. A., and N. J. White, 2011: Sea-Level Rise from the Late 19th to the Early 21st Century. *Surveys in Geophysics*, **32,** 585-602.
Church, J. A., J. R. Hunter, K. L. McInnes, and N. J. White, 2006: Sea-level rise around the Australian coastline and the changing frequency of extreme sea-level events. *Australian Meteorological Magazine*, **55,** 253-260.
Church, J. A., N. J. White, R. Coleman, K. Lambeck, and J. X. Mitrovica, 2004: Estimates of the regional distribution of sea level rise over the 1950-2000 period. *Journal of Climate*, **17,** 2609-2625.
Cianca, A., P. Helmke, B. Mourino, M. J. Rueda, O. Llinas, and S. Neuer, 2007: Decadal analysis of hydrography and in situ nutrient budgets in the western and eastern North Atlantic subtropical gyre. *Journal of Geophysical Research-Oceans*, **112**.
Cooley, S. R., H. L. Kite-Powell, and S. C. Doney, 2009: Ocean Acidification's Potential to Alter Global Marine Ecosystem Services. *Oceanography*, **22,** 172-181.
Cravatte, S., T. Delcroix, D. X. Zhang, M. McPhaden, and J. Leloup, 2009: Observed freshening and warming of the western Pacific Warm Pool. *Climate Dynamics*, **33,** 565-589.
Cummins, P. F., and H. J. Freeland, 2007: Variability of the North Pacific current and its bifurcation. *Progress in Oceanography*, **75,** 253-265.
Cunningham, S., et al., 2010: The present and future system for measuring the Atlantic meridional overturning circulation and heat transport. *Proceedings of OceanObs'09: Sustained Ocean Observations and Information for Society (Vol. 2)*, Venice, Italy, European Space Agency Publication, 16.
Cunningham, S. A., S. G. Alderson, B. A. King, and M. A. Brandon, 2003: Transport and variability of the Antarctic Circumpolar Current in Drake Passage. *Journal of Geophysical Research-Oceans*, **108**.
Cunningham, S. A., et al., 2007: Temporal variability of the Atlantic meridional overturning circulation at 26.5 degrees N. *Science*, **317,** 935-938.
Curry, R., and C. Mauritzen, 2005: Dilution of the northern North Atlantic Ocean in recent decades. *Science*, **308,** 1772-1774.
Curry, R., B. Dickson, and I. Yashayaev, 2003: A change in the freshwater balance of the Atlantic Ocean over the past four decades. *Nature*, **426,** 826-829.
D'Onofrio, E. E., M. M. E. Fiore, and J. L. Pousa, 2008: Changes in the regime of storm surges at Buenos Aires, Argentina. *Journal of Coastal Research*, **24,** 260-265.
Delcroix, T., S. Cravatte, and M. J. McPhaden, 2007: Decadal variations and trends in tropical Pacific sea surface salinity since 1970. *Journal of Geophysical Research-Oceans*, **112**.
Deng, Z. W., and Y. M. Tang, 2009: Reconstructing the Past Wind Stresses over the Tropical Pacific Ocean from 1875 to 1947. *Journal of Applied Meteorology and Climatology*, **48,** 1181-1198.
Deutsch, C., S. Emerson, and L. Thompson, 2006: Physical-biological interactions in North Pacific oxygen variability. *Journal of Geophysical Research-Oceans*, **111**.
Di Lorenzo, E., et al., 2009: Nutrient and salinity decadal variations in the central and eastern North Pacific. *Geophysical Research Letters*, **36**.
Diaz, R. J., and R. Rosenberg, 2008: Spreading dead zones and consequences for marine ecosystems. *Science*, **321,** 926-929.
Dickson, B., I. Yashayaev, J. Meincke, B. Turrell, S. Dye, and J. Holfort, 2002: Rapid freshening of the deep North Atlantic Ocean over the past four decades. *Nature*, **416,** 832-837.
Dickson, R. R., et al., 2008: The overflow flux west of Iceland: variability, origins and forcing. *Arctic-Subarctic Ocean Fluxes*, R. R. Dickson, J. Meincke, and P. B. Rhines, Eds., Springer Verlag.
Dmitrenko, I. A., et al., 2008: Toward a warmer Arctic Ocean: Spreading of the early 21st century Atlantic Water warm anomaly along the Eurasian Basin margins. *Journal of Geophysical Research-Oceans*, **113,** 13.
Dodet, G., X. Bertin, and R. Taborda, 2010: Wave climate variability in the North-East Atlantic Ocean over the last six decades. *Ocean Modelling*, **31,** 120-131.
Dohan, K., et al., 2010: Measuring the Global Ocean Surface Circulation with Satellite and In Situ Observations. *Proceedings of OceanObs'09: Sustained Ocean Observations and Information for Society (Vol. 2)*, Venice, Italy.
Domingues, C. M., J. A. Church, N. J. White, P. J. Gleckler, S. E. Wijffels, P. M. Barker, and J. R. Dunn, 2008: Improved estimates of upper-ocean warming and multi-decadal sea-level rise. *Nature*, **453,** 1090-U1096.
Doney, S. C., V. J. Fabry, R. A. Feely, and J. A. Kleypas, 2009: Ocean Acidification: The Other CO2 Problem. *Annual Review of Marine Science*, **1,** 169-192.
Dore, J. E., R. Lukas, D. W. Sadler, M. J. Church, and D. M. Karl, 2009: Physical and biogeochemical modulation of ocean acidification in the central North Pacific. *Proceedings of the National Academy of Sciences of the United States of America*, **106,** 12235-12240.
Douglas, B. C., 2001: Sea level change in the era of the recording tide gauge. *Sea Level Rise: History and Consequences*, B. C. Douglas, M. S. Kearney, and S. P. Leatherman, Eds., Academic Press, 37–64.

Douglass, E., D. Roemmich, and D. Stammer, 2006: Interannual variability in northeast pacific circulation. *Journal of Geophysical Research-Oceans*, **111**.
Dragani, W. C., P. B. Martin, C. G. Simionato, and M. I. Campos, 2010: Are wind wave heights increasing in south-eastern south American continental shelf between 32°S and 40°S? *Continental Shelf Research*, **30,** 481-490.
Ducet, N., P. Y. Le Traon, and G. Reverdin, 2000: Global high-resolution mapping of ocean circulation from TOPEX/Poseidon and ERS-1 and-2. *Journal of Geophysical Research-Oceans*, **105,** 19477-19498.
Durack, P. J., and S. E. Wijffels, 2010: Fifty-Year Trends in Global Ocean Salinities and Their Relationship to Broad-Scale Warming. *Journal of Climate*, **23,** 4342-4362.
Egleston, E. S., C. L. Sabine, and F. M. M. Morel, 2010: Revelle revisited: Buffer factors that quantify the response of ocean chemistry to changes in DIC and alkalinity. *Global Biogeochemical Cycles*, **24**.
Fabry, V. J., B. A. Seibel, R. A. Feely, and J. C. Orr, 2008: Impacts of ocean acidification on marine fauna and ecosystem processes. *Ices Journal of Marine Science*, **65,** 414-432.
Feely, R. A., S. C. Doney, and S. R. Cooley, 2009: Ocean Acidification: Present Conditions and Future Changes in a High-CO2 World. *Oceanography*, **22,** 36-47.
Feely, R. A., T. Takahashi, R. Wanninkhof, M. J. McPhaden, C. E. Cosca, S. C. Sutherland, and M. E. Carr, 2006: Decadal variability of the air-sea CO2 fluxes in the equatorial Pacific Ocean. *Journal of Geophysical Research-Oceans*, **111,** -.
Fine, R. A., K. A. Maillet, K. F. Sullivan, and D. Willey, 2001: Circulation and ventilation flux of the Pacific Ocean. *Journal of Geophysical Research-Oceans*, **106,** 22159-22178.
Fischer, J., M. Visbeck, R. Zantopp, and N. Nunes, 2010: Interannual to decadal variability of outflow from the Labrador Sea. *Geophysical Research Letters*, **37**.
Freeland, H., et al., 2010: Argo - A Decade of Progress. *Proceedings of OceanObs'09: Sustained Ocean Observations and Information for Society (Vol. 2)*, Venice, Italy.
Friis, K., A. Körtzinger, J. Pätsch, and D. W. R. Wallace, 2005: On the temporal increase of anthropogenic CO2 in the subpolar North Atlantic. *Deep-Sea Research I*, **52,** 681-698.
Fukasawa, M., H. Freeland, R. Perkin, T. Watanabe, J. Uchida, and A. Nishina, 2004: Bottom water warming in the North Pacific Ocean. 825–827.
Fyfe, J. C., and O. A. Saenko, 2006: Simulated changes in the extratropical Southern Hemisphere winds and currents. *Geophysical Research Letters*, **33**.
Garabato, A. C. N., L. Jullion, D. P. Stevens, K. J. Heywood, and B. A. King, 2009: Variability of Subantarctic Mode Water and Antarctic Intermediate Water in the Drake Passage during the Late-Twentieth and Early-Twenty-First Centuries. *Journal of Climate*, **22,** 3661-3688.
Giese, B. S., G. A. Chepurin, J. A. Carton, T. P. Boyer, and H. F. Seidel, 2011: Impact of bathythermograph temperature bias models on an ocean reanalysis. *Journal of Climate*, **24,** 84-93.
Gilbert, D., N. N. Rabalais, R. J. Diaz, and J. Zhang, 2010: Evidence for greater oxygen decline rates in the coastal ocean than in the open ocean. *Biogeosciences*, **7,** 2283-2296.
Gille, S. T., 2008: Decadal-scale temperature trends in the Southern Hemisphere ocean. *Journal of Climate*, **21,** 4749-4765.
Gladyshev, S. V., M. N. Koshlyakov, and R. Y. Tarakanov, 2008: Currents in the Drake Passage based on observations in 2007. *Oceanology*, **48,** 759-770.
Gloor, M., J. L. Sarmiento, and N. Gruber, 2010: What can be learned about carbon cycle climate feedbacks from the CO2 airborne fraction? *Atmos. Chem. Phys.*, **10,** 7739-7751.
Goni, G. J., F. Bringas, and P. N. DiNezio, 2011: Observed low frequency variability of the Brazil Current front. *Journal of Geophysical Research-Oceans*, **116**.
Gonzalez-Davila, M., J. M. Santana-Casiano, M. J. Rueda, and O. Llinas, 2010: The water column distribution of carbonate system variables at the ESTOC site from 1995 to 2004. *Biogeosciences*, **7,** 3067-3081.
Gouretski, V., and K. P. Koltermann, 2007: How much is the ocean really warming? *Geophysical Research Letters*, **34,** 5.
Gouretski, V., and F. Reseghetti, 2010: On depth and temperature biases in bathythermograph data: Development of a new correction scheme based on analysis of a global ocean database. *Deep-Sea Research Part I-Oceanographic Research Papers*, **57,** 812-833.
Grist, J. P., R. Marsh, and S. A. Josey, 2009: On the Relationship between the North Atlantic Meridional Overturning Circulation and the Surface-Forced Overturning Streamfunction. *Journal of Climate*, **22,** 4989-5002.
Gu, G. J., R. F. Adler, G. J. Huffman, and S. Curtis, 2007: Tropical rainfall variability on interannual-to-interdecadal and longer time scales derived from the GPCP monthly product. *Journal of Climate*, **20,** 4033-4046.
Gulev, S., T. Jung, and E. Ruprecht, 2007: Estimation of the impact of sampling errors in the VOS observations on air-sea fluxes. Part II: Impact on trends and interannual variability. *Journal of Climate*, **20,** 302-315.
Gulev, S., et al., 2010: Surface Energy and CO2 Fluxes in the Global Ocean-Atmosphere-Ice System. *OceanObs'09: Sustained Ocean Observations and Information for Society*, Venice, Italy, 20 pp.
Gulev, S. K., and V. Grigorieva, 2006: Variability of the winter wind waves and swell in the North Atlantic and North Pacific as revealed by the voluntary observing ship data. *Journal of Climate*, **19,** 5667-5685.
Haigh, I., R. Nicholls, and N. Wells, 2010: Assessing changes in extreme sea levels: Application to the English Channel, 1900-2006. *Continental Shelf Research*, **30,** 1042-1055.

Hakkinen, S., and P. B. Rhines, 2009: Shifting surface currents in the northern North Atlantic Ocean. *Journal of Geophysical Research-Oceans*, **114**.
Hallberg, R., and A. Gnanadesikan, 2006: The role of eddies in determining the structure and response of the wind-driven southern hemisphere overturning: Results from the Modeling Eddies in the Southern Ocean (MESO) project. *Journal of Physical Oceanography*, **36,** 2232-2252.
Hansen, B., and S. Osterhus, 2007: Faroe Bank Channel overflow 1995-2005. *Progress in Oceanography*, **75,** 817-856.
Hatun, H., A. B. Sando, H. Drange, B. Hansen, and H. Valdimarsson, 2005: Influence of the Atlantic subpolar gyre on the thermohaline circulation. *Science*, **309,** 1841-1844.
Held, I. M., and B. J. Soden, 2006: Robust responses of the hydrological cycle to global warming. *Journal of Climate*, **19,** 5686-5699.
Helm, K. P., N. L. Bindoff, and J. A. Church, 2010: Changes in the global hydrological-cycle inferred from ocean salinity. *Geophysical Research Letters*, **37**.
Hemer, M. A., 2010: Historical trends in Southern Ocean storminess: Long-term variability of extreme wave heights at Cape Sorell, Tasmania. *Geophysical Research Letters*, **37**.
Hemer, M. A., J. A. Church, and J. R. Hunter, 2010: Variability and trends in the directional wave climate of the Southern Hemisphere. *International Journal of Climatology*, **30,** 475-491.
Hendriks, I. E., C. M. Duarte, and M. Alvarez, 2010: Vulnerability of marine biodiversity to ocean acidification: A meta-analysis. *Estuarine Coastal and Shelf Science*, **86,** 157-164.
Hill, K. L., S. R. Rintoul, R. Coleman, and K. R. Ridgway, 2008: Wind forced low frequency variability of the East Australia Current. *Geophysical Research Letters*, **35**.
Hinkelman, L. M., P. W. Stackhouse, B. A. Wielicki, T. P. Zhang, and S. R. Wilson, 2009: Surface insolation trends from satellite and ground measurements: Comparisons and challenges. *Journal of Geophysical Research-Atmospheres*, **114**.
Holgate, S. J., 2007: On the decadal rates of sea level change during the twentieth century. *Geophysical Research Letters*, **34**.
Holland, P. R., A. Jenkins, and D. M. Holland, 2008: The response of ice shelf basal melting to variations in ocean temperature. *Journal of Climate*, **21,** 2558-2572.
Holliday, N., et al., 2008: Reversal of the 1960s to 1990s freshening trend in the northeast North Atlantic and Nordic Seas. *Geophysical Research Letters*, ARTN L03614, DOI 10.1029/2007GL032675**,** -.
Hood, M., et al., 2010: Ship-based Repeat Hydrography: A Strategy for a Sustained Global Program. *Proceedings of OceanObs'09: Sustained Ocean Observations and Information for Society (Vol. 2)*, Venice, Italy.
Hosoda, S., T. Suga, N. Shikama, and K. Mizuno, 2009: Global Surface Layer Salinity Change Detected by Argo and Its Implication for Hydrological Cycle Intensification. *Journal of Oceanography*, **65,** 579-586.
Houston, J. R., and R. G. Dean, 2011: Sea-Level Acceleration Based on US Tide Gauges and Extensions of Previous Global-Gauge Analyses. *Journal of Coastal Research*, **27,** 409-417.
Hughes, C. W., P. L. Woodworth, M. P. Meredith, V. Stepanov, T. Whitworth, and A. R. Pyne, 2003: Coherence of Antarctic sea levels, Southern Hemisphere Annular Mode, and flow through Drake Passage. *Geophysical Research Letters*, **30**.
Ishii, M., and M. Kimoto, 2009: Reevaluation of historical ocean heat content variations with time-varying XBT and MBT depth bias corrections. *Journal of Oceanography*, **65,** 287-299.
Ishii, M., N. Kosugi, D. Sasano, S. Saito, T. Midorikawa, and H. Y. Inoue, 2011: Ocean acidification off the south coast of Japan: A result from time series observations of CO(2) parameters from 1994 to 2008. *Journal of Geophysical Research-Oceans*, **116**.
Jackson, J. M., E. C. Carmack, F. A. McLaughlin, S. E. Allen, and R. G. Ingram, 2010: Identification, characterization, and change of the near-surface temperature maximum in the Canada Basin, 1993-2008. *Journal of Geophysical Research-Oceans*, **115,** 16.
Jacobs, S., 2004: Bottom water production and its links with the thermohaline circulation. *Antarctic Science*, DOI 10.1017/S095410200400224X**,** 427-437.
Jacobs, S. S., and C. F. Giulivi, 2010: Large Multidecadal Salinity Trends near the Pacific-Antarctic Continental Margin. *Journal of Climate*, **23,** 4508-4524.
Jacobs, S. S., A. Jenkins, C. F. Giulivi, and P. Dutrieux, 2011: Stronger ocean circulation and increased melting under Pine Island Glacier ice shelf. *Nature Geoscience*, **4,** 519-523.
Jevrejeva, S., A. Grinsted, J. C. Moore, and S. Holgate, 2006: Nonlinear trends and multiyear cycles in sea level records. *Journal of Geophysical Research-Oceans*, **111**.
Jevrejeva, S., J. C. Moore, A. Grinsted, and P. L. Woodworth, 2008: Recent global sea level acceleration started over 200 years ago? *Geophysical Research Letters*, **35**.
Johns, W. E., et al., 2011: Continuous, Array-Based Estimates of Atlantic Ocean Heat Transport at 26.5 degrees N. *Journal of Climate*, **24,** 2429-2449.
Johnson, G. C., and S. C. Doney, 2006: Recent western South Atlantic bottom water warming. *Geophys. Res. Lett.*, **33,** L14614.
Johnson, G. C., and N. Gruber, 2007: Decadal water mass variations along 20 degrees W in the Northeastern Atlantic Ocean. *Progress in Oceanography*, **73,** 277-295.

Johnson, G. C., S. G. Purkey, and J. L. Bullister, 2008a: Warming and Freshening in the Abyssal Southeastern Indian Ocean. *Journal of Climate*, **21,** 5351-5363.
Johnson, G. C., S. G. Purkey, and J. M. Toole, 2008b: Reduced Antarctic meridional overturning circulation reaches the North Atlantic Ocean. *Geophysical Research Letters*, **35**.
Johnson, G. C., S. Mecking, B. M. Sloyan, and S. E. Wijffels, 2007: Recent bottom water warming in the Pacific Ocean. *Journal of Climate*, **20,** 5365-5375.
Josey, S. A., 2011: Air-Sea Fluxes of Heat, Freshwater and Momentum. *Operational Oceanography in the 21st Century*, A. Schiller, and G. B. Brassington, Eds., Springer, 155-184.
Josey, S. A., J. P. Grist, and R. Marsh, 2009: Estimates of meridional overturning circulation variability in the North Atlantic from surface density flux fields. *Journal of Geophysical Research-Oceans*, **114**.
Kanzow, T., U. Send, and M. McCartney, 2008: On the variability of the deep meridional transports in the tropical North Atlantic. *Deep-Sea Research Part I-Oceanographic Research Papers*, **55,** 1601-1623.
Kanzow, T., et al., 2009: Basinwide Integrated Volume Transports in an Eddy-Filled Ocean. *Journal of Physical Oceanography*, **39,** 3091-3110.
Kanzow, T., et al., 2007: Observed flow compensation associated with the MOC at 26.5 degrees N in the Atlantic. *Science*, **317,** 938-941.
Kanzow, T., et al., 2010: Seasonal Variability of the Atlantic Meridional Overturning Circulation at 26.5 degrees N. *Journal of Climate*, **23,** 5678-5698.
Katsumata, K., and H. Yoshinari, 2010: Uncertainties in Global Mapping of Argo Drift Data at the Parking Level. *Journal of Oceanography*, **66,** 553-569.
Kawai, Y., T. Doi, H. Tomita, and H. Sasaki, 2008: Decadal-scale changes in meridional heat transport across 24 degrees N in the Pacific Ocean. *Journal of Geophysical Research-Oceans*, **113**.
Kawano, T., et al., 2006: Bottom water warming along the pathway of lower circumpolar deep water in the Pacific Ocean. *Geophys. Res. Lett.*, **33,** L23613.
Keeling, R. F., A. Kortzinger, and N. Gruber, 2010: Ocean Deoxygenation in a Warming World. *Annual Review of Marine Science*, **2,** 199-229.
Khatiwala, S., F. Primeau, and T. Hall, 2009: Reconstruction of the history of anthropogenic CO2 concentrations in the ocean. *Nature*, **462,** 346-U110.
Kieke, D., M. Rhein, L. Stramma, W. M. Smethie, D. A. LeBel, and W. Zenk, 2006: Changes in the CFC inventories and formation rates of Upper Labrador Sea Water, 1997-2001. *Journal of Physical Oceanography*, **36,** 64-86.
Kieke, D., M. Rhein, L. Stramma, W. Smethie, J. Bullister, and D. LeBel, 2007: Changes in the pool of Labrador Sea Water in the subpolar North Atlantic. *Geophysical Research Letters*, ARTN L06605, DOI 10.1029/2006GL028959**,** -.
Kobayashi, T., K. Mizuno, and T. Suga, 2011: Long-term variations of surface and intermediate waters in the southern Indian Ocean along 32°S. *JO*, **accepted**.
Komar, P. D., and J. C. Allan, 2008: Increasing hurricane-generated wave heights along the US East Coast and their climate controls. *Journal of Coastal Research*, **24,** 479-488.
Koshlyakov, M. N., Lisina, II, E. G. Morozov, and R. Y. Tarakanov, 2007: Absolute geostrophic currents in the Drake Passage based on observations in 2003 and 2005. *Oceanology*, **47,** 451-463.
Koshlyakov, M. N., S. V. Gladyshev, R. Y. Tarakanov, and D. A. Fedorov, 2011: Currents in the western Drake Passage by the observations in January 2010. *Oceanology*, **51,** 187-198.
Kouketsu, S., et al., 2009: Changes in water properties and transports along 24 degrees N in the North Pacific between 1985 and 2005. *Journal of Geophysical Research-Oceans*, **114**.
Kouketsu, S., et al., 2011: Deep ocean heat content changes estimated from observation and reanalysis product and their influence on sea level change. *Journal of Geophysical Research-Oceans*, **116**.
Kroeker, K. J., R. L. Kordas, R. N. Crim, and G. G. Singh, 2010: Meta-analysis reveals negative yet variable effects of ocean acidification on marine organisms. *Ecology Letters*, **13,** 1419-1434.
Kwok, R., G. F. Cunningham, M. Wensnahan, I. Rigor, H. J. Zwally, and D. Yi, 2009: Thinning and volume loss of the Arctic Ocean sea ice cover: 2003-2008. *Journal of Geophysical Research-Oceans*, **114**.
Large, W. G., and S. G. Yeager, 2009: The global climatology of an interannually varying air-sea flux data set. *Climate Dynamics*, **33,** 341-364.
Le Quere, C., M. R. Raupach, J. G. Canadell, G. Marland, and et al., 2009: Trends in the sources and sinks of carbon dioxide. *Nature Geosci*, **2,** 831-836.
LeBel, D. A., et al., 2008: The formation rate of North Atlantic Deep Water and Eighteen Degree Water calculated from CFC-11 inventories observed during WOCE. *Deep-Sea Research Part I-Oceanographic Research Papers*, **55,** 891-910.
Letetrel, C., M. Marcos, B. M. Miguez, and G. Woppelmann, 2010: Sea level extremes in Marseille (NW Mediterranean) during 1885-2008. *Continental Shelf Research*, **30,** 1267-1274.
Leuliette, E. W., and L. Miller, 2009: Closing the sea level rise budget with altimetry, Argo, and GRACE. *Geophysical Research Letters*, **36**.
Leuliette, E. W., and R. Scharroo, 2010: Integrating Jason-2 into a Multiple-Altimeter Climate Data Record. *Marine Geodesy*, **33,** 504-517.
Leuliette, E. W., and J. K. Willis, 2011: Balancing the Sea Level Budget. *Oceanography*, **24,** 122-129.

Levitus, S., J. Antonov, and T. Boyer, 2005: Warming of the world ocean, 1955-2003. *Geophysical Research Letters*, **32,** 4.
Levitus, S., J. I. Antonov, T. P. Boyer, R. A. Locarnini, H. E. Garcia, and A. V. Mishonov, 2009: Global ocean heat content 1955-2008 in light of recently revealed instrumentation problems. *Geophysical Research Letters*, **36,** 5.
Li, G., B. Ren, J. Zheng, and C. Yang, 2011: Trend Singular Value Decomposition Analysis and Its Application to the Global Ocean Surface Latent Heat Flux and SST Anomalies. *Journal of Climate*, **24,** 2931-2948.
Llovel, W., B. Meyssignac, and A. Cazenave, 2011: Steric sea level variations over 2004-2010 as a function of region and depth: Inference on the mass component variability in the North Atlantic Ocean. *Geophysical Research Letters*, **38**.
Llovel, W., A. Cazenave, P. Rogel, A. Lombard, and M. B. Nguyen, 2009: Two-dimensional reconstruction of past sea level (1950-2003) from tide gauge data and an Ocean General Circulation Model. *Climate of the Past*, **5,** 217-227.
Lowe, J. A., et al., 2010: Past and future changes in extreme sea levels and waves. *Understanding sea-level rise and variability*, J. A. Church, P. L. Woodworth, T. Aarup, and W. S. Wilson, Eds., Wiley-Blackwell.
Lozier, M. S., and N. M. Stewart, 2008: On the temporally varying northward penetration of Mediterranean Overflow Water and eastward penetration of Labrador Sea water. *Journal of Physical Oceanography*, **38,** 2097-2103.
Lumpkin, R., and K. Speer, 2007: Global ocean meridional overturning. *Journal of Physical Oceanography*, **37,** 2550-2562.
Lumpkin, R., and S. Garzoli, 2011: Interannual to decadal changes in the western South Atlantic's surface circulation. *Journal of Geophysical Research-Oceans*, **116**.
Luthi, D., et al., 2008: High-resolution carbon dioxide concentration record 650,000-800,000 years before present. *Nature*, **453,** 379-382.
Lyman, J. M., and G. C. Johnson, 2008: Estimating Annual Global Upper-Ocean Heat Content Anomalies despite Irregular In Situ Ocean Sampling. *Journal of Climate*, **21,** 5629-5641.
Lyman, J. M., et al., 2010: Robust warming of the global upper ocean. *Nature*, **465,** 334-337.
Macrander, A., U. Send, H. Valdimarsson, S. Jonsson, and R. H. Kase, 2005: Interannual changes in the overflow from the Nordic Seas into the Atlantic Ocean through Denmark Strait. *Geophysical Research Letters*, **32**.
Manning, A. C., and R. F. Keeling, 2006: Global oceanic and land biotic carbon sinks from the Scripps atmospheric oxygen flask sampling network. *Tellus Series B-Chemical and Physical Meteorology*, **58,** 95-116.
Marcos, M., M. N. Tsimplis, and A. G. P. Shaw, 2009: Sea level extremes in southern Europe. *Journal of Geophysical Research-Oceans*, **114**.
Marsh, R., 2000: Recent variability of the North Atlantic thermohaline circulation inferred from surface heat and freshwater fluxes. *Journal of Climate*, **13,** 3239-3260.
Marshall, G. J., 2003: Trends in the southern annular mode from observations and reanalyses. *Journal of Climate*, **16,** 4134-4143.
Masuda, S., et al., 2010: Simulated Rapid Warming of Abyssal North Pacific Waters. *Science*, **329,** 319-322.
Matear, R. J., and B. I. McNeil, 2003: Decadal accumulation of anthropogenic CO2 in the Southern Ocean: A comparison of CFC-age derived estimates to multiple-linear regression estimates. *Global Biogeochemical Cycles*, **17,** 24.
Mauritzen, C., et al., 2011: Closing the loop - Approaches to monitoring the state of the Arctic Mediterranean during the International Polar Year 2007-2008. *Progress in Oceanography*, **90,** 62-89.
McCarthy, G., E. McDonagh, and B. King, 2011: Decadal Variability of Thermocline and Intermediate Waters at 24°S in the South Atlantic. *Journal of Physical Oceanography*, **41,** 157-165.
McPhee, M. G., A. Proshutinsky, J. H. Morison, M. Steele, and M. B. Alkire, 2009: Rapid change in freshwater content of the Arctic Ocean. *Geophysical Research Letters*, **36**.
Mears, C. A., and F. J. Wentz, 2009a: Construction of the Remote Sensing Systems V3.2 Atmospheric Temperature Records from the MSU and AMSU Microwave Sounders. *Journal of Atmospheric and Oceanic Technology*, **26,** 1040-1056.
——, 2009b: Construction of the RSS V3.2 Lower-Tropospheric Temperature Dataset from the MSU and AMSU Microwave Sounders. *Journal of Atmospheric and Oceanic Technology*, **26,** 1493-1509.
Mecking, S., M. J. Warner, and J. L. Bullister, 2006: Temporal changes in pCFC-12 ages and AOU along two hydrographic sections in the eastern subtropical North Pacific. *Deep-Sea Research Part I-Oceanographic Research Papers*, **53,** 169-187.
Mecking, S., C. Langdon, R. A. Feely, C. L. Sabine, C. A. Deutsch, and D.-H. Min, 2008: Climate variability in the North Pacific thermocline diagnosed from oxygen measurements: An update based on the US CLIVAR/CO(2) Repeat Hydrography cruises. *Global Biogeochemical Cycles*, **22**.
Meijers, A. J. S., N. L. Bindoff, and S. R. Rintoul, 2011: Frontal movements and property fluxes: Contributions to heat and freshwater trends in the Southern Ocean. *Journal of Geophysical Research-Oceans*, **116**.
Meinen, C. S., M. O. Baringer, and R. F. Garcia, 2010: Florida Current transport variability: An analysis of annual and longer-period signals. *Deep-Sea Research Part I-Oceanographic Research Papers*, **57,** 835-846.
Menendez, M., and P. L. Woodworth, 2010: Changes in extreme high water levels based on a quasi-global tide-gauge data set. *Journal of Geophysical Research-Oceans*, **115**.

Menendez, M., F. J. Mendez, I. J. Losada, and N. E. Graham, 2008: Variability of extreme wave heights in the northeast Pacific Ocean based on buoy measurements. *Geophysical Research Letters*, **35**.
Meredith, M. P., P. L. Woodworth, C. W. Hughes, and V. Stepanov, 2004: Changes in the ocean transport through Drake Passage during the 1980s and 1990s, forced by changes in the Southern Annular Mode. *Geophysical Research Letters*, **31**.
Merrifield, M. A., S. T. Merrifield, and G. T. Mitchum, 2009: An Anomalous Recent Acceleration of Global Sea Level Rise. *Journal of Climate*, **22,** 5772-5781.
Metzl, N., 2009: Decadal increase of oceanic carbon dioxide in Southern Indian Ocean surface waters (1991-2007). *Deep-Sea Research Part Ii-Topical Studies in Oceanography*, **56,** 607-619.
Midorikawa, T., et al., 2010: Decreasing pH trend estimated from 25-yr time series of carbonate parameters in the western North Pacific. *Tellus Series B-Chemical and Physical Meteorology*, **62,** 649-659.
Mishchenko, M. I., and I. V. Geogdzhayev, 2007: Satellite remote sensing reveals regional tropospheric aerosol trends. *Optics Express*, **15,** 7423-7438.
Mitas, C. M., and A. Clement, 2005: Has the Hadley cell been strengthening in recent decades? *Geophysical Research Letters*, **32**.
Murata, A., Y. Kumamoto, S. Watanabe, and M. Fukasawa, 2007: Decadal increases of anthropogenic CO2 in the South Pacific subtropical ocean along 32 degrees S. *Journal of Geophysical Research-Oceans*, **112,** -.
Murata, A., Y. Kumamoto, K. Sasaki, S. Watanabe, and M. Fukasawa, 2008: Decadal increases of anthropogenic CO2 in the subtropical South Atlantic Ocean along 30 degrees S. *Journal of Geophysical Research-Oceans*, **113,** -.
Murata, A., Y. Kumamoto, K.-i. Sasaki, S. Watanabe, and M. Fukasawa, 2010: Decadal increases in anthropogenic CO2 along 20°S in the South Indian Ocean. *J. Geophys. Res.*, **115,** C12055.
Murata, A., Y. Kumamoto, K. Sasaki, ichi, S. Watanabe, and M. Fukasawa, 2009: Decadal increases of anthropogenic CO2 along 149°E in the western North Pacific. *J. Geophys. Res.*, **114,** C04018.
Murphy, D. M., S. Solomon, R. W. Portmann, K. H. Rosenlof, P. M. Forster, and T. Wong, 2009: An observationally based energy balance for the Earth since 1950. *Journal of Geophysical Research-Atmospheres*, **114,** 14.
Myers, P. G., and C. Donnelly, 2008: Water mass transformation and formation in the Labrador sea. *Journal of Climate*, **21,** 1622-1638.
Nakano, T., I. Kaneko, T. Soga, H. Tsujino, T. Yasuda, H. Ishizaki, and M. Kamachi, 2007: Mid-depth freshening in the North Pacific subtropical gyre observed along the JMA repeat and WOCE hydrographic sections. *Geophysical Research Letters*, **34**.
Nakanowatari, T., K. Ohshima, and M. Wakatsuchi, 2007: Warming and oxygen decrease of intermediate water in the northwestern North Pacific, originating from the Sea of Okhotsk, 1955-2004. *Geophysical Research Letters*, ARTN L04602, DOI 10.1029/2006GL028243**,** -.
Nerem, R. S., D. P. Chambers, C. Choe, and G. T. Mitchum, 2010: Estimating Mean Sea Level Change from the TOPEX and Jason Altimeter Missions. *Marine Geodesy*, **33,** 435-446.
Nerem, R. S., D. P. Chambers, E. W. Leuliette, G. T. Mitchum, and B. S. Giese, 1999: Variations in global mean sea level associated with the 1997-1998 ENSO event: Implications for measuring long term sea level change. *Geophysical Research Letters*, **26,** 3005-3008.
Olafsson, J., S. R. Olafsdottir, A. Benoit-Cattin, M. Danielsen, T. S. Arnarson, and T. Takahashi, 2009: Rate of Iceland Sea acidification from time series measurements. *Biogeosciences*, **6,** 2661-2668.
Olsen, A., A. M. Omar, E. Jeansson, L. G. Anderson, and R. G. J. Bellerby, 2010: Nordic seas transit time distributions and anthropogenic CO2. *J. Geophys. Res.*, **115,** C05005.
Olsen, A., et al., 2006: Magnitude and origin of the anthropogenic CO2 increase and C-13 Suess effect in the Nordic seas since 1981. *Global Biogeochemical Cycles*, **20,** -.
Olsen, S. M., B. Hansen, D. Quadfasel, and S. Osterhus, 2008: Observed and modelled stability of overflow across the Greenland-Scotland ridge. *Nature*, **455,** 519-U535.
Orr, J. C., 2011: Recent and future changes in ocean carbonate chemistry. *Ocean Acidification*, J.-P. Guttuso, and L. Hansson, Eds., Oxford University Press, 41-66.
Orr, J. C., S. Pantoja, and H. O. Portner, 2005: Introduction to special section: The ocean in a high-CO2 world. *Journal of Geophysical Research-Oceans*, **110**.
Orsi, A. H., G. C. Johnson, and J. L. Bullister, 1999: Circulation, mixing, and production of Antarctic Bottom Water. *Progress in Oceanography*, **43,** 55-109.
Park, G. H., et al., 2006: Large accumulation of anthropogenic CO2 in the East (Japan) Sea and its significant impact on carbonate chemistry. *Global Biogeochemical Cycles*, **20,** -.
Peltier, W. R., 2001: Global glacial isostatic adjustment and modern instrumental records of relative sea level history. *Sea Level Rise*, B. C. Douglas, M. S. Kearney, and S. P. Leatherman, Eds., Elsevier, 65-95.
——, 2004: Global glacial isostasy and the surface of the ice-age earth: The ice-5G (VM2) model and grace. *Annual Review of Earth and Planetary Sciences*, **32,** 111-149.
Peng, T.-H., R. Wanninkhof, and R. A. Feely, 2003: Increase of anthropogenic CO2 in the Pacific Ocean over the last two decades. *Deep-Sea Research A*, **50,** 3065-3082.
Peng, T.-H., R. Wanninkhof, J. L. Bullister, R. A. Feely, and T. Takahashi, 1998: Quantification of decadal anthropogenic CO2 uptake in the ocean based on dissolved inorganic carbon measurements. *Nature*, **396,** 560-563.

Perez, F. F., V.-R. M., E. Louarn, X. A. Padín, H. Mercier, and A. F. Ríos, 2008: Temporal variability of the anthropogenicv CO2 storage in the Irminger Sea. *Biogeosciences*, **5,** 1669-1679.

Pérez, F. F., M. Vázquez-Rodríguez, H. Mercier, A. Velo, P. Lherminier, and A. F. RÃos, 2010a: Trends of anthropogenic CO2 storage in North Atlantic water masses. *Biogeosciences*, **7,** 1789-1807.

Pérez, F. F., et al., 2010b: Plankton response to weakening of the Iberian coastal upwelling. *Global Change Biology*, **16,** 1258-1267.

Pierce, D. W., T. P. Barnett, K. M. AchutaRao, P. J. Gleckler, J. M. Gregory, and W. M. Washington, 2006: Anthropogenic warming of the oceans: Observations and model results. *Journal of Climate*, **19,** 1873-1900.

Polyakov, I. V., V. A. Alexeev, U. S. Bhatt, E. I. Polyakova, and X. D. Zhang, 2010: North Atlantic warming: patterns of long-term trend and multidecadal variability. *Climate Dynamics*, **34,** 439-457.

Polyakov, I. V., U. S. Bhatt, H. L. Simmons, D. Walsh, J. E. Walsh, and X. Zhang, 2005: Multidecadal variability of North Atlantic temperature and salinity during the twentieth century. *Journal of Climate*, **18,** 4562-4581.

Polyakov, I. V., et al., 2008: Arctic ocean freshwater changes over the past 100 years and their causes. *Journal of Climate*, **21,** 364-384.

Potemra, J. T., and N. Schneider, 2007: Interannual variations of the Indonesian throughflow. *Journal of Geophysical Research-Oceans*, **112**.

Proshutinsky, A., et al., 2009: Beaufort Gyre freshwater reservoir: State and variability from observations. *Journal of Geophysical Research-Oceans*, **114**.

Purkey, S. G., and G. C. Johnson, 2010: Warming of Global Abyssal and Deep Southern Ocean Waters Between the 1990s and 2000s: Contributions to Global Heat and Sea Level Rise Budgets. *Journal of Climate*, **23,** 6336 - 6351.

——, 2011: Global contraction of Antarctic Bottom Water between the 1980s and 2000s. *Journal of Climate*, **submitted**.

Qiu, B., and S. M. Chen, 2006: Decadal variability in the large-scale sea surface height field of the South Pacific Ocean: Observations and causes. *Journal of Physical Oceanography*, **36,** 1751-1762.

Qiu, B., and S. C. Chen, 2010: Interannual-to-Decadal Variability in the Bifurcation of the North Equatorial Current off the Philippines. *Journal of Physical Oceanography*, **40,** 2525-2538.

Qiu, B., and S. Chen, 2011: Multi-Decadal Sea Level and Gyre Circulation Variability in the Northwestern Tropical Pacific Ocean. *Journal of Physical Oceanography*, **accepted**.

Rabe, B., et al., 2011: An assessment of Arctic Ocean freshwater content changes from the 1990s to the 2006-2008 period. *Deep-Sea Research Part I-Oceanographic Research Papers*, **58,** 173-185.

Rahmstorf, S., and M. Vermeer, 2011: Discussion of: Houston, J.R. and Dean, R.G., 2011. Sea-Level Acceleration Based on U.S. Tide Gauges and Extensions of Previous Global-Gauge Analyses. Journal of Coastal Research, 27(3), 409-417. *Journal of Coastal Research*, **27,** 784-787.

Rawlins, M. A., et al., 2010: Analysis of the Arctic System for Freshwater Cycle Intensification: Observations and Expectations. *Journal of Climate*, **23,** 5715-5737.

Ren, L., and S. C. Riser, 2010: Observations of decadal time scale salinity changes in the subtropical thermocline of the North Pacific Ocean. *Deep-Sea Research Part Ii-Topical Studies in Oceanography*, **57,** 1161-1170.

Reverdin, G., 2010: North Atlantic Subpolar Gyre Surface Variability (1895-2009). *Journal of Climate*, **23,** 4571-4584.

Reverdin, G., F. Durand, J. Mortensen, F. Schott, H. Valdimarsson, and W. Zenk, 2002: Recent changes in the surface salinity of the North Atlantic subpolar gyre. *Journal of Geophysical Research-Oceans*, **107**.

Rhein, M., et al., 2011: Deep water formation, the subpolar gyre, and the meridional overturning circulation in the subpolar North Atlantic. *Deep-Sea Research Part Ii-Topical Studies in Oceanography*, **58,** 1819-1832.

Ridgway, K. R., 2007: Long-term trend and decadal variability of the southward penetration of the East Australian Current. *Geophysical Research Letters*, **34**.

Ridgway, K. R., and J. R. Dunn, 2007: Observational evidence for a Southern Hemisphere oceanic supergyre. *Geophysical Research Letters*, **34**.

Rignot, E., J. L. Bamber, M. R. Van Den Broeke, C. Davis, Y. H. Li, W. J. Van De Berg, and E. Van Meijgaard, 2008: Recent Antarctic ice mass loss from radar interferometry and regional climate modelling. *Nature Geoscience*, **1,** 106-110.

Rintoul, S. R., 2007: Rapid freshening of Antarctic Bottom Water formed in the Indian and Pacific oceans. *Geophysical Research Letters*, **34**.

Rintoul, S. R., S. Sokolov, and J. Church, 2002: A 6 year record of baroclinic transport variability of the Antarctic Circumpolar Current at 140 degrees E derived from expendable bathythermograph and altimeter measurements. *Journal of Geophysical Research-Oceans*, **107**.

Roemmich, D., and J. Gilson, 2009: The 2004-2008 mean and annual cycle of temperature, salinity, and steric height in the global ocean from the Argo Program. *Progress in Oceanography*, **82,** 81-100.

Roemmich, D., J. Gilson, R. Davis, P. Sutton, S. Wijffels, and S. Riser, 2007: Decadal spinup of the South Pacific subtropical gyre. *Journal of Physical Oceanography*, **37,** 162-173.

Romanou, A., W. B. Rossow, and S. H. Chou, 2006: Decorrelation scales of high-resolution turbulent fluxes at the ocean surface and a method to fill in gaps in satellite data products. *Journal of Climate*, **19,** 3378-3393.

Romanou, A., B. Liepert, G. A. Schmidt, W. B. Rossow, R. A. Ruedy, and Y. Zhang, 2007: 20th century changes in surface solar irradiance in simulations and observations. *Geophysical Research Letters*, **34**.

Rykaczewski, R. R., and J. P. Dunne, 2010: Enhanced nutrient supply to the California Current Ecosystem with global warming and increased stratification in an earth system model. *Geophysical Research Letters*, **37**.
Sabine, C. L., 2005: Global Ocean Data Analysis Project (GLODAP): Results and data, 110 pp. plus 116 Appendices pp.
Sabine, C. L., R. A. Feely, F. Millero, A. G. Dickson, C. Langdon, S. Mecking, and D. Greeley, 2008: Decadal changes in Pacific Carbon. *Journal of Geophysical Research-Oceans*, **113,** C07021.
Sabine, C. L., et al., 2004: The Oceanic sink for Anthropogenic CO2. *Science*, **305,** 367-371.
Santana-Casiano, J. M., M. Gonzalez-Davila, M. J. Rueda, O. Llinas, and E. F. Gonzalez-Davila, 2007: The interannual variability of oceanic CO2 parameters in the northeast Atlantic subtropical gyre at the ESTOC site. *Global Biogeochemical Cycles*, **21**.
Sarafanov, A., A. Falina, A. Sokov, and A. Demidov, 2008: Intense warming and salinification of intermediate waters of southern origin in the eastern subpolar North Atlantic in the 1990s to mid-2000s. *Journal of Geophysical Research-Oceans*, ARTN C12022, DOI 10.1029/2008JC004975**,** -.
Sarmiento, J. L., et al., 2010: Trends and regional distributions of land and ocean carbon sinks. *Biogeosciences*, **7,** 2351-2367.
Sasaki, W., S. I. Iwasaki, T. Matsuura, and S. Iizuka, 2005: Recent increase in summertime extreme wave heights in the western North Pacific. *Geophysical Research Letters*, **32**.
Schanze, J. J., R. W. Schmitt, and L. L. Yu, 2010: The global oceanic freshwater cycle: A state-of-the-art quantification. *Journal of Marine Research*, **68,** 569-595.
Schauer, U., and A. Beszczynska-Möller, 2009: Problems with estimation and interpretation of oceanic heat transport – conceptual remarks for the case of Fram Strait in the Arctic Ocean. *Ocean Science*, **5,** 487–494.
Schmidtko, S., and G. C. Johnson, 2011: Multi-decadal warming and shoaling of Antarctic Intermediate Water. *Journal of Climate*, **in press, doi:10.1175/JCLI-D-11-00021.1**.
Schmitt, R. W., 2008: Salinity and the Global Water Cycle. *Oceanography*, **21,** 12-19.
Schneider, T., P. A. O'Gorman, and X. J. Levine, 2010: WATER VAPOR AND THE DYNAMICS OF CLIMATE CHANGES. *Reviews of Geophysics*, **48**.
Schuster, U., and A. J. Watson, 2007: A variable and decreasing sink for atmospheric CO2 in the North Atlantic. *Journal of Geophysical Research-Oceans*, **112,** -.
Semedo, A., K. Suselj, A. Rutgersson, and A. Sterl, 2011: A Global View on the Wind Sea and Swell Climate and Variability from ERA-40. *Journal of Climate*, **24,** 1461-1479.
Send, U., M. Lankhorst, and T. Kanzow, 2011: Observation of decadal change in the Atlantic Meridional Overturning Circulation using 10 years of continuous transport data. *Geophys. Res. Lett.*, **in press**.
Shepherd, A., D. Wingham, and E. Rignot, 2004: Warm ocean is eroding West Antarctic Ice Sheet. *Geophysical Research Letters*, **31**.
Shiklomanov, A. I., and R. B. Lammers, 2009: Record Russian river discharge in 2007 and the limits of analysis. *Environmental Research Letters*, **4**.
Smith, T. M., P. A. Arkin, and M. R. P. Sapiano, 2009: Reconstruction of near-global annual precipitation using correlations with sea surface temperature and sea level pressure. *Journal of Geophysical Research-Atmospheres*, **114**.
Sokolov, S., and S. R. Rintoul, 2009: Circumpolar structure and distribution of the Antarctic Circumpolar Current fronts: 2. Variability and relationship to sea surface height. *Journal of Geophysical Research-Oceans*, **114,** 15.
Speer, K. G., 1997: A note on average cross-isopycnal mixing in the North Atlantic ocean. *Deep-Sea Research Part I-Oceanographic Research Papers*, **44,** 1981-1990.
Speich, S., B. Blanke, and W. Cai, 2007: Atlantic meridional overturning circulation and the Southern Hemisphere supergyre. *Geophysical Research Letters*, **34**.
Spence, P., J. C. Fyfe, A. Montenegro, and A. J. Weaver, 2010: Southern Ocean Response to Strengthening Winds in an Eddy-Permitting Global Climate Model. *Journal of Climate*, **23,** 5332-5343.
Sprintall, J., S. Wijffels, T. Chereskin, and N. Bray, 2002: The JADE and WOCE I10/IR6 Throughflow sections in the southeast Indian Ocean. Part 2: velocity and transports. *Deep-Sea Research Part Ii-Topical Studies in Oceanography*, **49,** 1363-1389.
Sprintall, J., S. E. Wijffels, R. Molcard, and I. Jaya, 2009: Direct estimates of the Indonesian Throughflow entering the Indian Ocean: 2004-2006. *Journal of Geophysical Research-Oceans*, **114**.
Steinfeldt, R., M. Rhein, J. L. Bullister, and T. Tanhua, 2009: Inventory changes in anthropogenic carbon from 1997-2003 in the Atlantic Ocean between 20 degrees S and 65 degrees N. *Global Biogeochemical Cycles*, **23,** GB3010.
Sterl, A., and S. Caires, 2005: Climatology, variability and extrema of ocean waves: The web-based KNMI/ERA-40 wave atlas. *International Journal of Climatology*, **25,** 963-977.
Stott, P. A., R. T. Sutton, and D. M. Smith, 2008: Detection and attribution of Atlantic salinity changes. *Geophysical Research Letters*, **35**.
Stramma, L., G. C. Johnson, J. Sprintall, and V. Mohrholz, 2008: Expanding oxygen-minimum zones in the tropical oceans. *Science*, **320,** 655-658.
Stramma, L., S. Schmidtko, L. A. Levin, and G. C. Johnson, 2010: Ocean oxygen minima expansions and their biological impacts. *Deep-Sea Research Part I-Oceanographic Research Papers*, **57,** 587-595.

Straneo, F., et al., 2010: Rapid circulation of warm subtropical waters in a major glacial fjord in East Greenland. *Nature Geoscience*, **3,** 182-186.
Sturges, W., and B. C. Douglas, 2011: Wind effects on estimates of sea level rise. *Journal of Geophysical Research-Oceans*, **116**.
Sugimoto, S., and K. Hanawa, 2010: The Wintertime Wind Stress Curl Field in the North Atlantic and Its Relation to Atmospheric Teleconnection Patterns. *Journal of the Atmospheric Sciences*, **67,** 1687-1694.
Swart, S., S. Speich, I. J. Ansorge, G. J. Goni, S. Gladyshev, and J. R. E. Lutjeharms, 2008: Transport and variability of the antarctic circumpolar current South of Africa. *Journal of Geophysical Research-Oceans*, **113**.
Takahashi, T., et al., 2009: Climatological mean and decadal change in surface ocean pCO(2), and net sea-air CO2 flux over the global oceans (vol 56, pg 554, 2009). *Deep-Sea Research Part I-Oceanographic Research Papers*, **56,** 2075-2076.
Tanaka, H. L., N. Ishizaki, and A. Kitoh, 2004: Trend and interannual variability of Walker, monsoon and Hadley circulations defined by velocity potential in the upper troposphere. *Tellus Series a-Dynamic Meteorology and Oceanography*, **56,** 250-269.
Tanhua, T., A. Koertzinger, K. Friis, D. W. Waugh, and D. W. R. Wallace, 2007: An estimate of anthropogenic CO(2) inventory from decadal changes in oceanic carbon content. *Proceedings of the National Academy of Sciences of the United States of America*, **104,** 3037-3042.
Tanhua, T., E. P. Jones, E. Jeansson, S. Jutterstrom, W. M. Smethie, D. W. R. Wallace, and L. G. Anderson, 2009: Ventilation of the Arctic Ocean: Mean ages and inventories of anthropogenic CO2 and CFC-11. *Journal of Geophysical Research-Oceans*, **114,** -.
Timmermann, A., S. McGregor, and F. F. Jin, 2010: Wind Effects on Past and Future Regional Sea Level Trends in the Southern Indo-Pacific. *Journal of Climate*, **23,** 4429-4437.
Toole, J. M., R. G. Curry, T. M. Joyce, M. McCartney, and B. Pena-Molino, 2011: Transport of the North Atlantic Deep Western Boundary Current about 39 degrees N, 70 degrees W: 2004-2008. *Deep-Sea Research Part Ii-Topical Studies in Oceanography*, **58,** 1768-1780.
Trenberth, K. E., and L. Smith, 2005: The mass of the atmosphere: A constraint on global analyses. *Journal of Climate*, **18,** 864-875.
Trenberth, K. E., J. T. Fasullo, and J. Kiehl, 2009: EARTH'S GLOBAL ENERGY BUDGET. *Bulletin of the American Meteorological Society*, **90,** 311-+.
Trenberth, K. E., J. T. Fasullo, and J. Mackaro, 2011: Atmospheric Moisture Transports from Ocean to Land and Global Energy Flows in Reanalyses. *Journal of Climate*, **24,** 4907-4924.
Trenberth, K. E., et al., 2007: Observations: Surface and Atmospheric Climate Change. *Climate Change 2007: The Physical Science Basis. Contribution of Working Group I to the Fourth Assessment Report of the Intergovernmental Panel on Climate Change*, S. Solomon, et al., Eds., Cambridge University Press.
Tsimplis, M. N., and A. G. P. Shaw, 2010: Seasonal sea level extremes in the Mediterranean Sea and at the Atlantic European coasts. *Natural Hazards and Earth System Sciences*, **10,** 1457-1475.
Vecchi, G. A., B. J. Soden, A. T. Wittenberg, I. M. Held, A. Leetmaa, and M. J. Harrison, 2006: Weakening of tropical Pacific atmospheric circulation due to anthropogenic forcing. *Nature (London)*, **441,** 73-76.
Vilibic, I., and J. Sepic, 2010: Long-term variability and trends of sea level storminess and extremes in European Seas. *Global and Planetary Change*, **71,** 1-12.
Wahlin, A. K., X. Yuan, G. Bjork, and C. Nohr, 2010: Inflow of Warm Circumpolar Deep Water in the Central Amundsen Shelf. *Journal of Physical Oceanography*, **40,** 1427-1434.
Wainwright, L., G. Meyers, S. Wijffels, and L. Pigot, 2008: Change in the Indonesian Throughflow with the climatic shift of 1976/77. *Geophysical Research Letters*, **35**.
Wakita, M., S. Watanabe, A. Murata, N. Tsurushima, and M. Honda, 2010: Decadal change of dissolved inorganic carbon in the subarctic western North Pacific Ocean. *Tellus B*, **62,** 608-620.
Wang, C. Z., S. F. Dong, and E. Munoz, 2010: Seawater density variations in the North Atlantic and the Atlantic meridional overturning circulation. *Climate Dynamics*, **34,** 953-968.
Wang, X. L. L., and V. R. Swail, 2006: Climate change signal and uncertainty in projections of ocean wave heights. *Climate Dynamics*, **26,** 109-126.
Wang, X. L. L., V. R. Swail, F. W. Zwiers, X. B. Zhang, and Y. Feng, 2009: Detection of external influence on trends of atmospheric storminess and northern oceans wave heights. *Climate Dynamics*, **32,** 189-203.
Wanninkhof, R., W. E. Asher, D. T. Ho, C. Sweeney, and W. R. McGillis, 2009: Advances in Quantifying Air-Sea Gas Exchange and Environmental Forcing. *Annual Review of Marine Science*, **1,** 213-244.
Wanninkhof, R., S. C. Doney, J. L. Bullister, N. M. Levine, M. Warner, and N. Gruber, 2010: Detecting anthropogenic CO2 changes in the interior Atlantic Ocean between 1989 and 2005. *J. Geophys. Res.*, **115,** C11028.
WASA-Group, 1998: Changing waves and storm in the Northern Atlantic? *Bulletin of the American Meteorological Society*, **79,** 741-760.
Watson, A. J., et al., 2009: Tracking the Variable North Atlantic Sink for Atmospheric CO2. *Science*, **326,** 1391-1393.
Waugh, D. W., T. M. Hall, B. I. McNeil, R. Key, and R. J. Matear, 2006: Anthropogenic CO2 in the Oceans estimated using transit-time distributions. *Tellus*, **58B,** 376-389.
Wentz, F. J., L. Ricciardulli, K. Hilburn, and C. Mears, 2007: How much more rain will global warming bring? *Science*, **317,** 233-235.

Whitney, F. A., H. J. Freeland, and M. Robert, 2007: Persistently declining oxygen levels in the interior waters of the eastern subarctic Pacific. *Progress in Oceanography*, **75,** 179-199.
Wijffels, S. E., et al., 2008: Changing Expendable Bathythermograph Fall Rates and Their Impact on Estimates of Thermosteric Sea Level Rise. *Journal of Climate*, **21,** 5657-5672.
Wild, M., 2009: Global dimming and brightening: A review. *Journal of Geophysical Research-Atmospheres*, **114**.
Wild, M., et al., 2005: From dimming to brightening: Decadal changes in solar radiation at Earth's surface. *Science*, **308,** 847-850.
Willis, J. K., 2010: Can in situ floats and satellite altimeters detect long-term changes in Atlantic Ocean overturning? *Geophysical Research Letters*, **37**.
Willis, J. K., D. P. Chambers, and R. S. Nerem, 2008: Assessing the globally averaged sea level budget on seasonal to interannual timescales. *Journal of Geophysical Research-Oceans*, **113**.
Willis, J. K., D. P. Chambers, C.-Y. Kuo, and C. K. Shum, 2010: Global sea level rise: Recent Progress and challenges for the decade to come. *Oceanography*, **23,** 26 - 35.
Woeppelmann, G., et al., 2009: Rates of sea-level change over the past century in a geocentric reference frame. *Geophysical Research Letters*, **36**.
Wong, A. P. S., N. L. Bindoff, and J. A. Church, 1999: Large-scale freshening of intermediate waters in the Pacific and Indian oceans. *Nature*, **400,** 440-443.
Wong, C. S., L. S. Xie, and W. W. Hsieh, 2007: Variations in nutrients, carbon and other hydrographic parameters related to the 1976/77 and 1988/89 regime shifts in the sub-arctic Northeast Pacific. *Progress in Oceanography*, **75,** 326-342.
Woodworth, P. L., and D. L. Blackman, 2004: Evidence for systematic changes in extreme high waters since the mid-1970s. *Journal of Climate*, **17,** 1190-1197.
Woodworth, P. L., M. Menendez, and W. R. Gehrels, 2011: Evidence for Century-Timescale Acceleration in Mean Sea Levels and for Recent Changes in Extreme Sea Levels. *Surveys in Geophysics*, **32,** 603-618.
Woodworth, P. L., N. J. White, S. Jevrejeva, S. J. Holgate, J. A. Church, and W. R. Gehrels, 2009: Evidence for the accelerations of sea level on multi-decade and century timescales. *International Journal of Climatology*, **29,** 777-789.
Xue, Y., B. Huang, Z.-Z. Hu, A. Kumar, C. Wen, D. Behringer, and S. Nadiga, 2010: An assessment of oceanic variability in the NCEP climate forecast system reanalysis. *Climate Dynamics*, 10.1007/s00382-010-0954-4**,** 1-29.
Yamamoto-Kawai, M., F. A. McLaughlin, E. C. Carmack, S. Nishino, K. Shimada, and N. Kurita, 2009: Surface freshening of the Canada Basin, 2003-2007: River runoff versus sea ice meltwater. *Journal of Geophysical Research-Oceans*, **114**.
Yang, X. Y., R. X. Huang, and D. X. Wang, 2007: Decadal changes of wind stress over the Southern Ocean associated with Antarctic ozone depletion. *Journal of Climate*, **20,** 3395-3410.
Yashayaev, I., 2007: Hydrographic changes in the Labrador Sea, 1960-2005. *Progress in Oceanography*, **73,** 242-276.
Yashayaev, I., and J. W. Loder, 2009: Enhanced production of Labrador Sea Water in 2008. *Geophysical Research Letters*, **36**.
Young, I. R., S. Zieger, and A. V. Babanin, 2011: Global Trends in Wind Speed and Wave Height. *Science*, **332,** 451-455.
Yu, L., 2011: A global relationship between the ocean water cycle and near-surface salinity. *Journal of Geophysical Research-Oceans*, **116**.
Yu, L., and R. A. Weller, 2007: Objectively analyzed air-sea flux fields for the global ice-free oceans (1981-2005). *Bulletin of the American Meteorological Society*, **88,** 527-539.
Yu, L. S., 2007: Global variations in oceanic evaporation (1958-2005): The role of the changing wind speed. *Journal of Climate*, **20,** 5376-5390.
Yu, L. S., X. Z. Jin, and R. A. Weller, 2007: Annual, seasonal, and interannual variability of air-sea heat fluxes in the Indian Ocean. *Journal of Climate*, **20,** 3190-3209.
Zenk, W., and E. Morozov, 2007: Decadal warming of the coldest Antarctic Bottom Water flow through the Vema Channel.

Chapter 3: Observations: Ocean

Coordinating Lead Authors: Monika Rhein (Germany), Stephen R. Rintoul (Australia)

Lead Authors: Shigeru Aoki (Japan), Edmo Campos (Brazil), Don Chambers (USA), Richard Feely (USA), Sergey Gulev (Russia), Gregory C. Johnson (USA), Simon Josey (UK), Andrey Kostianoy (Russia), Cecilie Mauritzen (Norway), Dean Roemmich (USA), Lynne Talley (USA), Fan Wang (China)

Contributing Authors: Michio Aoyama, Molly Baringer, Nick Bates, Timothy Boyer, Robert Byrne, Stuart Cunningham, Thierry Delcroix, John Dore, Paul Durack, Rana Fine, Melchor González-Dávila, Nicolas Gruber, Mark Hemer, David Hydes, Stanley Jacobs, Torsten Kanzow, David Karl, Alexander Kazmin, Samar Khatiwala, Joan Kleypas, Kitack Lee, Calvin Mordy, Jon Olafsson, James Orr, Alejandro Orsi, Igor Polyakov, Sarah G. Purkey, Bo Qiu, Gilles Reverdin, Anastasia Romanou, Raymond Schmitt, Koji Shimada, Lothar Stramma, Toshio Suga, Taro Takahashi, Toste Tanhua, Hans von Storch, Xialoan Wang, Rik Wanninkhof, Susan Wijffels, Philip Woodworth, Igor Yashayaev, Lisan Yu

Review Editors: Howard Freeland (Canada), Yukihiro Nojiri (Japan), Ilana Wainer (Brazil)

Date of Draft: 16 December 2011

Notes: TSU Compiled Version

Figures

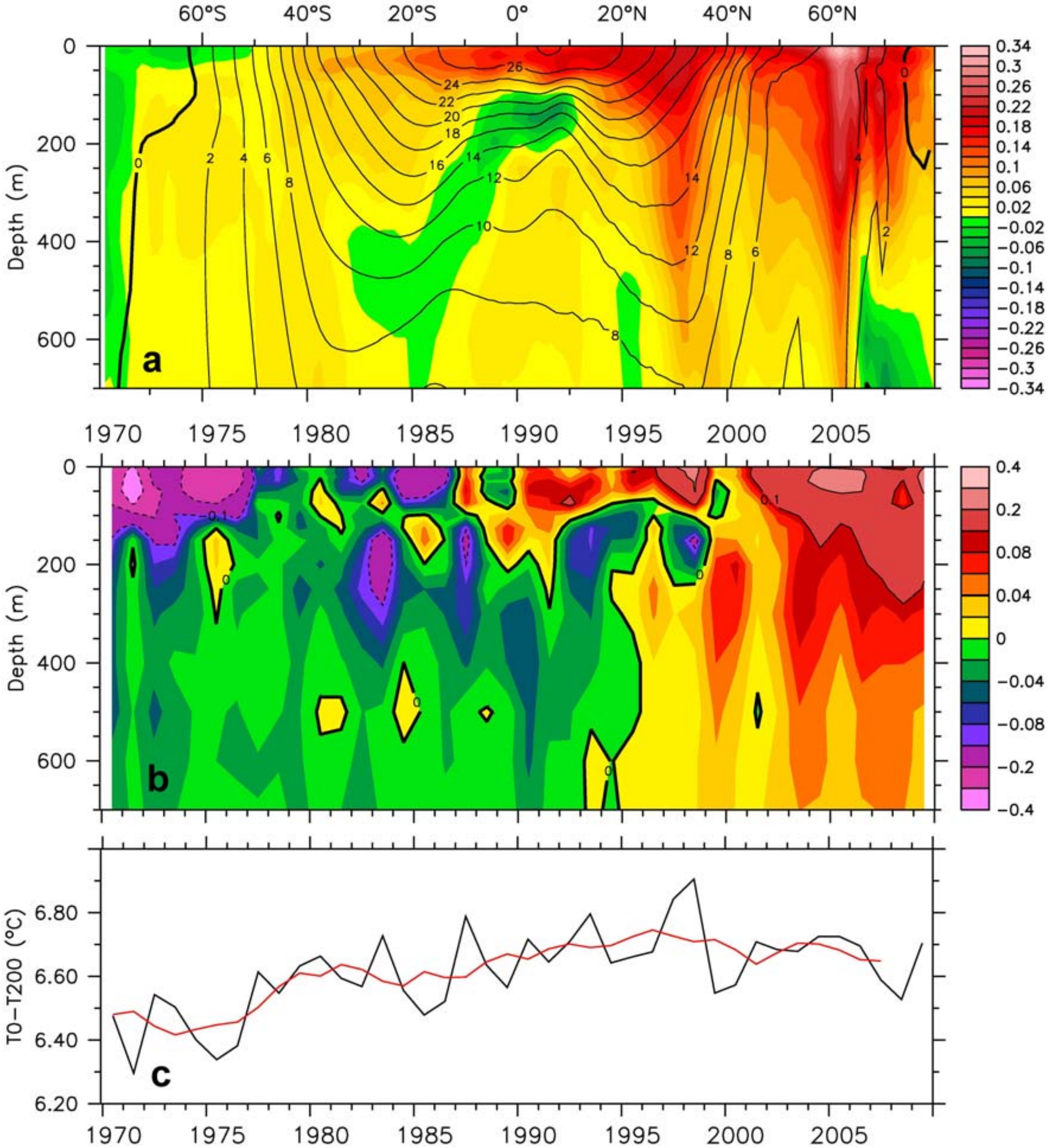

Figure 3.1: a) Zonally-averaged temperature trends (latitude versus depth, colors in °C per decade) for 1970–2009, with zonally averaged mean temperature over-plotted (black contours in °C). **b)** Globally-averaged temperature anomaly (time versus depth, colors in °C). **c)** Globally-averaged temperature difference between the ocean surface and 200-m depth (black: annual values, red: 5-year running mean). All plots are constructed from the optimal interpolation analysis of Levitus et al. (2009).

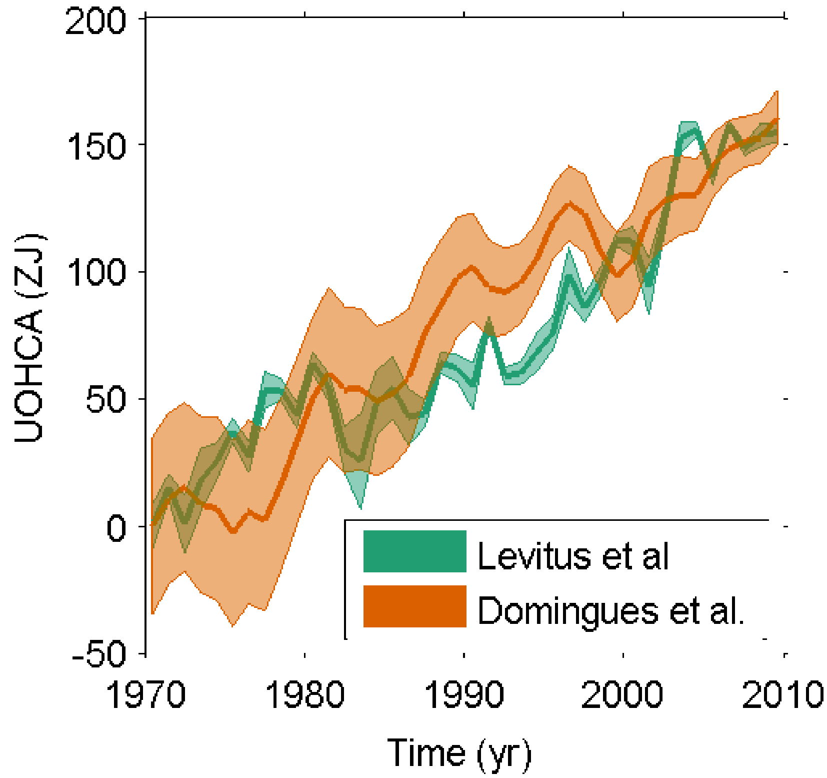

Figure 3.2: Observation-based estimates of annual global mean ocean heat content anomaly in ZJ (10^{21} J) from 0–700 m from Levitus et al. (2009) (green line) and Domingues et al. (2008) (orange line) with one standard error uncertainty estimates (shading). The error estimates of Levitus et al. (2009) are simply the standard deviation of four seasonal estimates for each year, and do not reflect the full uncertainty, whereas the larger error estimates of Domingues et al. (2008) reflect data distributions and ocean statistics. The curves are plotted relative to their 1970 values.

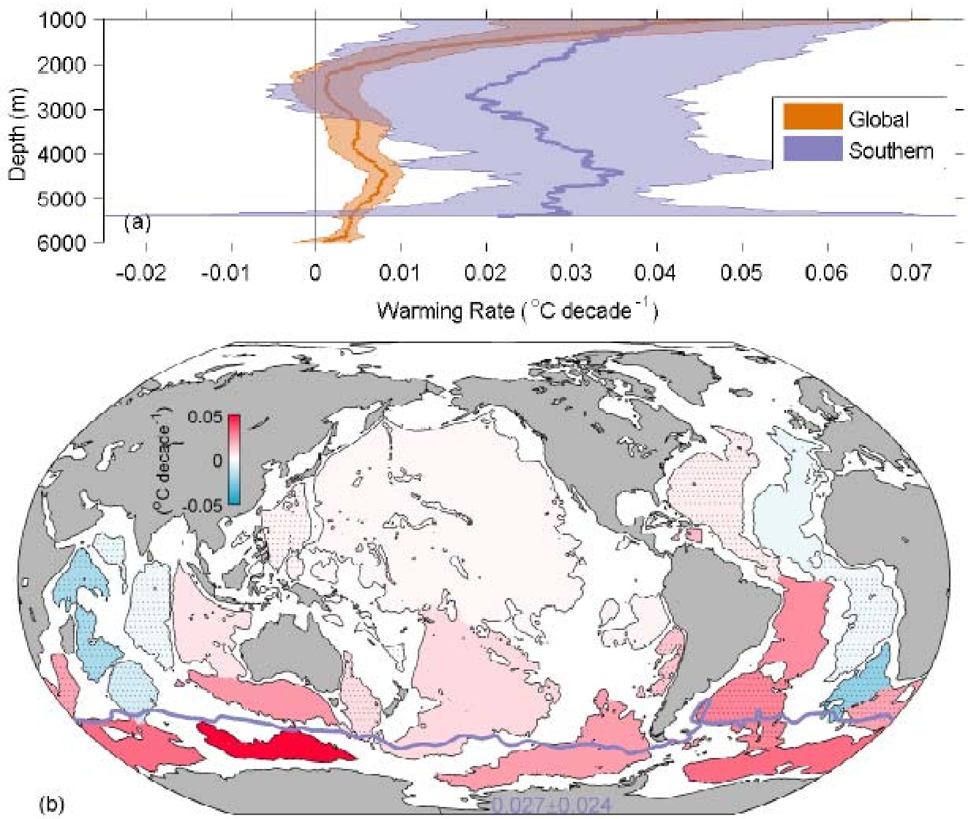

Figure 3.3: a) Areal mean warming rates versus depth (thick lines) with 95% confidence limits (shading), both global (orange) and for the Southern Ocean south of the Sub-Antarctic Front SAF (purple). **b)** Mean warming rate below 4000 m (colorbar) estimated for deep ocean basins (thin black outlines) and centred on 1992–2005. Stippled basin warming rates are not significantly different from zero at 95% confidence. The mean warming rate for 1000–4000 m south of the SAF (purple line) is also given (purple number) with its 95% confidence interval. Data from Purkey and Johnson (2010).

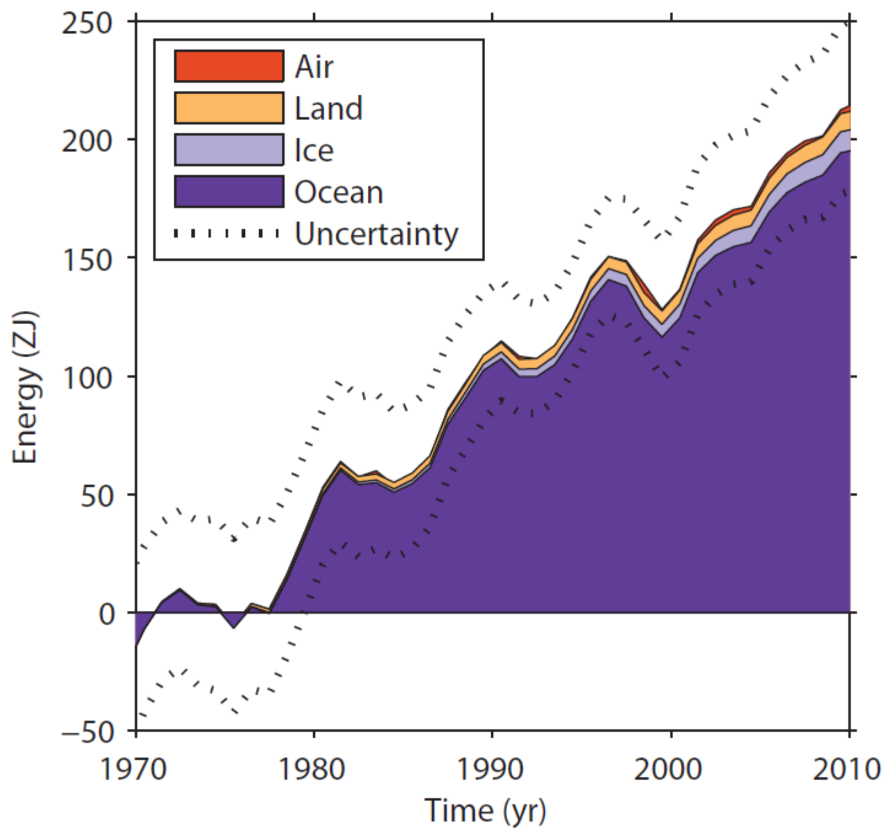

Box 3.1, Figure 1: Plot of energy change inventory in ZJ (10^{21} J) within distinct components of Earth's climate system relative to and starting from 1970 unless otherwise indicated. The combined upper and deep ocean warming (dark purple) dominates; ice melt (light purple; for glaciers and ice caps, Greenland starting from 1992, Antarctica starting from 1992, and Arctic sea ice starting from 1979); continental warming (orange); and atmospheric warming (red; starting from 1979) make smaller contributions. The ocean uncertainty also dominates the total uncertainty (dotted lines about the sum of all four components).

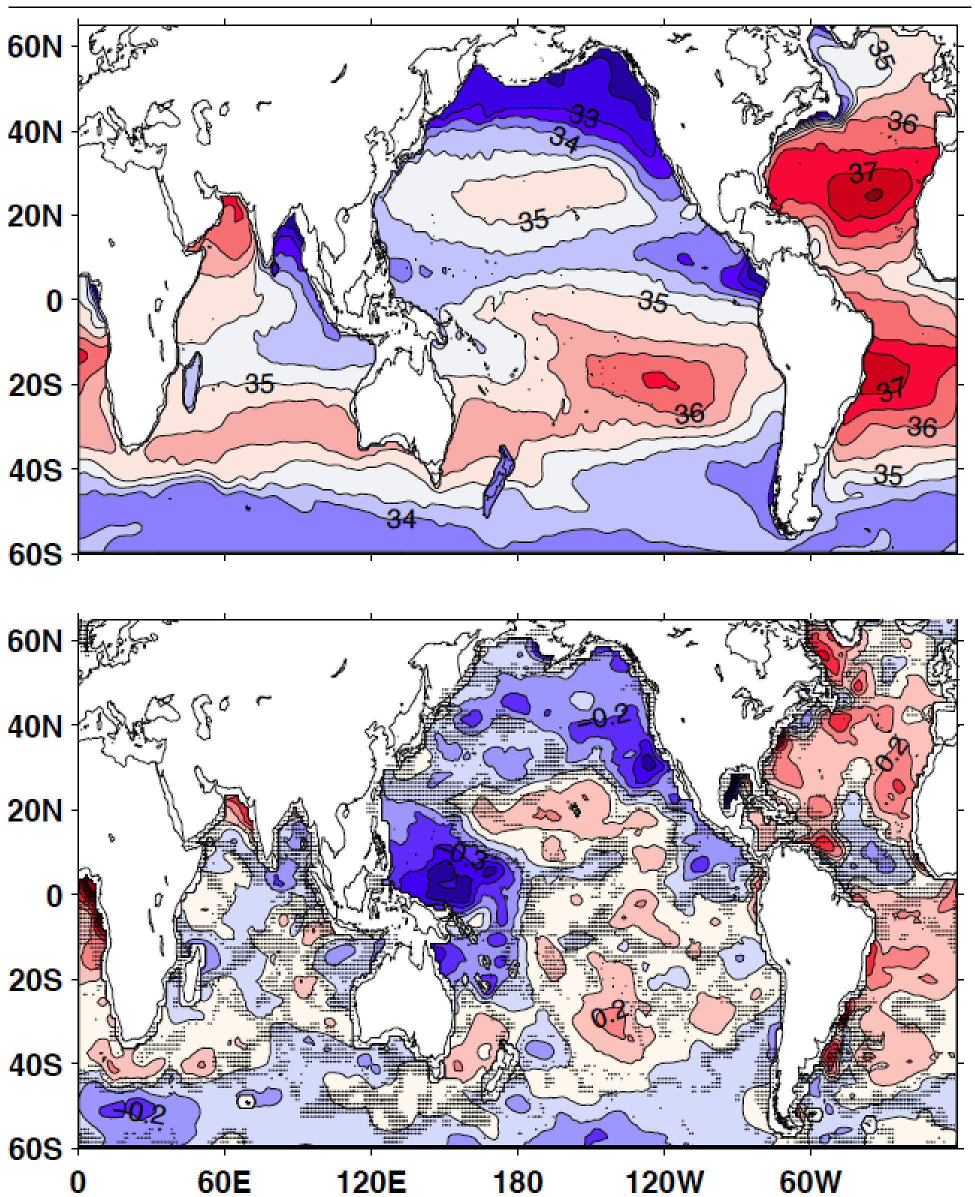

Figure 3.4: a) The 1950–2000 climatological-mean surface salinity. Contours every 0.5 are plotted in black. **b)** The 50-year linear surface salinity trend [(50 year)$^{-1}$]. Contours every 0.2 are plotted in white. Regions where the resolved linear trend is not significant at the 99% confidence level are stippled in grey. Composite of Durack and Wijffels (2010) and Hosoda et al. (2009).

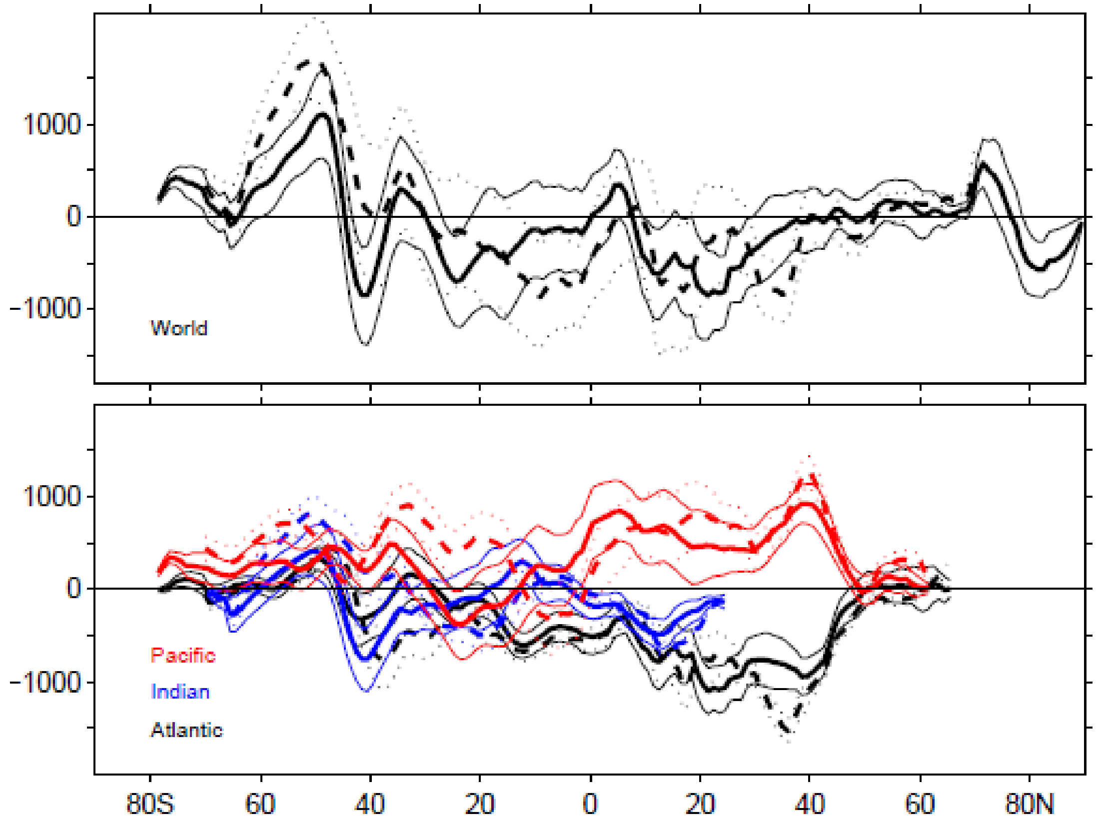

Figure 3.5: Zonally integrated freshwater content changes (km^3 per degree of latitude) for the latter half of the 20th century in the upper 500 m over the one-degree zonal belt of the World Ocean (upper panel), and Atlantic, Pacific, and Indian Oceans (lower panel). The time period is from the late 1950s to 2000s (Boyer et al., 2005; solid lines) and 1950–2000 (Durack and Wijffels, 2010; broken lines). Calculations are done according to the method of Boyer et al. (2007). Error estimates are 90% confidence intervals.

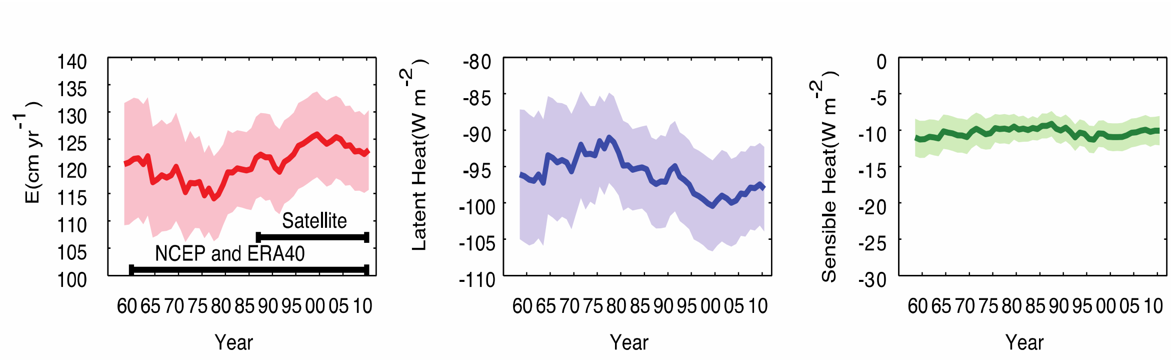

Figure 3.6: Time series of globally averaged annual mean ocean evaporation (E), latent and sensible heat flux from 1958 to 2010 determined from OAFlux (shaded bands show uncertainty estimates; updated from Yu (2007)).

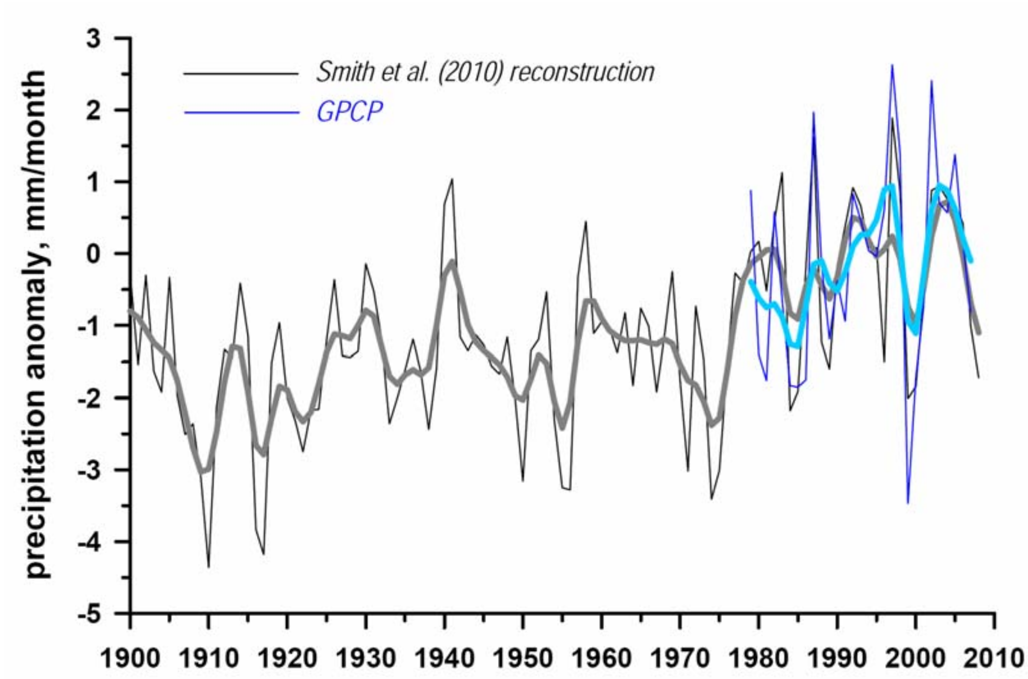

Figure 3.7: Long-term reconstruction of ocean precipitation (annual values – thin black line, low-pass filtered data – bold grey line) over 75°S – 75°N by Smith et al. (2009) as well as GPCP-derived ocean precipitation over the same latitudinal range (annual values – thin blue line, low-pass filtered data – cyan bold line). Precipitation anomalies were taken relative to the 1979–2007 period.

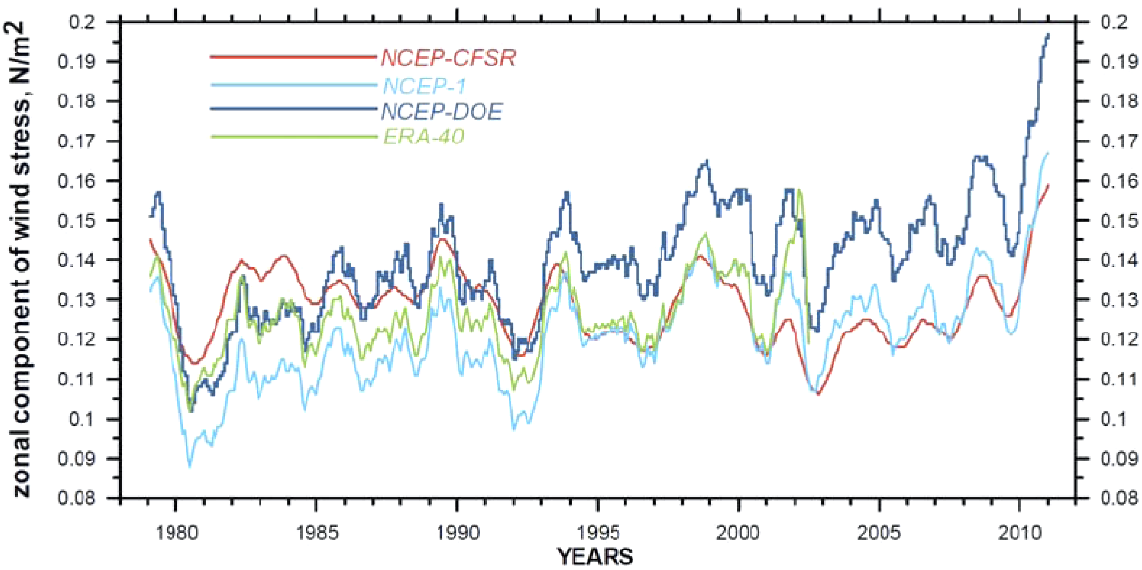

Figure 3.8: Time series of 1-year running mean of zonal mean wind stress over the Southern Ocean (45–70°S) for NCEP-CFSR (red), NCEP R1 (cyan, labelled NCEP-1), NCEP/NCAR R2 (dark blue line, labelled NCEP-DOE) and ERA-40 (green line). Units are N m^{-2} (Xue et al., 2010).

Figure 3.9: [PLACEHOLDER FOR SECOND ORDER DRAFT: Global map of trends in SWH. Figure will be available for Second Order Draft.]

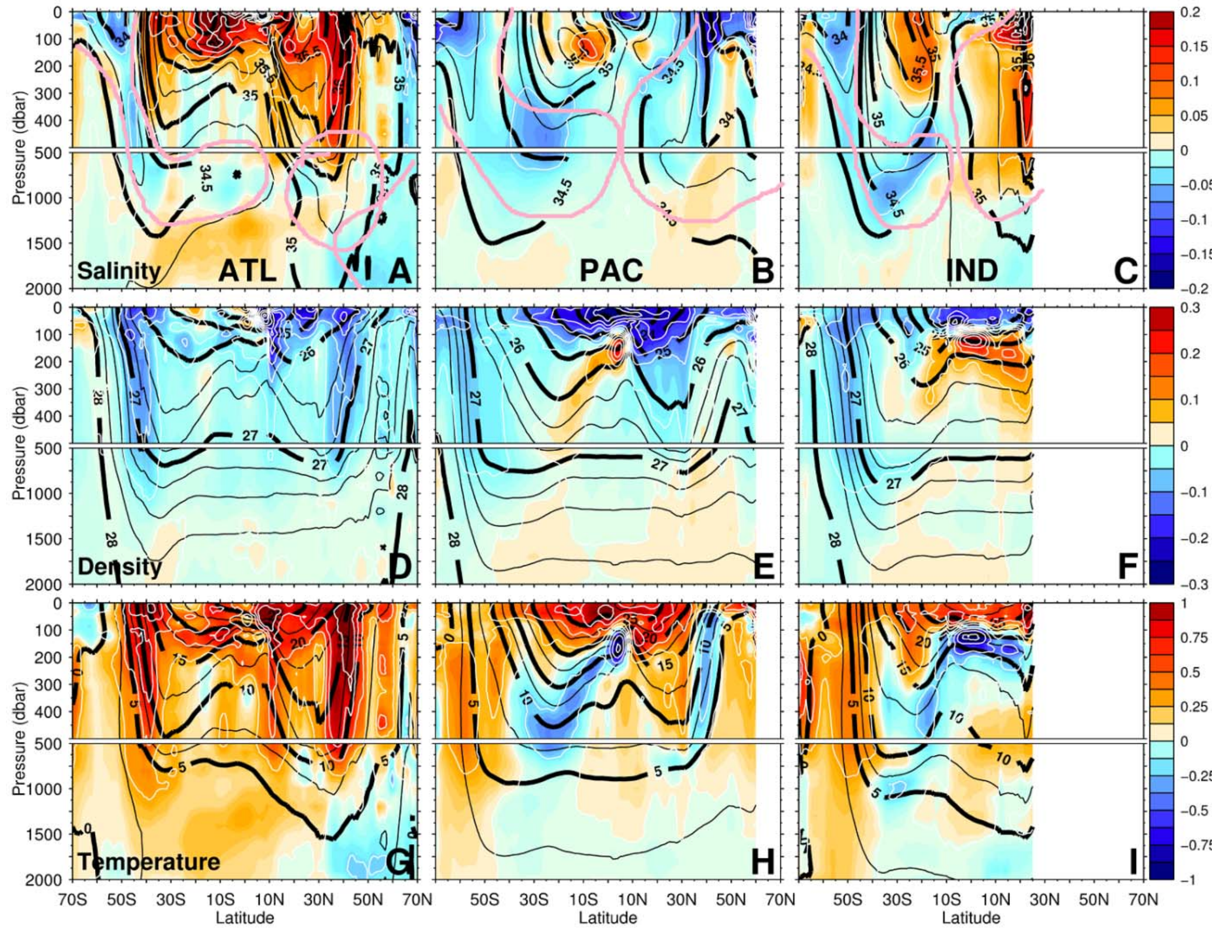

Global averages:

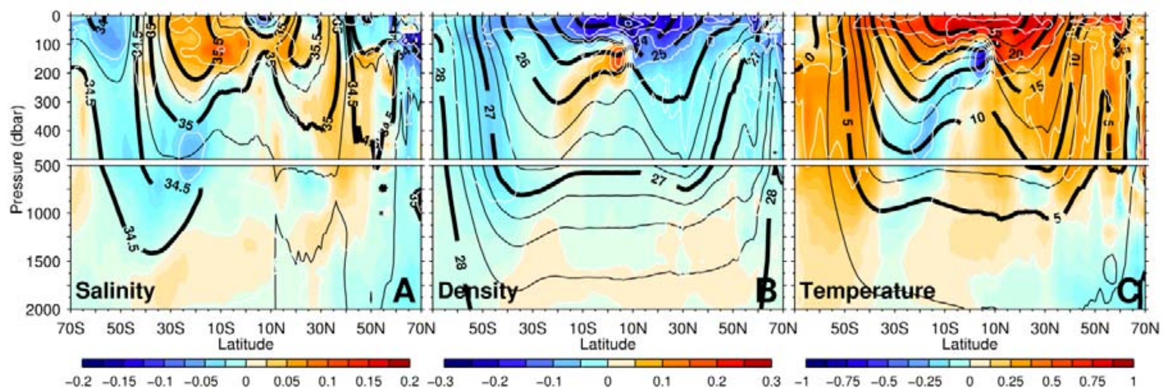

Figure 3.10: [PLACEHOLDER FOR SECOND ORDER DRAFT] Upper 2000 m zonal average distribution of changes in salinity (row 1), neutral density (row 2), and potential temperature (row 3), for the Atlantic (column 1), Pacific (column 2) and Indian (column 3) oceans over the past 50 years (1950–2000). Mean density is overlaid in black (contour interval 1.0 kg m^{-3} – thick contours, and 26.5 to 27.75 in increments of 0.25 kg m^{-3} – thin contours), and density changes are contoured in white (contour interval 0.1 kg m^{-3} from -0.3 to +0.3 kg m^{-3}). Data from Durack and Wijffels (2010). Main intermediate water masses are indicated in row 1.

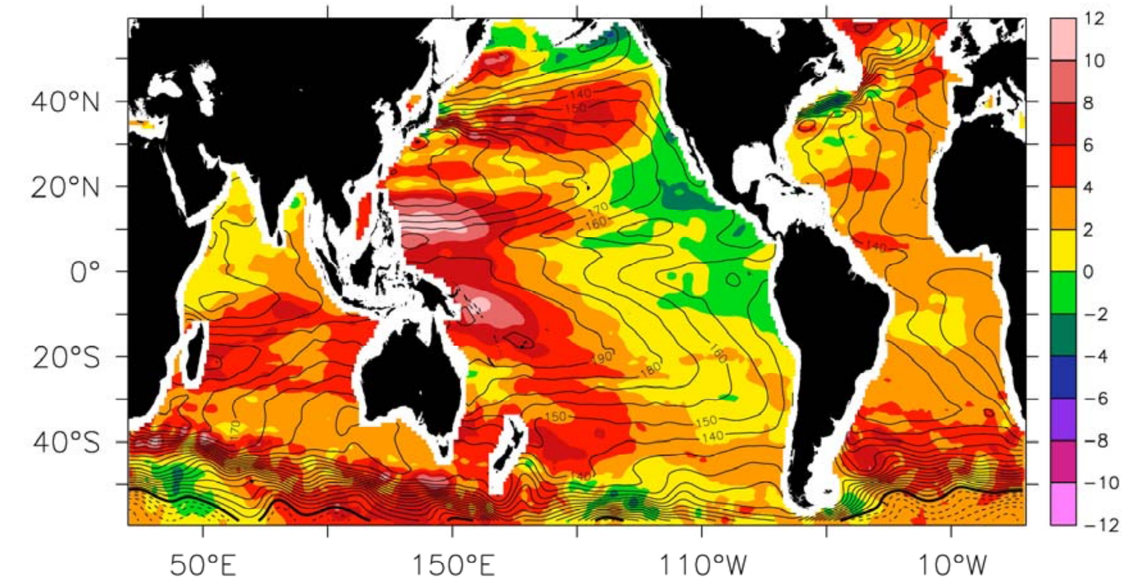

Figure 3.11: The mean SSH (cm, black contours) for the Argo era is the sum of the geostrophic pressure field at 1000 m based on Argo trajectory data (Katsumata and Yoshinari, 2010) plus the relative pressure field (0/1000 dbar steric height) based on Argo profile data from Roemmich and Gilson (2009). The SSH trend (cm decade^{-1}, color shading) for the period 1993–2009 is based on the AVISO altimetry "reference" product (Ducet et al., 2000). Spatial gradients in the SSH trend are proportional to changes in surface geostrophic velocity.

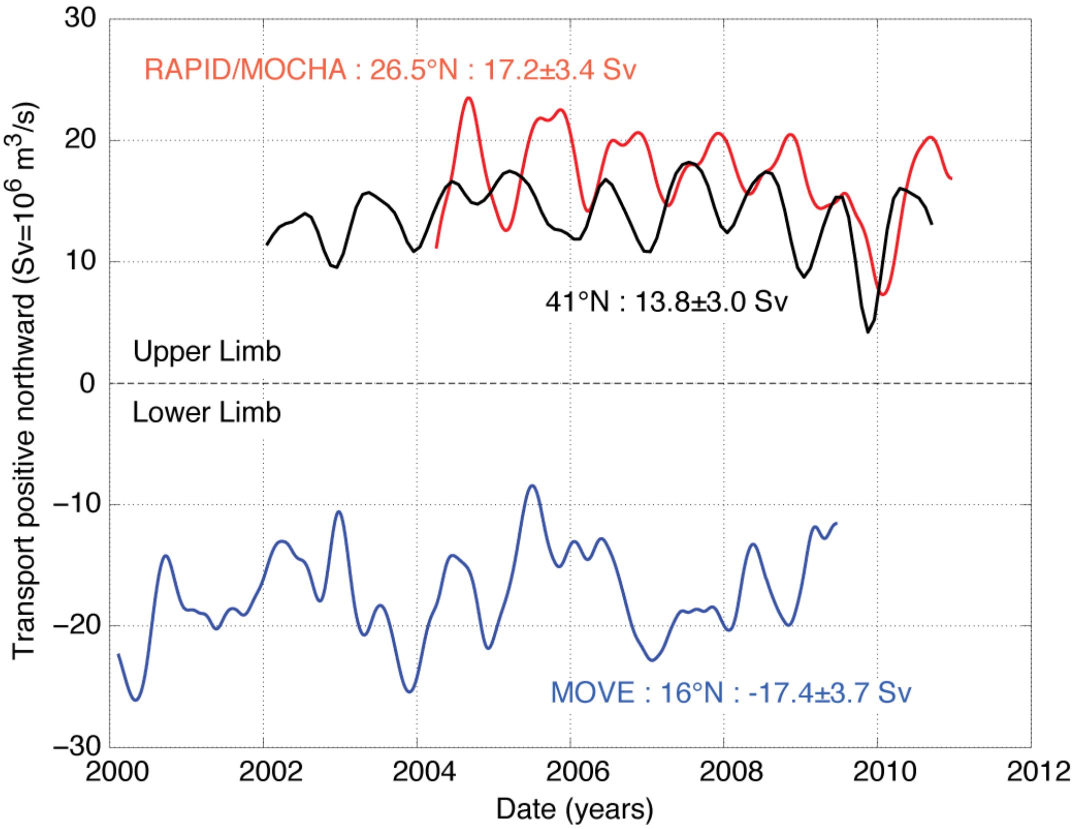

Figure 3.12: The AMOC is a time-varying streamfunction in the vertical-meridional plane that can be calculated from the zonal integral of the meridional velocity in an east–west section across an ocean basin The AMOC is primarily a two-layer system, with an upper limb moving northward between the surface and approximately 1200 m depth and a mass-balancing lower limb return flow between approximately 1200 m and 5000 m. Transports are given in units of Sverdrups (Sv; where 1 Sv = 10^6 m^3 s^{-1}). 1. RAPID/MOCHA array at 26.5°N (red): The array monitors the top-to-bottom Atlantic wide circulation, ensuring a closed mass balance across the section, and hence a direct measure of the upper and lower limbs of the AMOC. 2. 41°N (black): An index of maximum AMOC strength from Argo float measurements in the upper 2000 m only, combined with satellite altimeter data. The lower limb is not measured. 3. MOVE at 16°N (blue): Transport of North Atlantic Deep Water in the lower limb of the AMOC between 1100m and 4800m depth between the Caribbean and the mid-Atlantic Ridge. This transport is thought to be representative of maximum MOC variability based on model validation experiments. The temporal resolution of the three timeseries is ten days for 16°N and 26°N and one month for 41°N. In this figure the data have been three month low-pass filtered and the means and standard deviations are of the low-pass timeseries.

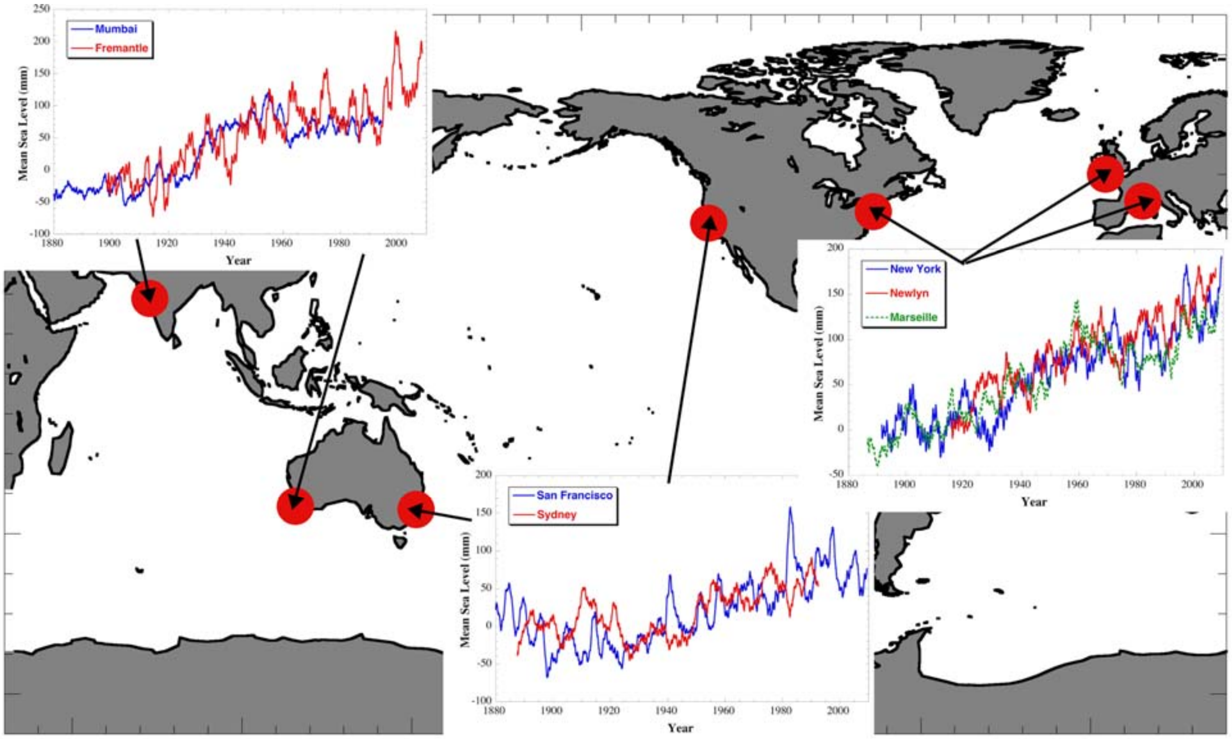

Figure 3.13: 3-year running mean sea level from long tide gauge records from the Permanent Service for Mean Sea Level (PSMSL), corrected for Glacial Isostatic Adjustment (GIA) (Peltier, 2004), after Woodworth et al. (2009).

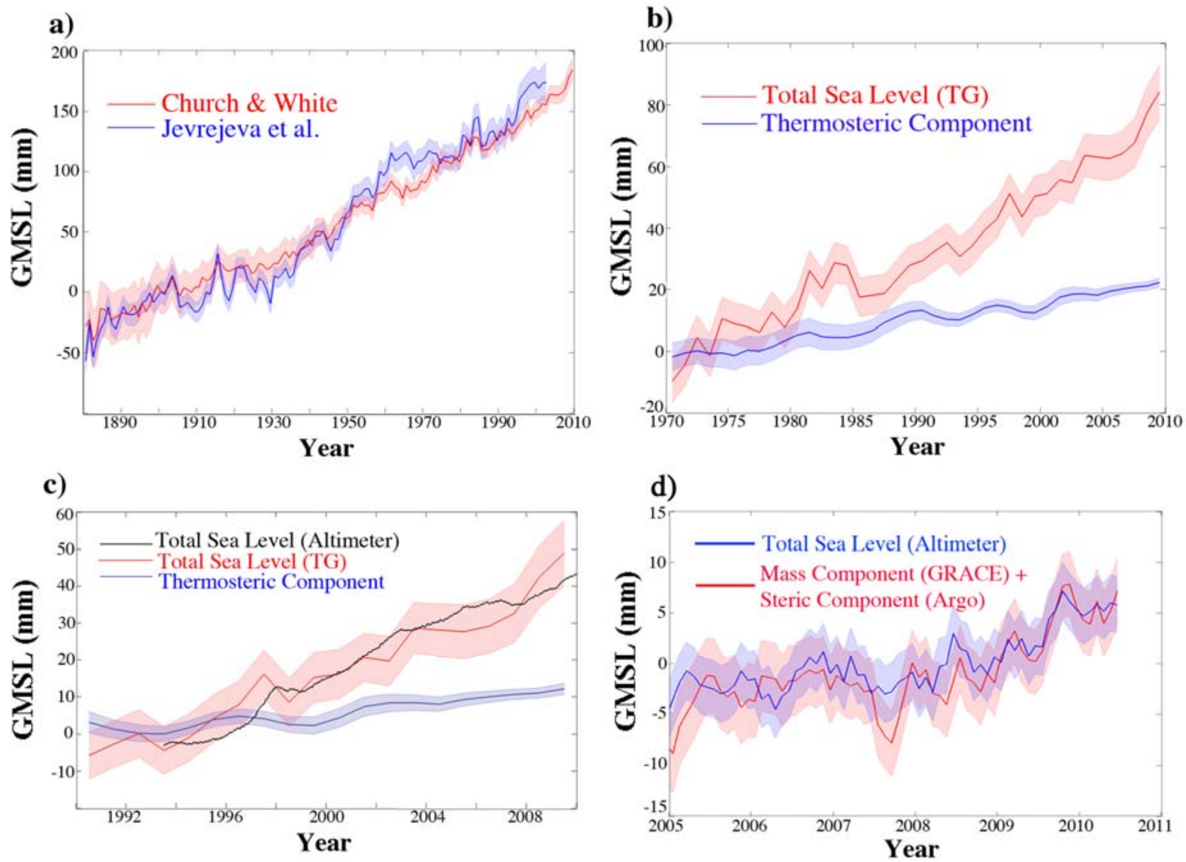

Figure 3.14: Global mean sea level from the different measuring systems as they have evolved in time. **a)** Yearly average GMSL reconstructed from tide gauges (1900–2010) by two different approaches (Church and White, 2011; Jevrejeva et al., 2008), **b)** total GMSL (1970–2010) from tide gauges along with the thermosteric component (3-year running mean) estimated from in situ temperature profiles (updated from Domingues et al., 2008), **c)** total GMSL (1993–2010) from tide gauges, along with measurement from altimetry (Nerem et al., 2010) smoothed with a 1-year running mean, and thermosteric component, **d)** the total sea level (nonseasonal) from altimetry and computed from the mass component (GRACE) and steric component (Argo) from 2005–2010 (Leuliette and Willis, 2011). All uncertainty bars are one standard error as reported by the authors. The thermosteric component is just a portion of total sea level, and is not expected to agree individually with total sea level. The time-series are plotted relative to 5-year mean values that start at **a)** 1900, **b)** 1970, **c)** 1993, and **d)** 2005.

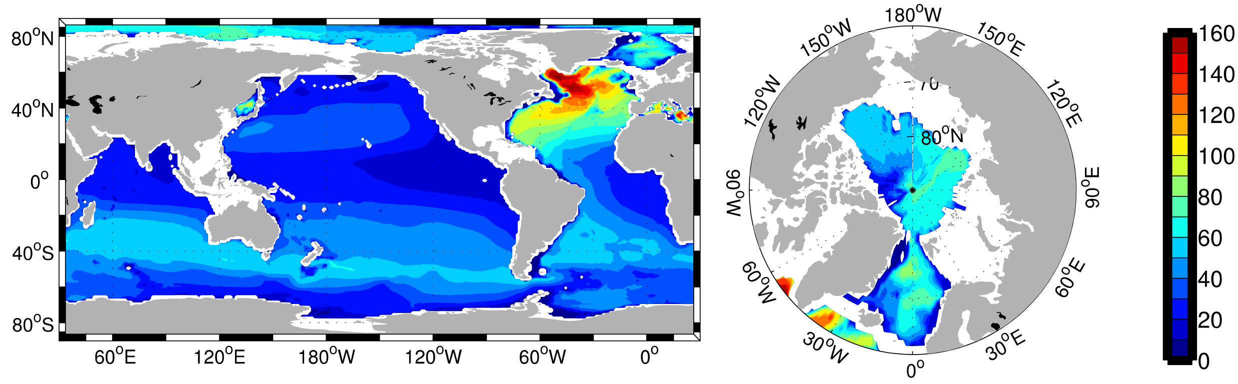

Figure 3.15: Compilation of the 2010 column inventories (mol m^{-2}) of anthropogenic CO_2: the global Ocean excluding the marginal seas (updated from Khatiwala et al., 2009) 151 ± 26 PgC; Arctic Ocean (Tanhua et al., 2009) 2.6 – 3.4 PgC; the Nordic Seas (Olsen et al., 2010) 1.0 – 1.5 PgC; the Mediterranean Sea (Schneider et al., 2010) 1.5 – 2.4 PgC; the East Sea (Sea of Japan) (Park et al., 2006) 0.40 ± 0.06 Pg C.

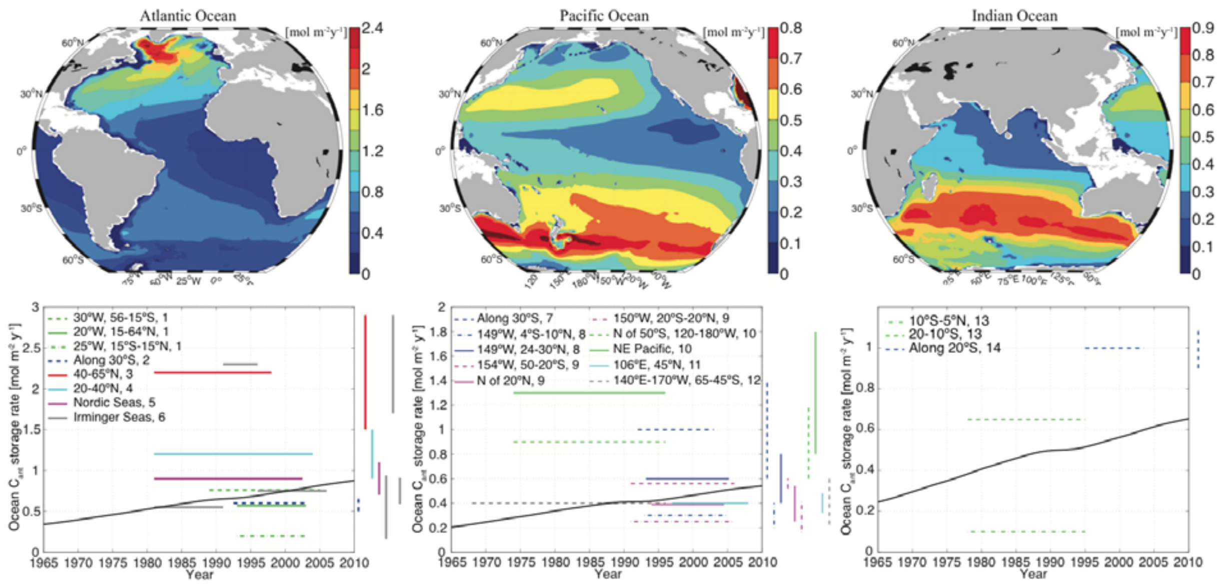

Figure 3.16: Top: maps of storage rate distribution of anthropogenic carbon (mol m^{-2} y^{-1}) for the three ocean basins (Atlantic, Pacific, and Indian Ocean) averaged over 1980–2005 estimated by the Green function approach (Khatiwala et al., 2009). Bottom: Corresponding storage rates as observed from repeat hydrography cruises. Measurements for the northern hemisphere are drawn as solid lines, the tropics as dash-dotted lines, and dashed lines for the southern hemisphere; the color schemes refer to different studies. Estimates of uncertainties are shown as vertical bars with matching colors on the right hand side of the panels. The solid black line represents the basin average storage rate using the same Green function approach (Khatiwala et al., 2009). Data sources as indicated in the legend are: 1) (Wanninkhof et al., 2010), 2) (Murata et al., 2008), 3) (Friis et al., 2005), 4) (Tanhua et al., 2007), 5) (Olsen et al., 2006), 6) (Perez et al., 2008), 7) (Murata et al., 2007), 8) (Murata et al., 2009), 9) (Sabine et al., 2008), 10) (Peng et al., 2003), 11) (Wakita et al., 2010), 12) (Matear and McNeil, 2003), 13) (Peng et al., 1998), and 14) (Murata et al., 2010).

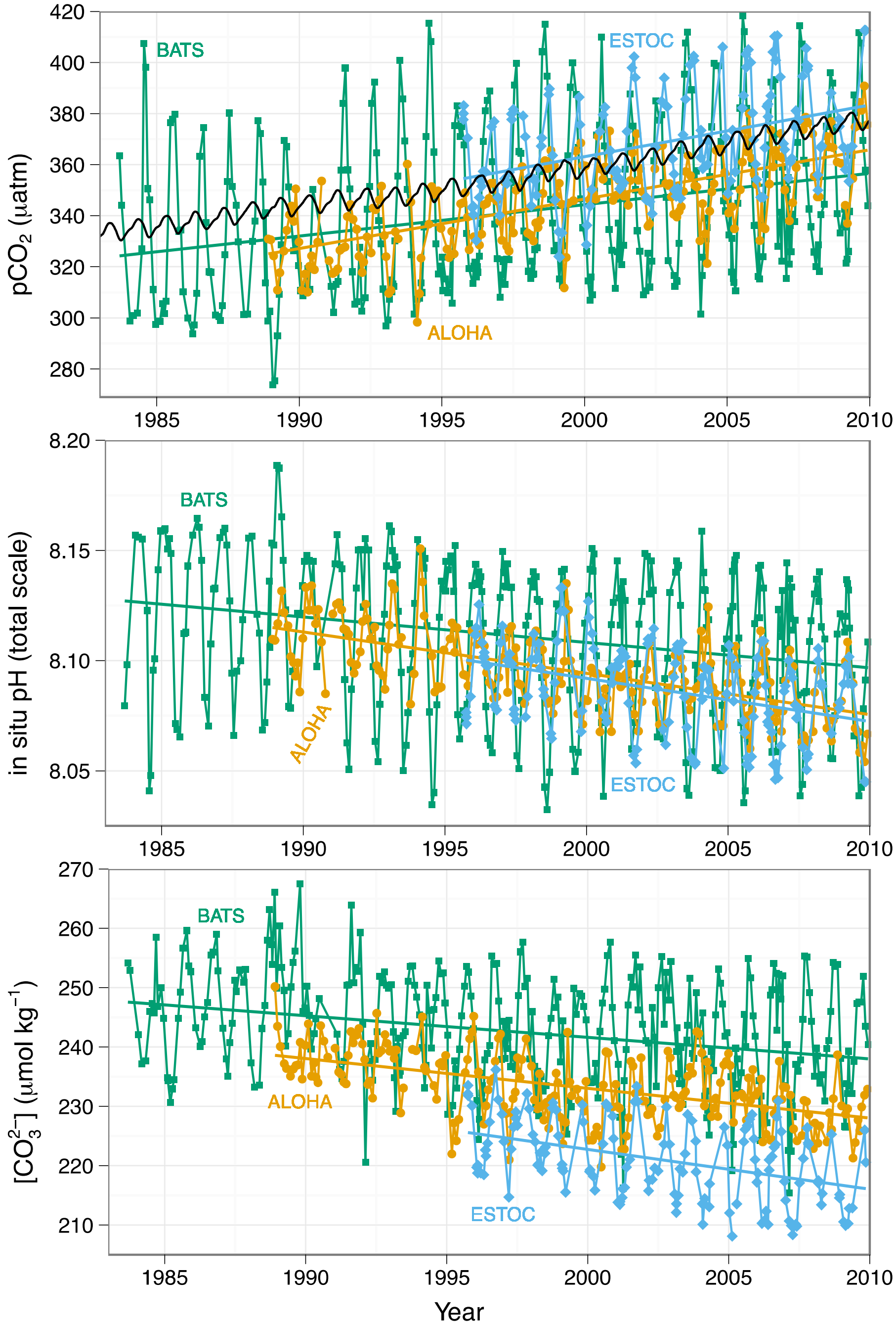

Figure 3.17: Long-term trends of surface seawater pCO_2 (top), pH (middle), and carbonate ion (bottom) concentration at three subtropical ocean time series in the North Atlantic and North Pacific Oceans, including: **a)** Bermuda Atlantic Time-series Study (BATS, 31°40′N, 64°10′W; **green**) and Hydrostation S (32°10′, 64°30′W) from 1983 to present (published and updated from Bates, 2007); **b)** Hawaii Ocean Time-series (HOT) at Station ALOHA (A Long-term Oligotrophic Habitat Assessment; 22°45′N, 158°00′W; **orange**) from 1988 to present (published and updated from Dore et al., 2009), and; **c)** European Station for Time-series in the Ocean (ESTOC, 29°10′N, 15°30′W; **blue**) from 1994 to present (published and updated from Gonzalez-Davila et al., 2010). Atmospheric pCO_2 (**black**) from Hawaii is shown in the top panel. Lines show linear fits to the data, whereas Table 3.2 give results for harmonic fits to the data (updated from Orr, 2011).

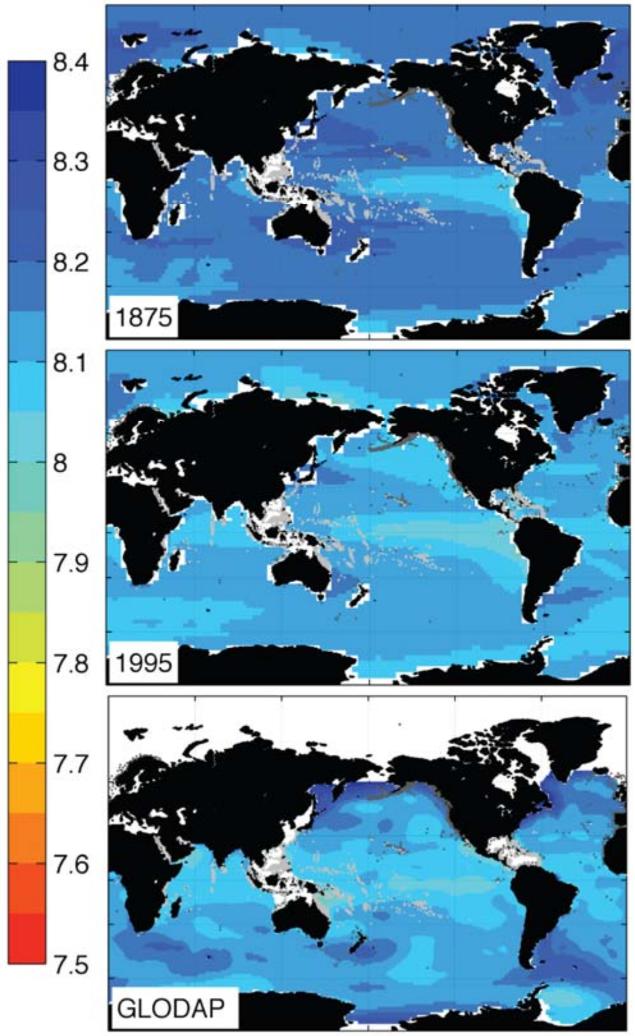

Box 3.2, Figure 1: National Center for Atmospheric Research Community Climate System Model 3.1 (CCSM3)-modeled decadal mean pH at the sea surface centered around the years 1875 (top) and 1995 (middle). Global Ocean Data Analysis Project (GLODAP)-based pH at the sea surface, nominally for 1995 (bottom). Deep coral reefs are indicated with darker gray dots; shallow-water coral reefs are indicated with lighter gray dots. White areas indicate regions with no data (after Feely et al., 2009).

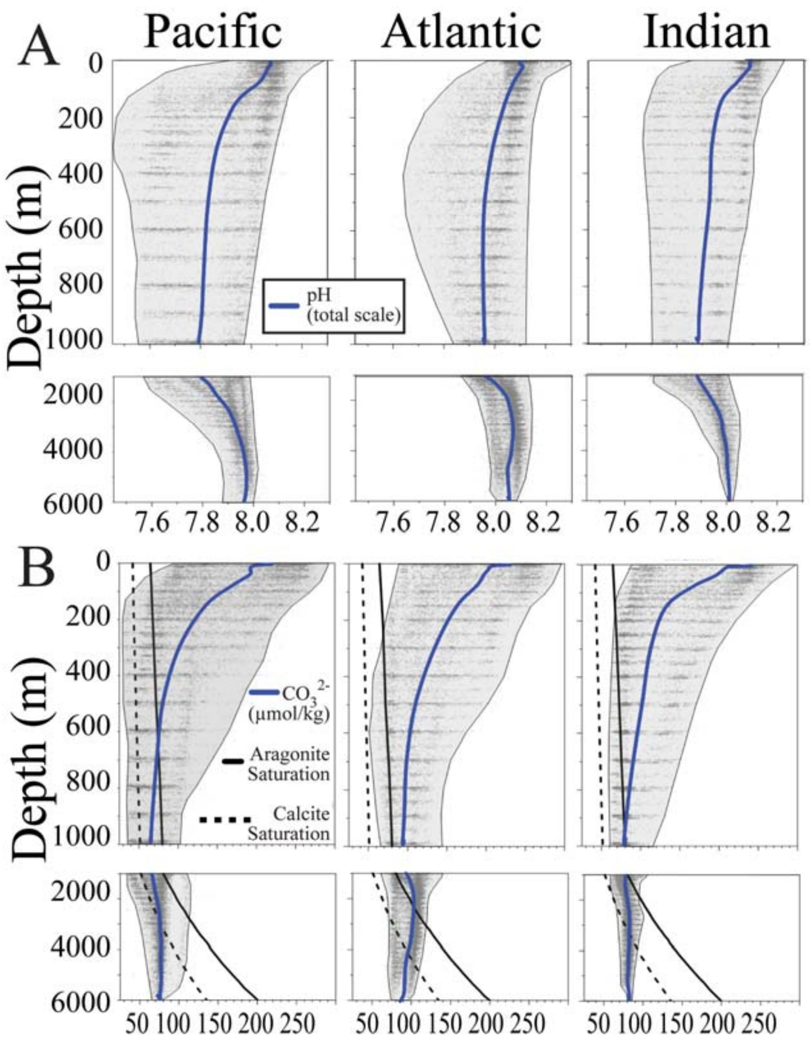

Box 3.2, Figure 2: Distribution of: **a)** pH and **b)** CO_3^{2-} ion concentration in the Pacific, Atlantic, and Indian oceans. The data are from the World Ocean Circulation Experiment/Joint Global Ocean Flux Study/Ocean Atmosphere Carbon Exchange Study global CO_2 survey (Sabine, 2005). The lines show the mean pH (solid line to panel), aragonite (solid line bottom panel), and calcite (dashed line bottom panel) saturation CO_3^{2-} concentration for each of these basins (modified from Feely et al., 2009).

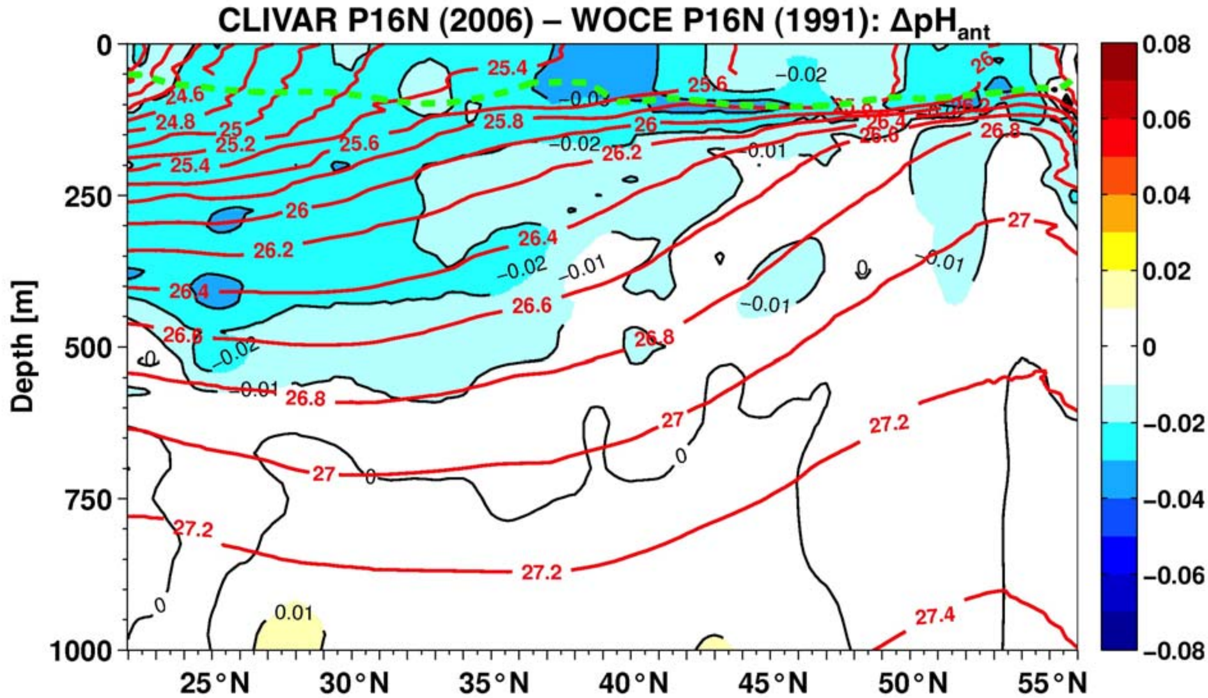

Figure 3.18: ΔpH_{ant}: pH change attributed to the uptake of anthropogenic carbon between 1991 and 2006, at about 150°W, Pacific Ocean (from Byrne et al., 2010).

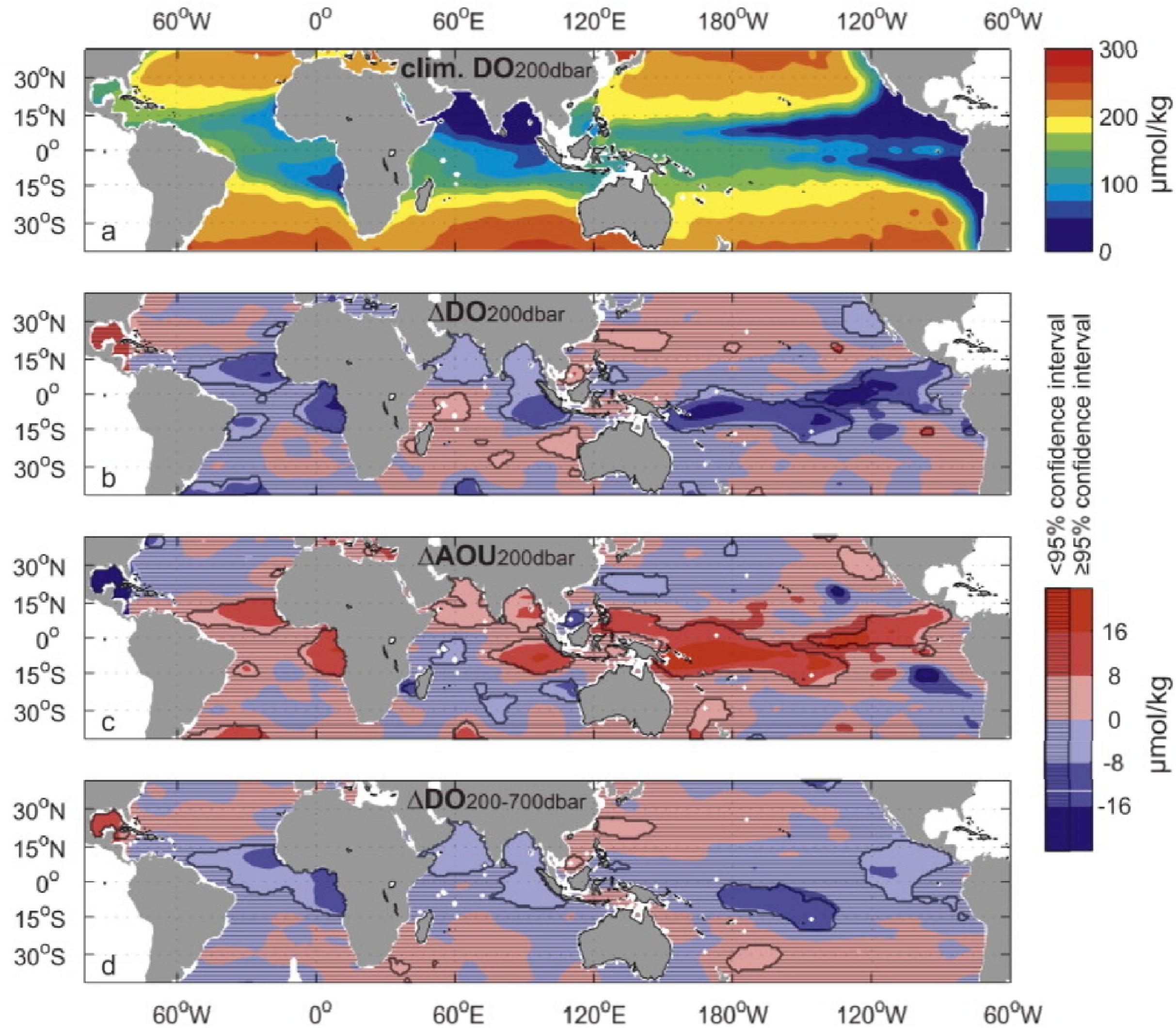

Figure 3.19: Dissolved oxygen (DO) distributions (in µmol kg^{-1}) between 40°S and 40°N for: **a)** the climatological mean (World Ocean Database 2005) at 200 dbar, as well as changes between 1960 and 1974 and 1990 and 2008 of **b)** dissoved oxygen (ΔDO) at 200 dbar, **c)** apparent oxygen utilization at 200 dbar relative to oxgen saturation at the surface, and **d)** ΔDO vertically-averaged over 200–700 dbar. In **b)-d)** increases are red and decreases blue, and areas with differences below the 95% confidence interval are shaded by black horizontal lines (after Stramma et al., 2010).

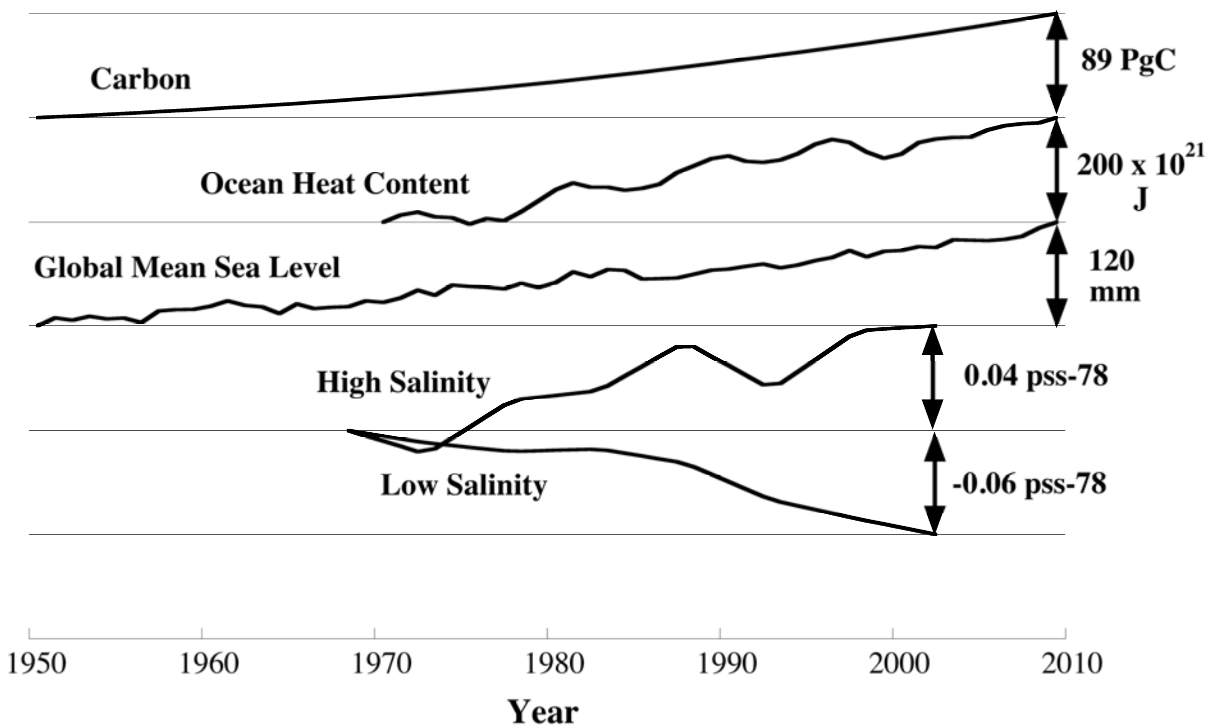

Figure 3.20: Time series of changes in large-scale ocean climate properties. Global ocean inventory of anthropogenic carbon dioxide is updated from Khatiwala et al. (2009). Global upper ocean heat content anomaly is updated from Domingues et al. (2008). Global mean sea level (GMSL) is from Church and White (2011). “High salinity” refers to the salinity averaged over regions where the sea surface salinity is greater than the global mean sea surface salinity from the World Ocean Database (2009) and "Low Salinity" to an average over regions with values below the global mean. Time series amplitudes are normalized by the differences between the last and first years of the records for easier comparison of trends in different properties.

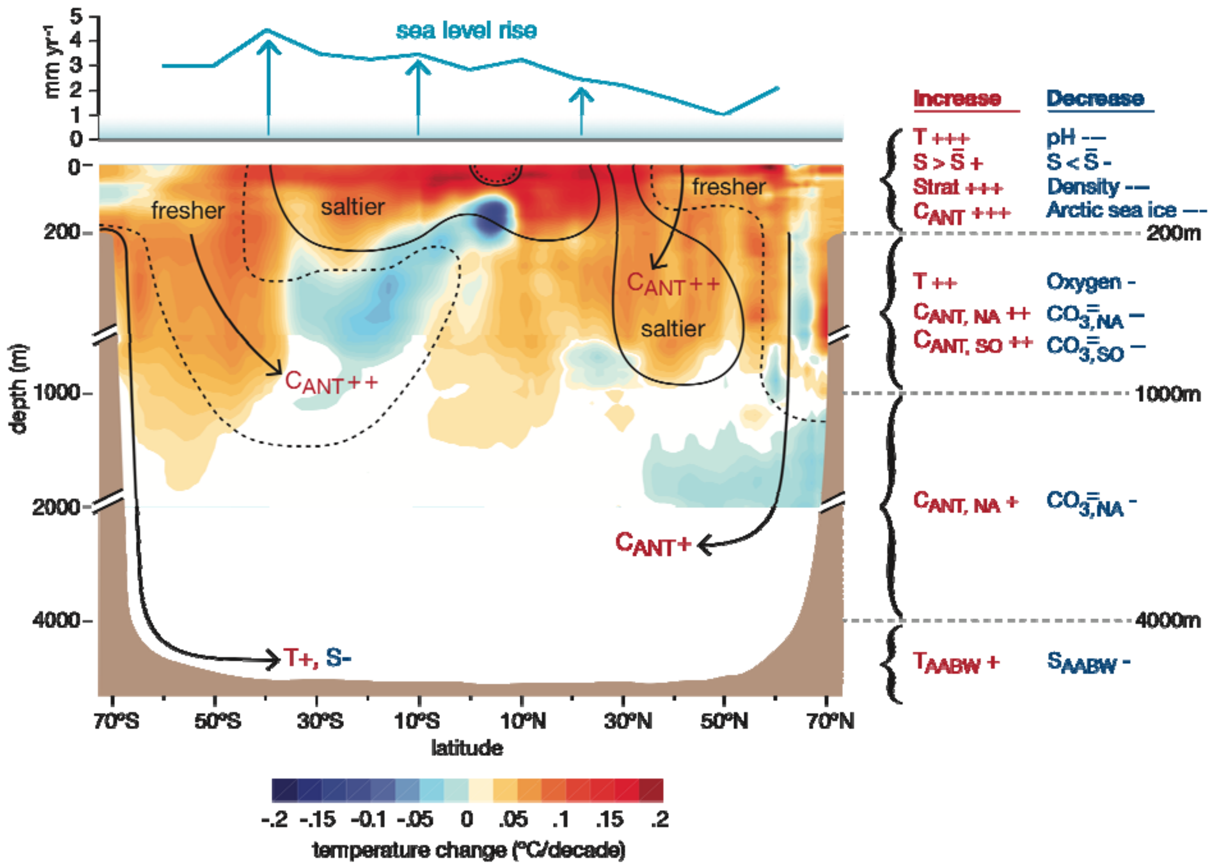

Figure 3.21: Summary of observed changes in zonal averages of global ocean properties. Temperature trends (°C decade^{-1}) are indicated in color (red = warming, blue = cooling); salinity trends are indicated by contour lines (dashed = fresher; solid = saltier) for the upper 2000 m of the water column (50-year trends from data set of Durack and Wijffels (2010); trends significant at >90% confidence are shown). Arrows indicate primary ventilation pathways. The top panel shows the zonal mean trend in sea level from 1993-2007 from satellite altimetry (Merrifield et al., 2009). Changes in other physical and chemical properties are summarised to the right of the figure, for each depth range (broken axes symbols delimit changes in vertical scale). Increases are shown in red, followed by a plus sign; decreases are shown in blue, followed by a minus sign; the number of + and – signs indicates the level of confidence associated with the observation of change (+++ = high confidence; ++ = medium confidence; + = low confidence). T = temperature, S = salinity, Strat = stratification, C_{ANT} = anthropogenic carbon, $CO_3^{=}$ = carbonate ion, NA = North Atlantic, SO = Southern Ocean, AABW = Antarctic Bottom Water. $S > \overline{S}$ refers to the salinity averaged over regions where the sea surface salinity is greater than the global mean sea surface salinity; $S < \overline{S}$ refers to the average over regions with values below the global mean.

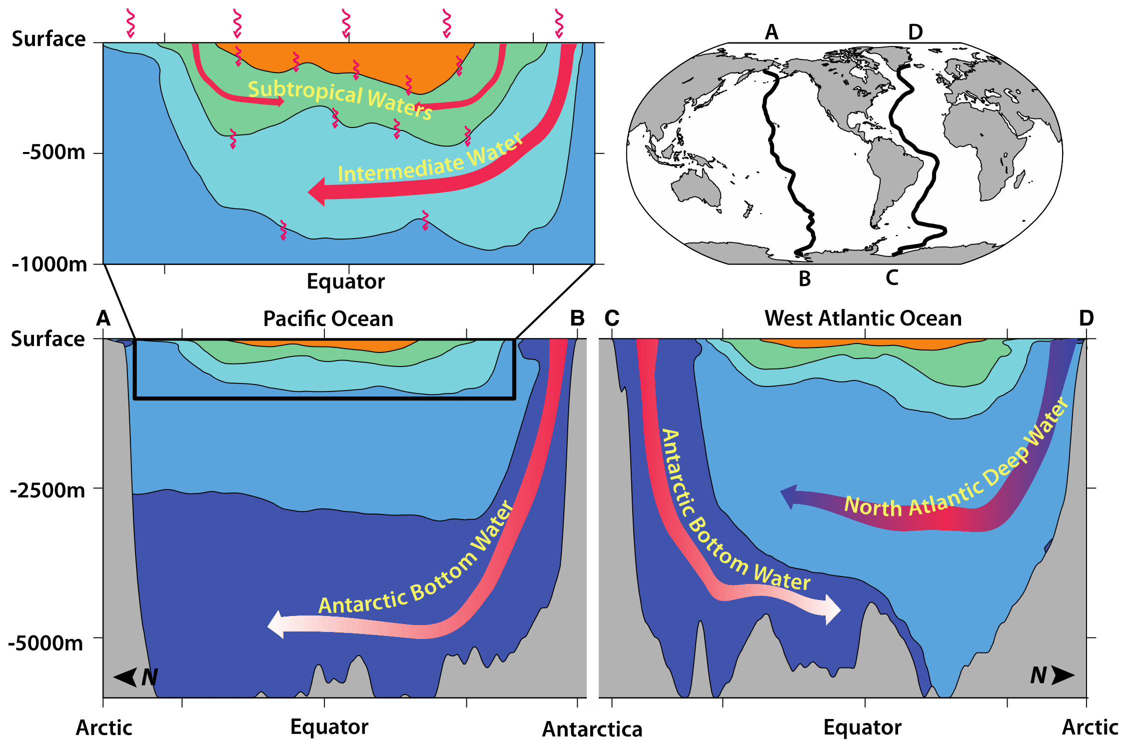

FAQ 3.1, Figure 1: Ocean variability pathways. The ocean is stratified, with the coldest water in the deep ocean (lower panels, use upper right panel for orientation). Antarctic Bottom Water (dark blue) sinks around Antarctica and spreading northward along the ocean floor into the central Pacific (left, red arrow fading to white indicating warming with time) and western Atlantic (right, red arrow fading to white indicating warming with time) oceans, as well as the Indian Ocean (not shown). North Atlantic Deep Water, slightly warmer and lighter (lighter blue) sinks in the northern North Atlantic Ocean (right, red and blue arrow indicating decadal warming and cooling) and spreads south above the Antarctic Bottom Water and then around Antarctica and into the Pacific and Indian Oceans. Similarly, in the upper ocean (upper left panel, only Southern Hemisphere shown, but Northern Hemisphere similar) Intermediate Waters, still warmer (cyan) sink in subpolar regions (red arrows indicating warming with time) and slip equatorward under Subtropical Waters, yet warmer (green), which in turn sink (red arrows indicating warming with time) slip equatorward under tropical waters, the warmest and lightest (orange) in all three oceans. Excess heat or cold entering at the ocean surface (top squiggly red arrows) also mixes slowly downward (interior squiggly red arrows).

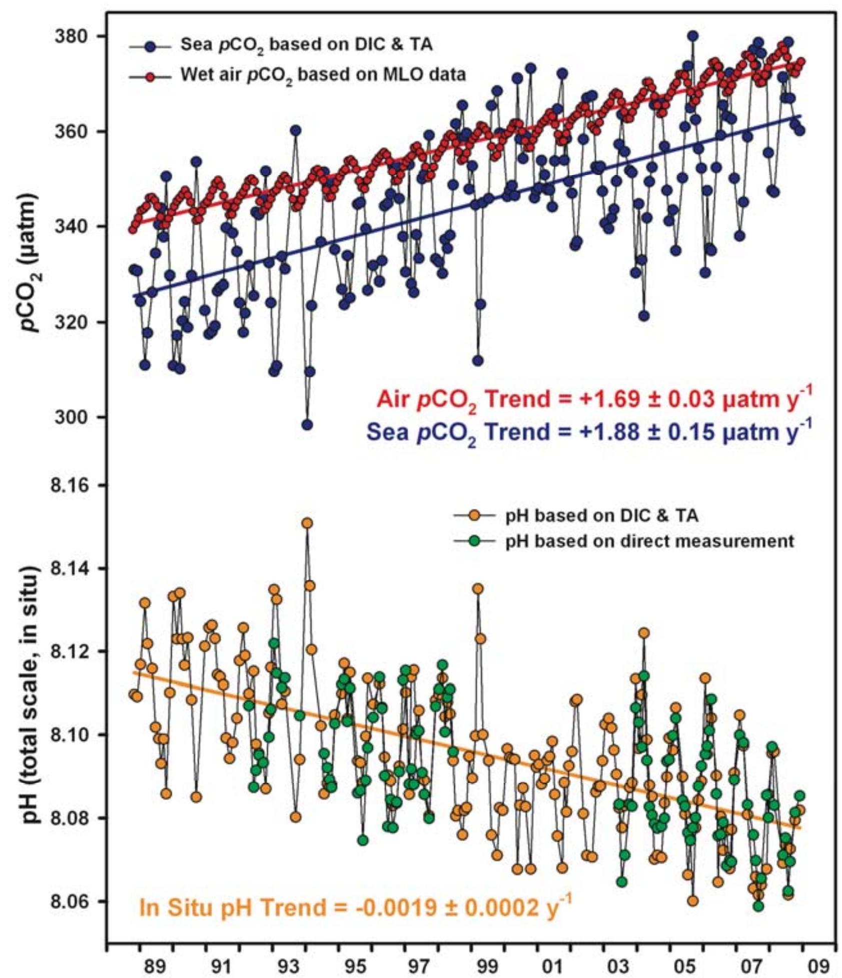

FAQ 3.2, Figure 1: Time series of atmospheric pCO_2 at the atmospheric Mauna Loa Observatory (top), surface ocean pCO_2 (middle), and surface ocean pH (bottom) on the island of Hawaii and Station ALOHA in the subtropical North Pacific north of Hawaii, 1988–2008 (after Doney et al., 2009; data from Dore et al., 2009).